1 An Experimental and Theoretical Approach to the Dynamic Behavior of Emulsions

Stanislav S. Dukhin, Johan Sjöblom, and Øystein Sæther

CONTENTS

1.1 General 5
1.1.1 Stability Mechanisms 5
1.1.2 Hydrodynamics of Flocculation: Main Notions 6
1.1.3 Importance of Flocculation Kinetics 6
1.1.4 Scope of the Chapter 7
1.2 Surface Forces 8
1.2.1 van der Waals Interaction 8
1.2.1.1 Macroscopic Approach 8
1.2.1.2 Hamaker Expressions 9
1.2.1.3 Retardation 9
1.2.2 Electrical Interaction 10
1.2.2.1 Electrical Double Layer 10
1.2.2.2 Double-Layer Interaction 11
1.2.2.3 The Problem of the Determination of the Stern Potential 12
1.2.3 Hydrophobic Interaction 12
1.2.4 Hydration Effects 12
1.3 Rapid Brownian Coagulation 13
1.3.1 von Smoluchowski Theory 13
1.3.2 Incorporation of Hydrodynamic Interaction and Attractive Surface Forces in the Theory of Rapid Coagulation 16
1.3.3 Brownian Collisions in Emulsions 17
1.3.3.1 Specification of the Fuchs Equation for Emulsions 18
1.3.3.2 Expression for the Drop Collision Rate 19
1.3.3.3 Brownian Collisions without Interparticle Forces 21
1.3.3.4 Brownian Collisions with van der Waals Forces 21
1.3.4 Experiments 22
1.4 Kinetics of Rapid Gravitational Coagulation in the Absence of Repulsive Surface Forces 24
1.4.1 Orthokinetic Coagulation and Particle Capture from Flow 24
1.4.2 Primitive Model of Gravitational Flocculation and its Specification for Emulsions 25

1.4.3 Long-Range and Short-Range Hydrodynamic Interaction 27
1.4.4 The Effect of Droplet Inertia 29
1.4.5 Collision Efficiency Caused by Long-Range Hydrodynamic Interaction 31
1.4.5.1 The Grazing Trajectory Method 31
1.4.5.2 Equation for the Smaller Drop Flux on the Surface of a Larger Drop 32
1.4.5.3 Long-Range Hydrodynamic Interaction at Intermediate Reynolds Numbers 33
1.4.5.3.1 Complete Surface Retardation 34
1.4.5.3.2 Incomplete Surface Retardation 34
1.4.5.3.3 Experiments 34
1.4.6 Flocculation in a Centrifugal Field and Dynamic Adsorption Layer 35
1.4.7 Incorporation of Short-Range Hydrodynamic Interaction and Attractive Surface Forces in the Theory of Inertialess Collision 37
1.4.7.1 Quantitative Theory of Short-Range Hydrodynamic Interaction Given Attractive Surface Forces 38
1.4.7.2 Theory Specification for Different Models 40
1.4.7.3 Peculiarities of Gravitational Coagulation at Small Aggregation Numbers 42
1.4.7.4 Estimation of the Size of Emulsion Drops Stable Against Flocculation with Larger Drops 43
1.4.8 Experiments 44
1.4.8.1 Experiments with Packed Beds 44
1.4.8.2 Experimental Investigation of Collision Efficiency at a Small Radius Ratio 44
1.4.9 Long- and Short-Range Hydrodynamic Interaction and Collision Efficiency at Any Radius Ratio 45
1.4.10 Collision Efficiency for Interacting Drops 46
1.4.10.1 Mobility Functions for the Relative Motion of Two Drops 46
1.5 Gravitational Coagulation in Secondary Minimum 48
1.5.1 Secondary Minimum of Interaction Energy in Emulsions 48
1.5.1.1 Secondary Minimum in Potential Curve of Charged Emulsions 52
1.5.1.2 Repulsive Hydration Forces and the Secondary Minimum 52
1.5.2 Estimation of the Size of Drops Not Coagulating in the Secondary Minimum. Sedimentation–Hydrodynamic Stability Mechanism of Microheterogeneous Dispersed Systems 53
1.5.3 Wet Fractionation Method and Sedimentation–Hydrodynamic Mechanism of Aggregate Stability 56
1.5.4 Peculiarities of Secondary Flocculation in Emulsion and Their Fractionation 56
1.5.5 Gravitational Coagulation Kinetics in the Secondary Minimum 57
1.5.5.1 General 57
1.5.5.2 Similarity in Collision Efficiencies of Primary and Secondary Gravitational Coagulation 57
1.6 Gravitational Coagulation in the Primary Minimum 58
1.7 Classification of Regimes of Gravitational Coagulation 58
1.8 Delineation of Different Particle Loss Mechanisms. Rapid Coagulation 61
1.8.1 Gravity-Induced Flocculation versus Brownian Flocculation 61
1.8.2 Gravity-Induced Flocculation versus Creaming 64

1.8.3 Domains of Dominant Particle Loss Mechanisms . . . 65
1.8.4 Experiment . . . 68
1.9 Coupling of Flocculation and Coalescence in Dilute Oil-In-Water Emulsions . . . 70
1.9.1 General . . . 70
1.9.1.1 Kinetic and Thermodynamic Stability in Macroemulsions and Mini-Emulsions . . . 70
1.9.1.2 Current State of Emulsion Stability Science . . . 71
1.9.1.3 The Specificity of Emulsion Characterization . . . 72
1.9.1.4 Scope of Section 9 . . . 72
1.9.2 Coupling of Coalescence and Flocculation . . . 73
1.9.2.1 Singlet–Doublet Quasi-Equilibrium . . . 73
1.9.2.2 Kinetic Equation for Coupling of Flocculation and Intradoublet Coalescence in Monodisperse Emulsions . . . 74
1.9.2.3 Coalescence in a Singlet–Doublet System at Quasi-Equilibrium . . . 75
1.9.2.4 Reduced Role of Fragmentation with Decreasing τ_c . . . 76
1.9.2.5 Experimental . . . 77
1.9.2.5.1 Application of Video Enhanced Microscopy Combined with the Microslide Technique for Investigation of Singlet–Doublet Equilibrium and Intradoublet Coalescence . . . 77
1.9.2.5.2 Improving the Experimental Technique with the Use of Low Density Contrast Emulsions . . . 78
1.9.2.5.3 The Measurement of Coalescence Time and Doublet Fragmentation Time . . . 78
1.9.2.6 Perspective for Generalization of the Theory for Coupling of Coalescence and Flocculation . . . 79
1.9.3 Coupling of Coalescence and Coagulation . . . 80
1.9.3.1 General . . . 80
1.9.3.2 Average Models . . . 81
1.9.3.2.1 The Model by Borwankar et al. . . . 81
1.9.3.2.2 The Limiting Cases of Fast and Slow Coalescence . . . 82
1.9.3.3 DIGB Model for the Simultaneous Processes of Coagulation and Coalescence . . . 83
1.9.4 Doublet Fragmentation Time . . . 85
1.9.4.1 Theory of Doublet Fragmentation Time . . . 85
1.9.4.2 Doublet Fragmentation Time of Uncharged Droplets . . . 87
1.9.4.3 Lifetime of a Doublet of Charged Droplets and Coagulation/Flocculation . . . 89
1.9.5 Coalescence Coupled with Either Coagulation or Flocculation in Dilute Emulsions . . . 89
1.9.5.1 Fragmentation of Primary Flocs in Emulsions and the Subsequent Reduction of Coalescence . . . 89
1.9.5.2 Domains of Coalescence Coupled Either with Coagulation or with Flocculation . . . 92
1.9.5.3 Hydration Forces Initiate Flocculation . . . 94
1.9.6 Applications . . . 95
1.9.6.1 Long-Term Prediction of Emulsion Stability . . . 95
1.9.6.2 Perfection of Methods for Emulsion Stabilization (Destabilization) by Means of the Effect on Both Coalescence and Flocculation . . . 96

1.9.6.2.1 Combining Surfactants and Polymers in Emulsion Stabilization 96
1.9.6.2.2 Strong Influence of Low Concentrations of Ionic Surfactant on Doublet Fragmentation Time and Coalescence Time 96
1.9.6.3 Standardization of the Measurement of τ_c and τ_d 97
1.9.6.4 Experimental–Theoretical Emulsion Dynamics Modeling 97
1.9.6.4.1 General 97
1.9.6.4.2 Combined Approach in Investigations of Dilute and Concentrated Emulsions 98
1.9.6.4.3 Kernel Determination 98
1.9.6.4.4 Singlet–Doublet Quasi-Equilibrium 99
1.9.6.4.5 Substitution of the Coalescence Kernels 99
1.10 Summary 99
Symbols 100
References 101

Abstract

For emulsion stability the surface chemistry, the dynamic of adsorption, the surface rheology, and the physicochemical kinetics are important. In contrast to the large success in industrial application of the emulsion surface chemistry the physicochemical kinetics is almost not used in emulsion technology. Meanwhile, the population balance equation (PBE) enables prediction of the evolution in time for droplet size distribution if the family of subprocesses including droplet aggregation, aggregate fragmentation, droplet coalescence, and droplet (floccula) creaming are quantified. These subprocesses are characterized in PBE by means of kinetic coefficients (kernels). The coupling of these four subprocesses, droplet poly-dispersity, and immense variety in droplet aggregate configurations cause the extreme difficulty in emulsion dynamics modeling (EDM). Three subprocesses, namely aggregation, fragmentation, and creaming, can be quantified. The systematic consideration of these three subprocesses with account for both Brownian and gravitational aggregation is accomplished in this chapter as it is necessary for EDM. In contrast to those three subprocesses, the experimental approach only is effective now concerning the emulsion film stability and coalescence kernel quantification for EDM. Accordingly, an experimental theoretical approach for the coalescence time determination, based on a dilute emulsion characterization in its simplest state, namely at the singlet doublet quasi-equilibrium, is elaborated. Information about elementary acts of coalescence and fragmentation obtained in experiments with dilute emulsion preserves its significance for concentrated emulsion as well. For modeling of nondiluted emulsions the combining of experimental investigation of the simplest emulsion model system with computer simulation accounting for the characteristics of a concentrated emulsion is proposed. Emulsion dynamics modeling combined with experiments using dilute emulsions at singlet doublet equilibrium may result in: (1) the quantification of emulsion film stability, namely the establishment of the coalescence time dependence on the physicochemical specificity of the adsorption layer of a surfactant (polymer), its structure and the droplet dimensions. This quantification can

form a base for the optimization of emulsifier and demulsifier selection and their synthesis for emulsion technology applications, instead of the current empirical level applied in the area; (2) the elaboration of a commercial device for coalescence time measurement, which in combination with EDM will represent a useful approach to the optimization of emulsion technology with respect to stabilization and destabilization.

1.1 GENERAL

1.1.1 Stability Mechanisms

In emulsions, the water droplets in oil, or oil droplets in water, are large (of the order of microns). Because of the large surface area per drop, the excess Gibbs energy per drop is high and cannot be compensated for by entropy contributions as in microemulsions.

The stability of a disperse system is characterized by a constant behavior in time of its basis parameters, namely, the dispersity and the uniform distribution of the dispersed phase in the medium. The problem of stability is one that is most important and complicated in colloid chemistry.

Notwithstanding their thermodynamic instability, many emulsions are kinetically stable and do not change appreciably for a prolonged period (sometimes for decades). These systems exist in the metastable state, that is, the potential barrier preventing aggregation of the particles is sufficiently high.

To understand the reasons for the relative stability of such systems, it is necessary to first determine the stability [1] and mechanisms of destabilization. *Sedimentation stability* distinguishes the stability of the disperse phase with respect to the force of gravity. Phase separation due to sedimentation is a typical phenomenon for droplets in coarsely dispersed emulsions resulting in settling (or floating) of the drops. Highly dispersed emulsions are *kinetically* stable. They are characterized by diffusion–sedimentation subsequent equilibrium. Isothermal distillation of fine drops in coarser ones causes subsequent sedimentation. The loss of *aggregative* stability is due to a combination of drops.

Forces of molecular attraction may result in the formation of a continuously structured system with *phase* stability. *Coagulation* or *flocculation* is a process of particle cohesion, the formation of larger aggregates with a loss of sedimentation and phase stability and the subsequent phase separation, that is, a destruction of the emulsion. Hence, *aggregative stability* can be defined as the ability of emulsion to retain the dispersity and individuality of drops. In aggregates, notwithstanding the change of their mobility, the drops still remain as such for a certain time (the "lifetime") after which they can merge spontaneously with diminishing phase interface. The merging of droplets is called *coalescence*.

The aggregative *stability* or *instability* is most characteristic for colloid systems. This chapter is devoted to this type of instability.

Two types of the aggregative stability can be discriminated: a very low coagulation rate or an equilibrium in the aggregation and disaggregation processes (reversible coagulation).

The theoretical and experimental investigations of flocculation are focused on monodisperse systems because it simplifies to quantify the flocculation kinetics. Polydisperse emulsions are not usually chosen as a model system for the flocculation kinetics. Another reason for not choosing emulsion is the deformation of droplet surfaces upon interaction, which further complicates a quantitative treatment. In addition, the mentioned coupling of flocculation and coalescence creates difficulties in the modeling of the flocculation kinetics.

1.1.2 Hydrodynamics of Flocculation: Main Notions

When two particles approach each other, several types of interaction patterns may arise, affecting the flocculation process. There are two different but related ways in which colloid interactions influence flocculation. First, they have a direct effect on the *collision efficiency*, which is the probability that a pair of colliding particles will form a permanent aggregate. A strong long-range repulsion between the particles will reduce the chance of aggregate formation, and flocculation will occur very slowly, if at all. The other aspect of colloid interaction is their effect in the *strength* of aggregates, which is much less well understood but of great practical importance [2].

Flocculation occurs only if particles collide with each other and adhere when brought together by collision (i.e., the particles have low colloidal stability). To a large extent, these two processes, which could be termed *transport* and *attachment* steps, may be regarded as independent and can be treated separately.

Practically all colloidal interactions are of a short range, almost never extending over distances greater than the size of the particles. Hence, they have little influence over the transport of the particles, although they are crucial in determining the collision efficiency. To a large extent, this justifies the treatment of transport and attachment as separate steps. There is an important type of interaction to which this conclusion does not apply, the so-called *viscous* or *hydrodynamic* interaction, which arises during the approach of particles in a viscous fluid. The effect reduces the rate of approach and gives a lower collision efficiency.

The main qualitative difference in flocculation kinetics is caused by the sign of the surface forces. Naturally, the attractive force enhances the flocculation and repulsive forces retard it. This difference is reflected (expressed) in the notions of rapid and slow flocculation. If attractive forces predominate, the flocculation is called "rapid," whereas "slow" coagulation relates to the systems in which the repulsive interaction between particles predominates.

In addition, the surface force dependence on the interparticle distance is important. As is known, the van der Waals attractive forces can predominate at small and large distances, whereas the repulsive forces cause the electrostatic barrier at intermediate distances. The flocculation/coagulation in the primary minimum is slow because it is retarded by the electrostatic barrier. It is not valid for the flocculation/coagulation in secondary minimum, which is rapid.

The formation of the drop doublet is the basic process in the flocculation kinetics. In a polydisperse emulsion, a statistical ensemble of the pairs of the drops with the radius a_1 and a_2 is considered [3,4]. One of the drops is chosen as the reference sphere, and the flux of all drops with another radius to the surface of the reference drop is considered. Thus, the flux represents the result of the averaging over all drop pairs of the statistical ensemble. The flux determines the loss of the particle drop number during the flocculation and the rate of the doublet formation.

The drop loss rates can be computed from the distribution of drops around the reference sphere. In the case of coagulation, the steady-state capture rate is given by the net inward flux of drops through an arbitrary surface enclosing the test sphere. The net flux depends on the drop distribution as well as the relative sphere velocities, which are known functions of the relative drop positions. Once the drop loss rates are known, the overall stability of an emulsion can be determined by solving the governing population balance equations which incorporate these drop loss rates. The solution of this system of coupled nonlinear partial differential equations gives the drop size distribution as a function of time and position.

1.1.3 Importance of Flocculation Kinetics

Tadros and Vincent [5] classified emulsion-breakdown processes. The transport processes (Brownian diffusion and differential settling) can manifest themselves in any kind of breakdown

processes. For instance, it is clear that the first step in Ostwald ripening [6] is due to the molecular diffusion. However, the mutual approach of the droplets caused by the differential settling or Brownian movement influences the molecular diffusion and kinetics of the Ostwald ripening. Thus, one concludes that the role of the transport processes can be understood more widely than in this chapter.

In the case of flocculation, two final states have to be distinguished: creaming and emulsion gelling [7,8] which occupy the emulsion volume as a whole. The larger the difference in liquid densities, the larger the droplet dimensions and the lower the volume fraction, which is favorable for creaming.

The quantification of the conditions of the two final states in flocculated emulsions is, in principle, possible on the basis of the flocculation theory.

Flocculation kinetics is important because it is accompanied by the change of emulsion properties and finally leads to the creaming and phase separation. The coalescence process usually follows the flocculation; that is, the coalescence kinetics are coupled with flocculation kinetics. Thus, the flocculated state and the flocculated kinetics have independent significance [9–11].

1.1.4 Scope of the Chapter

In monographs and reviews, much more attention is paid to surface forces [12,13] and stable colloids than to flocculation kinetics. Exceptions are Refs. 14 and 15 and literature on aerosols [16,17] and flotation [18–20].

In emulsion science, the main attention is focused on interparticle forces or colloid interactions and, correspondingly, to emulsion stability or instability, in terms of demulsification. In this chapter we turn to the question of transport mechanism, the coagulation kinetics, and to a lesser degree to the floc properties.

Now, due to the success of the investigations of flocculation in disperse model systems, the prerequisites are created for the investigation of flocculation in emulsions. In this review, we try to couple the studies of coagulation in disperse systems with flocculation in emulsions.

In a manner similar to Tadros and Vincent [5] and Melik and Fogler [15], we are concerned solely with "dilute" emulsions and suspensions in which the particle behavior is dominated by two-body interactions. Consequently, for emulsions, the present analysis is valid only for conditions predominated by singlets and doublets. However, the true application of this chapter is with emulsion systems which are characterized by coalescence times much faster than the corresponding flocculation times. The present analysis remains rigorous for predicting the flocculation and creaming behavior of a new larger particle, which is the result of a coalescence process, in relation to the remaining particles in the system. At faster coalescence times, an emulsion consists of the singlet and temporary doublet. At faster flocculation times, the emulsion consists of flocs. The structure of these flocs will not be considered in this chapter.

Dilute emulsions play an important role in, for instance, oil-dewatering processes [21]. At high initial volume fractions, the dewatering rate is high as well. The smaller the volume fraction, the lower the dewatering rate. Thus, the efficiency of oil-dewatering technology is connected to the flocculation kinetics. Obviously, the same is true with respect to produced water purification in environmental protection [22]. These two examples prove the importance of the flocculation process in dilute emulsions.

Tadros and Vincent [5] classified a wide range of emulsion systems. The classification subdivides the different types into (1) the nature of the "stabilizing moieties" and (2) the basic "structure" of the system. In both cases, the list represents a hierarchy of increasing complexity. In this hierarchy, the simplest systems will be considered here, which is justified by the limited knowledge of emulsion flocculation. Systems with steric stabilization [23], polymer bridging [24],

and depletion stabilization [25] are beyond the scope of this chapter. This obviously does not mean that the Brownian and gravitational coagulations described earlier are not important for the more complicated emulsion systems.

A general mathematical formulation of the problem of evolution of liquid drops spectrum is given in Ref. 1. A deductive method is used for the presentation. Equations of doublet formation kinetics and population balance equations (PBEs) are written in the more general form. Then the stability problem is being considered as a purely mathematical one. In principle, such an approach is very efficient if reliable information is available about coagulation kinetics. Unfortunately, available information about surface forces in emulsions is incomplete and often inaccurate with a clear discrepancy between theory and experiment.

Along with a general approach characterized in Refs. 15, 26, and 27, it is very important at the present stage to discriminate between facts established reliably and the links in the complex process of coagulation in emulsions which need a systematic investigation. As applied to definite systems and conditions, the general model of coagulation kinetics in emulsions described in Ref. 15 can be used at present; however, without guarantee of the required accuracy. Generally, the use of potentially very wide possibilities of the general coagulation theory can lead to unreliable results because of incomplete information about surface forces and subprocesses. There is a possibility to provide efficiency of the general theory with regard to a wider range of problems and systems which can result in a qualitatively new level of the emulsions science. The objective of this review is to provide some movement in this direction. This has also determined the accepted inductive method of presentation from a simple to a complicated matter, from reliable established facts to those insufficiently studied.

During the last years, the influence of droplet surface mobility on collision efficiency and droplet deformation on colloidal interaction in emulsion have been quantified [28], a fact which stimulated the preparation of this paper.

1.2 SURFACE FORCES

Surface forces are described in all monographs and reviews concerning emulsion stability [5,15,29–31]. In the following section we deal with some general notions and some new results.

1.2.1 van der Waals Interaction

1.2.1.1 Macroscopic Approach

The universal attractive forces between atoms and molecules, known as van der Waals forces, also operate between macroscopic objects and play a very important role in the interaction of colloidal particles. Indeed, without these forces, aggregation of particles would usually be prevented by the hydrodynamic interaction.

The interaction between macroscopic bodies arises from spontaneous electric and magnetic polarizations, giving a fluctuating electromagnetic field within the media and in the gap between them. In order to calculate the force, the variation in electromagnetic wave energy with the separation distance has to be determined. Lifshitz derived an expression for the force between two semi-infinite media separated by a plane-parallel gap. His treatment was later extended by Dzyaloshinskii et al. to deal with the case of two bodies separated by a third medium. The expressions can be found in Refs. 12 and 29. In principle, these methods should enable the interaction between systems of interest to be calculated, and direct measurements of van der Waals forces between mica sheets [32] have confirmed the essential correctness of the Lifshitz or

macroscopic approach. However, proper application of this approach requires detailed knowledge of the dielectric responses of the interacting media over a very wide frequency range.

1.2.1.2 Hamaker Expressions

Because of difficulties in applying the macroscopic theory, an older approach, due mainly to Hamaker [33], is still widely used. This is based on the assumption of pairwise additivity of intermolecular forces. The interaction between two particles is calculated simply by summing the interactions of all molecules in one particle with all of the molecules in the other particle. Hamaker replaced the summation by a double integration procedure, which leads to very simple expressions, especially when the separation distance is small. For two spheres, radii a_1 and a_2, separated by a distance h, the interaction energy at close approach ($h \ll a$) is given by

$$V_A = -\frac{A_{12}}{6h}\frac{a_1 a_2}{a_1 + a_2} \tag{1.1}$$

where V_A is the attraction energy between the two spheres and A_{12} is the *Hamaker constant* for media 1 and 2, of which the spheres are composed. The results given above apply to the interaction of media across a vacuum.

A useful approximation for Hamaker constants of different media is the geometric mean assumption

$$A_{12} \cong (A_{11}A_{22})^{1/2} \tag{1.2}$$

For similar materials, medium 1 interacting across medium 3,

$$A_{131} \cong \left(A_{11}^{1/2} - A_{33}^{1/2}\right)^2 \tag{1.3}$$

Equation 1.3 led Hamaker to the conclusion that the van der Waals interaction between similar materials in a liquid would always be attractive (positive Hamaker constant) whatever the values of A_{11} and A_{33}.

Oil phases are characterized by fairly low dielectric constants ranging between 2 and 5, which makes the pure entropic term fairly constant. The nonretarded dispersion contribution is the major cause of differences in Hamaker constants between different emulsions. The Hamaker constant can be expected to vary between 3×10^{-21} and 10×10^{-21} J in most food emulsions [31].

1.2.1.3 Retardation

Because dispersion forces are electromagnetic in character, they are subject to a *retardation* effect. The finite time of propagation causes a reduced correlation between oscillations in the interacting bodies and a smaller interaction. Pailtorpe and Russel [34] considered the effect of retardation and found that the total Hamaker constant decreases by approximately 70% for $a = 0.1$ μm and 85% for $a = 0.25$ μm over the range $2.001 < S - 2 < 2.5$. Melik and Fogler [15] conclude that the equation proposed in Ref. 35 cannot be considered a reasonable quantitative approximation to the retarded interparticle potential. However, in light of the tedious calculations required to account rigorously for any spatial variation of the Hamaker constant, they used this equation in their calculations of flocculation in the secondary minimum. Its distance to the surface can be equal to 5–7 Debye radius, that is, 10–100 nm (Section 1.5.1.1). According to Lyklema [36] the

van der Waals energy dependence on distance can always be expressed through the Hamaker function $A(h)$. At a small separation, $A(h)$ becomes independent of h and identical to the *Hamaker constant*. At large h,

$$A(h) \sim h^{-1} \tag{1.4}$$

However, the systematic investigation of Rabinovich and Churaev [32,37,38] led them to the conclusion that for systems including water and a dielectric, the asymptotic equation [Equation 1.4] is not valid at any distance. In Ref. 32, they carried out a numerical calculation of $A(h)$ for 36 systems.

1.2.2 Electrical Interaction

1.2.2.1 Electrical Double Layer

Most particles in aqueous media are charged due to various reasons, such as the ionization of surface groups, specific adsorption of ions, and so forth. In an electrolyte solution, the distribution of ions around a charged particle is not uniform and gives rise to an *electric double layer* (DL). This topic has been the subject of several reviews [39,40] and details are not given here. The essential point is that the charge on a particle surface is balanced by an equivalent number of oppositely charged *counterions* in solution. These counterions are subject to two opposing effects: electrostatic attraction tending to localize the counterions close to the particles and the tendency of ions to diffuse randomly throughout the solution due to their thermal energy. The surface charge on a particle and the associated counterion charge together constitute the electrical double layer. A widely accepted model for the double layer is that of Stern, later modified by Graham (see Hunter [39]), in which part of the counterion charge is located close to the particle surface (the so-called *Stern layer*) and the remainder is distributed more broadly in the *diffuse layer*.

The interaction between charged particles is governed predominantly by the overlap of diffuse layers, so the potential most relevant to the interaction is that at the boundary between the Stern and diffuse layers (the Stern potential, Ψ_δ), rather than the potential at the particle surface. This boundary (the *Stern plane*) is generally considered to be at a distance of about 0.3–0.5 nm from the particle surface, corresponding to the diameter of a hydrated counterion.

There is no direct experimental method for determining the Stern potential. The two major influences on electrical interaction between particles are the magnitude of the effective "surface potential" (generally assumed to be Ψ_δ or ζ) and the extent of the diffuse layer because the latter governs the range of the interactions. Surface potentials can be modified in two distinct ways. If the ionic strength is raised, then a greater proportion of the potential drop occurs across the Stern layer, giving a smaller Stern potential. This effect can be produced by adding salt, and those which act in this way only are known as *indifferent electrolytes*. A more dramatic effect can be produced by the addition of salts with *specifically adsorbing counterions*. These adsorb on the particles because of some specific, nonelectrostatic affinity and can be regarded as located in the Stern layer. In many cases, such ions can adsorb to such an extent that they reverse the sign of the Stern potential.

The extent of the diffuse layer is also dependent on the ionic strength and is best seen through the variation of the potential as a function of distance from the Stern plane, for which the Poisson–Boltzmann approach is most commonly employed [39,40]. For fairly low potentials the linear form of the Poisson–Boltzmann expression is appropriate and a very simple result is

obtained:

$$\Psi = \Psi_\delta \exp(-\kappa x) \tag{1.5}$$

where Ψ is the potential at a distance x from the Stern plane and κ is the *Debye–Hückel* reciprocal length [39,40], which is of great importance in colloid stability. For aqueous solution at 25 °C, κ is given by

$$\kappa = 2.3 \times 10^9 \left(\sum c_i z_i^2\right)^{1/2} (m^{-1}) \tag{1.6}$$

where c_i is the molar concentration and z_i is the valence of ion i. The sum is made over all ions in solution.

The Debye–Hückel parameter has the dimensions of reciprocal length and $1/\kappa$ is a characteristic length which determines the extent of the diffuse layer.

1.2.2.2 Double-Layer Interaction

When two charged particles approach each other in an electrolyte solution, their diffuse layers overlap and, in the case of identical particles, a repulsion is experienced between them. The precise way in which the double layers respond to each other depends on a number of factors which cannot be treated in detail here. One distinction is between interaction at constant surface potential or constant surface charge.

The repulsion energy of identical spherical particles at constant potential is [39], according to DLVO theory [1],

$$V_R = \frac{4\pi a_1 a_2}{a_1 + a_2} \varepsilon \Psi^2 \ln(1 + e^{-\kappa h}) \tag{1.7}$$

When deriving Equation 1.7, it was assumed that the Stern potential is low, that is,

$$\tilde{\Psi} = \frac{e\Psi}{kT} < 1 \tag{1.8}$$

where e is the electron charge, k is the Boltzmann constant, T is the absolute temperature, and the double layer is thin, that is,

$$\kappa a \gg 1 \tag{1.9}$$

For larger potentials, the analytic equations for large separation and thin layers [41,42],

$$\kappa a > 2 \tag{1.10}$$

is

$$V_R = 32\pi\varepsilon \left(\frac{kT}{e}\right)^2 \tanh^2\left(\frac{\tilde{\Psi}}{4}\right) a e^{-\kappa h} \tag{1.11}$$

1.2.2.3 The Problem of the Determination of the Stern Potential

The electrostatic interaction is very sensitive to the value of the surface potential. Its identification with the ζ potential is correct for surfaces which can be described by the so-called standard electrokinetic model [39,40]. In this model, the surfaces are described as molecularly smooth, impermeable for ions, and under no conditions porous and rough. The surface of an emulsion droplet is usually covered by the adsorption layer of an organic substance and does not satisfy this condition. In Ref. 31, values concerning the size and penetration of the different polar groups of the adsorbed organic molecular into water are given as 0.3–1.6 nm. The ions of the diffuse layer are distributed partially outside the adsorption layer and partially inside it. The latter part is not small if the electrolyte concentration is not low. The counterions inside the adsorption layer participate in the electrostatic interaction of particles also. The ζ potential yields information about the counterions outside the adsorption layer. Thus, using the ζ potential instead of the Stern potential leads to an underestimation of the electrostatic interaction.

The ζ potential manifests itself in Bickerman surface conductivity. The counterions distributed between the slipping plane and the interface are mobile and produce the additional surface conductivity. Measurements of the surface conductivity enable the evaluation of the total charge of the diffuse layer and the efficient Stern potential [43]. Low-frequency dielectric dispersion is the most exact method for those measurements [44]. High-frequency conductometry is also useful for the Stern potential evaluation [45].

1.2.3 Hydrophobic Interaction

In some cases, surfaces may have significant areas with a hydrophobic (nonwettable) character, such as polymer latex particles with a low density of surface ionic groups, or negative particles with adsorbed cationic surfactant. The possibility then arises of another type of interaction which can give appreciable attraction – the so-called *hydrophobic interaction*. The extensive hydrogen bonding present in ordinary water is responsible for a considerable degree of association between water molecules and a significant "structuring" effect. A hydrophobic surface offers no possibility of hydrogen bonding or ion hydration, so there is no inherent affinity for water. However, the presence of such a surface tends to limit the contact with such surfaces as far as possible. In aqueous solutions, molecules with hydrophobic segments can associate with each other in such a way that contact between water and the hydrophobic regions is minimized. This is known as *hydrophobic bonding*. The best known examples of this are surfactant and protein solutions.

It has recently been found [46] that the same type of interaction occurs between macroscopic hydrophobic surfaces. The resulting attractive force can be surprisingly large and of quite long range [47].

With increasing hydrophilicity with the introduction of charged headgroups onto the surface, the measurable range of the hydrophobic attraction decreases rapidly [48]. No long-range hydrophobic interaction is observed for surfaces having contact angles below about 40–70° (water/air). It, thus, appears that a low density of hydrophilic groups on a hydrophobic surface is sufficient to considerably reduce the magnitude and range of the hydrophobic force. The hydrophobic interactions between macroscopic surfaces seem to be important only in rather pure systems [31] and not in technical emulsions.

1.2.4 Hydration Effects

The nature of water close to a particle surface is usually very different from bulk water. The major consequence of hydration at a particle surface is an increased repulsion between approaching

particles because of the need for ions to lose their water of hydration upon contact between particles. This involves work and, hence, an increase in free energy of the system.

The most direct evidence of hydration effects comes from measurements of the force between mica sheets in various electrolyte solutions [49]. At low ionic strengths, the repulsion follows the expected exponential form for the double-layer interaction (see Section 1.2.2.2). At salt concentrations above 1 mM, a monotonic short-range force is apparent, in addition to the double-layer repulsion, which is due to adsorbed hydrated cations. This extra force increases with the degree of hydration ($Li^+ \cong Na^+ > K^+ > Cs^+$) and is roughly exponential over the range 1.5–4 nm, with a decay length of the order of 1 nm. In their earlier studies, Derjaguin and Zorin [50] introduced the concept of a "structural component of disjoining pressure" to account for the anomalous behavior of thin films.

The range of these hydration forces is quite appreciable in relation to the range of double-layer repulsion, and they may be expected to have an effect on colloid stability, especially at high ionic strengths. Similarly, the way some flocculated colloids can be redispersed ("repetized") simply by washing away the electrolyte [51,52] is a clear indication that aggregation is not occurring in a true primary minimum, but in a "hydration minimum," where the particles are prevented from coming into true contact by the presence of hydrated ions. In these cases, the van der Waals attraction is not sufficiently strong to prevent separation of particles when the salt is diluted and double-layer repulsion is re-established.

Another type of hydration repulsion arises when adsorbed layers of hydrophilic material are present, but this is usually considered as a "steric" interaction. In Ref. 31, it is shown that the hydration forces acting between bilayers of different phosphatidylcholines have a comparable magnitude out to a bilayer of about 2–3 nm. The authors suggest the important role of the hydration forces in emulsion stabilization.

1.3 RAPID BROWNIAN COAGULATION

1.3.1 VON SMOLUCHOWSKI THEORY

The classical understanding of coagulation kinetics is given by von Smoluchowski theory [3,4], which follows from the assumption that the collisions are binary and that fluctuations in density are sufficiently small. Computer simulations [53–56] serve as a means to test the validity of the mean field approach.

An aggregate formed from i identical particles is called an i-mer. The average number of i-mers per unit volume is the particle concentration z_i.

The coagulation of two clusters of the kind i and j is given by the following relation:

$$i\text{-}mer + j\text{-}mer \xrightarrow{k_{ij}} (i+j)\text{-}mer = k\text{-}mer$$

where k_{ij} is the concentration-independent coagulation constant or kernel. Physically, it means that the coagulation rate between all kinds of i-mers and j-mers is the same.

For dilute dispersions with volume fractions less than 1%, only two-particle collisions need to be considered because the probability of three-particle collisions is small.

The equation describing the temporal evolution of the cluster of kind k is as follows:

$$\frac{dz_k}{dt} = \frac{1}{2} \sum_{i=1, j=k-1} k_{ij} z_i z_j - z_k \sum_{i=1}^{\infty} k_{ik} z_i \tag{1.12}$$

k_{ij} depends on details of the collision process between i-mers and j-mers. This kernel embodies the dependence on i and j of the meeting of an i-mer and a j-mer, including effects such as the volume dependence of the collision cross-section and the diffusion constant.

The first term in Equation 1.12 describes the increase in z_k owing to coagulation of an i-mer and a j-mer and the second term describes the decrease of z_k owing to the coagulation of a k-mer with other aggregates.

It is important to note that Equation 1.12 is for *irreversible* aggregation – no account is taken of the breakup of aggregates, which would require a third term on the right-hand side. Also, it is assumed, for the present, that each collision results in the formation of an aggregate (i.e., the collision efficiency and stability ratio are both unity).

In principle, it would be possible to use Equation 1.12 to derive the concentrations of all aggregate types at any time, but there are great difficulties, notably in assigning values to the rate coefficients, which depend not only on aggregate size and shape but also on the particle transport mechanism. By converting Equation 1.12 into an integral expression and considering continuous aggregate size distributions rather than discrete numbers, it is possible to derive solutions in certain cases but only for specific forms of the i-ate coefficients (or kernels), which may not be physically realistic. Nevertheless, such approaches can give some insight into the way aggregate size distributions may evolve during flocculation processes.

Particles in suspensions are subject to Brownian motion [57,58]. As a result, particles will collide. The Smoluchowski approach is to imagine a stationary central particle and to calculate the number of particles colliding with it in unit time. Allowance can then be made for the fact that the central particle itself is one of many similar particles undergoing Brownian motion and so the appropriate collision frequency can be derived:

$$J_{ij} = 4\pi R_{ij}(D_i + D_j)n_i n_j \tag{1.13}$$

J_{ij} is the total number of collisions occurring between particles of types i and j in unit volume per unit time. D_i and D_j, and n_i and n_j, are the diffusion coefficients and number concentrations, respectively. The term R_{ij} is the collision radius for the pair of particles and represents the center-to-center distance at which the particles may be assumed to be in contact. In many cases, the collision radius can be taken simply as the sum of the particle radii, but if there is long-range attraction between the particles, the effective collision radius will be somewhat larger. In what follows, we will assume spherical particles, radii a_i and a_j, and that $R_{ij} = a_i + a_j$. Also, for the diffusion coefficients, the Stokes–Einstein expression is used:

$$D_i = \frac{kT}{6\pi a_i \mu} \tag{1.14}$$

where μ is the viscosity of the fluid, k is the Boltzmann constant, and T is the temperature.

Equation 1.13 then becomes

$$J_{ij} = \frac{(2kT/3\mu)\, n_i n_j \left(a_i + a_j\right)^2}{a_i a_j} \tag{1.15}$$

and so, by comparison with Equation 1.12, the rate constant can be written as

$$k_{ij} = \frac{(2kT/3\mu) \left(a_i + a_j\right)^2}{a_i a_j} \tag{1.16}$$

For an initially monodisperse suspension of particles, radius a_1, the initial collision rate can be calculated easily from Equation 1.12 because only one type of collision (1-1) is involved. Also, the initial rate of decrease of the *total* particle concentration, n_T, follows directly from the collision rate because each collision reduces the number of particles by one (two primary particles lost, one aggregate gained). The result is

$$-\frac{dn_T}{dt} = \left(\frac{4kT}{3\mu}\right) n_T^2 = k_F n_T^2 \tag{1.17}$$

where k_F is known as the flocculation rate constant and has a value of 6.13×10^{-18} $m^3\,s^{-1}$ for aqueous dispersions at 25 °C.

The most noteworthy feature of Equation 1.17 is that it does not include the particle size because the size terms cancels from Equation 1.16 when $a_i = a_j$. As the particle size increases, the diffusion coefficients decreases, but the collision radius increases. These have opposing effects on the collision rate and, for equal particles, they balance exactly. Even for spheres of different size, the term $\left(a_i + a_j\right)^2 / a_i a_j \cong 4$, provided that the sizes do not differ too greatly (say, by no more than a factor of 3, in which case the size term has a value of about 5).

The simplest second-order rate expression of Equation 1.17 can be integrated to give the total number of particles as a function of time:

$$n_T = \frac{n_0}{1 + k_F n_0 t} \tag{1.18}$$

where n_0 is the initial concentration of primary particles.

There is a characteristic flocculation time t_F, in which the number of particles is reduced to half of the initial value ($n_T = n_0/2$) and this follows immediately from Equation 1.18:

$$t_F = \frac{1}{k_F n_0} \tag{1.19}$$

The flocculation time can also be thought of as the average time in which a particle experiences one collision. From the value of k_F quoted above, t_F turns out to be about $1.6 \times 10^{17}/n_0$ s and so for an initial particle concentration of 10^{16} m^{-3}, the flocculation time would be about 16 s. Particle concentrations are often much lower and the corresponding flocculation time would be greater.

As well as the total particle concentration, it is also possible to calculate the concentration of single particles and aggregates, assuming the rate constant is the same for all collisions. For single particles,

$$n_1 = \frac{n_0}{(1 + t/t_F)^2} \tag{1.20a}$$

and for doublets,

$$n_2 = \frac{n_0 t/t_F}{(1 + t/t_F)^3} \tag{1.20b}$$

The general Smoluchowski expression for k-fold aggregates is

$$n_k = \frac{n_0 (t/t_F)^{k-1}}{(1 + t/t_F)^{k+1}} \tag{1.21}$$

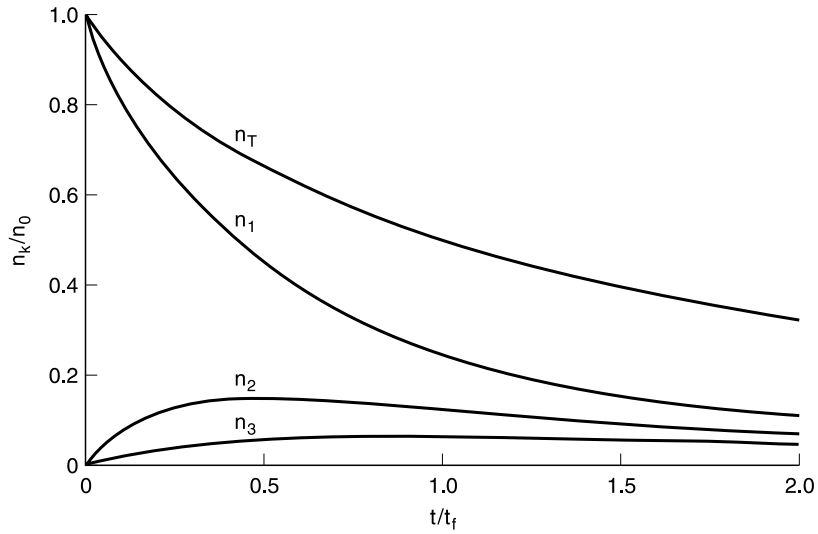

FIGURE 1.1 Reduced concentration of k-fold aggregates plotted against reduced time for $k = 1, 2, 3$ and for the total concentration n_T.

Results from these expressions are shown in the dimensionless form (n_k/n_0 versus t/t_F) in Figure 1.1, for aggregates up to three-fold. For all aggregates, the concentration rises to a maximum at a characteristic time and then declines slowly. Note that at all times the concentration of singlets exceeds that of any other aggregate.

Experimental data for rapid flocculation show reasonable agreement with Smoluchowski predictions, at least in the early stages of the process (see Section 1.3.4).

Rate constants determined for the rapid flocculation of latex particles are about half of the value given by Equation 1.17 and this is now known to be a result of hydrodynamic interaction between approaching particles. This effect will be considered briefly in Sections 1.3.2 and 1.3.3.

1.3.2 Incorporation of Hydrodynamic Interaction and Attractive Surface Forces in the Theory of Rapid Coagulation

Theory of perikinetic coagulation continued to develop along the way as proposed by Smoluchowski. Oversimplifications were not allowed, which led step by step to an improvement in theory. In the Smoluchowski model, every collision is accompanied by coagulation. The possibility of disaggregation is neglected. In other words, Smoluchowski proposed the theory of the irreversible coagulation, which corresponds to the case of strong attractive forces. However, the introduction of the notion of long-range surface forces necessitates the generalization of the model of the mutual free diffusion of the particles. At small interparticle distances, the additional flux caused by the particle attraction to each other has to be incorporated in the expression for the particles flux to the reference particle. This important generalization was made by Fuchs [59] with respect to repulsive forces. However, the attractive surface forces can be used in Fuchs expression for particle flux too. Fuchs has not paid attention to another shortcoming in the Smoluchowski model which was noticed by Derjaguin [60].

The particle approach leads to the necessity of a liquid flow out from the gap between them. The thinner the liquid interlayer dividing the particles, the higher the hydrodynamic resistance to its thinning. It leads to the decrease of the coefficient of the particle mutual diffusion. Instead of the constant particle diffusivity in Smoluchowski–Fuchs theory, Derjaguin and Krotova [61] introduced in the Fuchs equation the particle diffusivity which is proportional to h at a small interparticle distance and consequently equals zero at particle contact.

The Einstein equation for interconnection of diffusivity and friction coefficient f,

$$f\mathrm{D} = k\mathrm{T} \tag{1.22}$$

is valid for any interparticle distance. It allows one to obtain the dependence D(h) using the dependence $f(h)$. The asymptotic expression for $f(h)$ at small h is given by Taylor [62] without derivation. The derivation of this linear dependence is given by Derjaguin [60]. The diffusivity decreases to zero at $h \to 0$ and does not lead to the disappearance of particle flux because the attractive surface force causes the opposite influence. However, the neglect of the long-range surface forces leads to an erroneous conclusion about when the coagulation takes place. The elimination of this paradoxical result is the main consequence of the incorporation [61] of the attractive surface forces in the theory of perikinetic coagulation. This phenomenon has been considered in some articles [63,64]. To distinguish this from the analytical result of Derjaguin and Krotova [61], the numerical calculation was used [63,64]. The results obtained in Refs. 63 and 64 are less convenient for application and confirm the original investigation [61].

The collision of droplets of intermediate dimensions are controlled by the joint action of the Brownian movement and sedimentation. In this respect, the Fuchs equation was generalized by Batchelor [65]. The Batchelor equation was used by many investigators and led to noticeable progress in the kinetic theory. Taking this into account, we shall represent the Fuchs equation in the next section in the notation used by Batchelor and his successors.

1.3.3 Brownian Collisions in Emulsions

There are few studies available of the coalescence of fluid drops, presumably because of the more complex interactions which involve fluid flow both inside and outside of the drops. Further, there is a possibility that the drops will deform as they collide. A notable exception is that by Zinchenko [66–68] who has calculated the rate of gravity-induced coalescence of spherical drops of different sizes numerically, using a trajectory analysis for pairs of drops, without considering the effects of interparticle forces. His results confirm that, in contrast to rigid spheres, drop collision is possible at finite rates under the action of a finite external force only. He also showed how the rate of drop collisions decreases with an increasing ratio of the drop fluid viscosity and the surrounding fluid viscosity.

Under conditions of low Reynolds numbers, the relative motion of two spherical drops may be decomposed into motions along and normal to their line of centers. Hetsroni and Haber [69] used the method of reflections to describe the hydrodynamic interaction for widely separated drops in both configurations. More accurate image techniques, which are valid unless the separation distance is small relative to the radius of the smaller drop, have been developed by Fuentes et al. [70,71]. Exact solutions based on bispherical coordinate methods have been developed by Haber et al. [72] and Rushton and Davies [73] for axisymmetric motion along the line of centers, and by Zinchenko [67] for asymmetric motion normal to the line of centers. Each of these solution methods yields an infinite series for the hydrodynamic force between the drops, which diverges when the distance between the drops tends to zero. Because coalescence phenomena depend

critically on the near-contact interaction, these earlier solutions may be matched with the recent lubrication theories of Davis et al. [74]. In these, the nature of the hydrodynamic force resisting the near-contact relative motion of two spherical drops in the direction along their line of centers has been analyzed in detail.

1.3.3.1 Specification of the Fuchs Equation for Emulsions

Zhang and Davis [75] employ the above solutions for the hydrodynamic interactions of two spherical drops and calculate collision rates by extending the previous work by several authors for rigid particles and by Zinchenko [68] for spherical drops. According to Zhang and Davis [75], for creeping flow, the external driving forces on each drop balance the hydrodynamic forces, and the velocity $\mathbf{V}_{12}$ of drop 1 to drop 2 is linearly related to the sum of the external forces and depends only on the relative position of the two drops. An expression for this relative force has been presented by Batchelor [65] for rigid spheres.

Zhang and Davis [75] use Batchelor's expression for $\mathbf{V}_{12}$ and modify it for spherical drops:

$$\mathbf{V}_{12} = -\frac{D_{12}^{(0)}}{kT} G \left(\frac{dU_{12}}{dr} + kT \frac{d \ln p_{12}}{dr} \right) \tag{1.23}$$

where $\mathbf{r}$ is the vector from the center of drop 2 to the center of drop 1. Similarly, the relative diffusivity due to Brownian motion for two widely separated drops is

$$D_{12}^{(0)} = \frac{kT(\hat{\mu} + 1)(1 + \lambda^{-1})}{2\pi\mu(3\hat{\mu} + 2)a_1} \tag{1.24}$$

The pair-distribution function, p_{12}, represents the probability that drop 1 is at position $\mathbf{r}$ relative to drop 2, normalized such that $p_{12} \to 1$ as $r \to \infty$. The interparticle force is described by the potential function $U_{12}(\mathbf{r})$.

The relative mobility function for motion along the line of centers G describes the effects of hydrodynamic interactions between the two drops. The function depends on the size ratio of the two drops

$$\lambda = \frac{a_1}{a_2} \tag{1.25}$$

the viscosity ratio of the drop fluid and the surrounding fluid

$$\hat{\mu} = \frac{\mu_1}{\mu_2} \tag{1.26}$$

and the dimensionless distance between the drops, $s = 2r/(a_1 + a_2)$. It is unchanged when λ is replaced with λ^{-1}.

In the development by Davis et al. [74], the dimensionless lubrication force between two spherical drops in near contact is shown to depend on a single dimensionless parameter,

$$m = \hat{\mu} \left(\frac{a}{h_0} \right)^{1/2} \equiv \frac{a_1 a_2}{a_1 + a_2} \tag{1.27}$$

where $a_1 a_2/(a_1 + a_2)$ is the reduced radius of the two drops and $h_0 = r - (a_1 + a_2)$ is the closest separation between two drop surfaces. This parameter describes the mobility of the

interfaces: When $m \ll 1$, the drops behave as rigid spheres, whereas when $m \gg 1$, the drops have fully mobile interfaces and offer relatively little resistance to the drop relative motion. Note that the interface mobility, m, is not a property of the interfaces themselves but instead represents the viscous resistance of the fluid inside the drops to the flow exerted on their interfaces by the external fluid as it is squeezed out of the gap between the drops. Using this interface mobility, the lubrication forces acting on the drops in the direction along their line of centers can be simply expressed as

$$-F_{1,1} = F_{1,2} = 6\pi\mu a^2 \frac{V_{12}}{h_0} f(m) \tag{1.28}$$

where V_{12} is the component of $\mathbf{V}_{12}$ in the direction along the line of centers and $f(m)$ is a dimensionless function which is approximated by Davis et al. [74] using the following Pade-type expression:

$$f(m) = \frac{1 + 0.402m}{1 + 1.711m + 0.461m^2} \tag{1.29}$$

Note that the lubrication force for drops with mobile interfaces ($m \gg 1$) is inversely proportional to $(h_0/a)^{1/2}$, indicating that spherical drops can come into contact in a finite time under the action of a finite force, in contrast to that for immobile interfaces ($m \ll 1$) for which the lubrication force is inversely proportional to h_0/a. This lubrication force dominates the hydrodynamic resistance unless the droop viscosity is very small [$\hat{\mu} < O(h_0/a)^{1/2}$], in which case the fluid slips out of the gap with little resistance.

When the drops are close to one another ($\zeta \to 0$), the lubrication force dominates the hydrodynamic force and directly balances the external force on each of the drops, that is,

$$G(\xi) = \frac{2 + 3\hat{\mu}}{3 + 3\hat{\mu}} \frac{(1+\lambda)^2}{2\lambda} \frac{\xi}{f(m)} \tag{1.30}$$

1.3.3.2 Expression for the Drop Collision Rate

The rate at which drops of radius a_1 collide with drops of radius a_2 per unit volume is equal to the flux of pairs into the contact surface $r = a_1 + a_2$ and is expressed in terms of the pair-distribution function $p_{12}(\mathbf{r})$ and the drop relative velocity V_{12} by

$$J_{12} = -n_1 n_2 \int_{r=a_1+a_2} p_{12} \mathbf{V}_{12} \mathbf{n}\, dA \tag{1.31}$$

where $\mathbf{n} = \mathbf{r}/r$ is the outward unit normal to the spherical surface represented by $r = a_1 + a_2$, and n_1 and n_2 are the number of drops at the given time in the size categories characterized by radius a_1 and radius a_2, respectively, per unit volume of the dispersion.

For the dilute dispersion, the pair-distribution function is governed by a quasi-steady mass conservation equation for regions of space outside the contact surface:

$$\nabla \bullet (p_{12} \mathbf{V}_{12}) = 0 \tag{1.32}$$

As the colliding drops come into contact, they are assumed to coalesce, and so $p_{12} = 0$ for $r = a_1 + a_2$:

$$p_{12}\,|_{r=a_1+a_2} = 0 \tag{1.33}$$

Provided that all of the drop–drop encounters originate at wide separations in a homogeneous dispersion, the other boundary condition is

$$p_{12} \to 1 \text{ as } r \to \infty \tag{1.34}$$

Due to the spherical symmetry and quasi-steady mass conservation equation, the expression for rate can be simplified:

$$J_{12} = 4\pi r^2 n_1 n_2 p_{12}(\mathbf{r}) V_{12}(\mathbf{r}) \tag{1.35}$$

It does not depend on r. The substitution in it $V_{12}(\mathbf{r})$ according Equation 1.23 yields the linear differential equation of first order where J_{12} is an unknown constant. The integration of this equation and using the boundary conditions for p_{12}, Equations 1.33 and 1.34 yield the equation for the collision rate:

$$J_{12} = 4\pi n_1 n_2 D_{12}^{(0)} \left(\int_{a_1+a_2}^{\infty} \frac{\exp(U_{12}/kT)}{r^2 G} dr \right)^{-1} \tag{1.36}$$

If the drops are assumed to move independently, that is, without any hydrodynamic interactions ($G = 1$) or interparticle forces ($U_{12} = 0$), other than a sticking force on contact, the collision rate is that obtained by Smoluchowski (Equation 1.13). From Equation 1.13, Equation 1.12 for the total number of collisions occurring between particles of types i and j follows. We define the collision efficiency,

$$E_{12} \equiv \frac{J_{12}}{J_{12}^{(0)}} \tag{1.37}$$

as the ratio of the predicted collision rate with hydrodynamic and interparticle interactions to that obtained in their absence. Using the dimensionless center-to-center distance, s, this is then

$$E_{12} = \left(2 \int_2^{\infty} \frac{\exp\left[U_{12}(s)/kT\right]}{s^2 G(s)} ds \right)^{-1} \tag{1.38}$$

Note that the inverse of the collision efficiency is often called the "stability ratio." Of considerable interest is the influence of the viscosity ratio on the collision efficiency. For viscous drops, the relative mobility function G for the near-contact relative motion is inversely proportional to the square root of the distance between the drops when the interface mobility is large. It leads to the integration in Equation 1.38 being finite instead of being infinite as for rigid spheres. Furthermore, because G decreases with increasing viscosity ratio, Equation 1.38 indicates that the collision efficiency will decrease monotonically as the ratio of the drop phase viscosity to the suspending phase viscosity is increased. On the other hand, comparing the effects of the hydrodynamic interactions and interparticle force which are represented by G and U_{12}, respectively, on E_{12} through Equation 1.38, it is seen that the hydrodynamic interactions appear

in a pre-exponential factor and, therefore, are subordinate, for moderate values of A/kT, to the interparticle forces, which appear in the argument of the exponential.

1.3.3.3 Brownian Collisions without Interparticle Forces

Figure 1.2 shows the results for E_{12} as a function of λ for $\hat{\mu} = 0$, 0.1, 1.0, 10, 100, and 1000. As expected, E_{12} decreases as $\hat{\mu}$ increases because this corresponds to decreasing the interface mobility and internal drop flow, which leads to a higher hydrodynamic resistance to the close approach. In the limit as $\hat{\mu} \to \infty$, corresponding to that of rigid spheres, $E_{12} \to 0$, although this limit is approached only slowly.

As λ decreases from unity, E_{12} increases and it tends to unity when λ tends to zero. One reason for this is that when λ decreases, the influence of the smaller drop on the Brownian diffusion of the larger one is decreased. More important is that the contribution of the smaller drop to the relative Brownian diffusivity increases as λ decreases. As $\lambda \to 0$, the hydrodynamic interactions become important only within an increasingly small boundary layer around the larger drop, and so $E_{12} \to 0$ as $\lambda \to 0$.

1.3.3.4 Brownian Collisions with van der Waals Forces

In addition to λ and $\hat{\mu}$, the collision efficiency depends on A/kT. This dimensionless parameter is called the Hamaker group, and it provides a measure of the strength of the van der Waals forces relative to the Brownian motion. Typically, it attains a value of unity or less.

The effects of van der Waals attraction on the collision efficiency of Brownian drops are shown as a function of $A/6kT$ in Figure 1.3 for different viscosity ratios with $\lambda = 1$. As expected, the attractive force increases the collision rate. In fact, the collision efficiency becomes higher than unity for $A \gg 6kT$, but attractive forces of this magnitude are not usually encountered in practice.

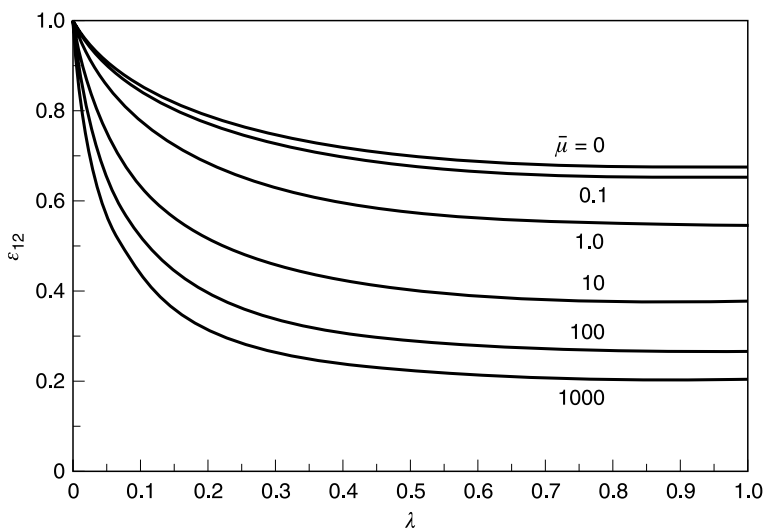

FIGURE 1.2 The collision efficiency for Brownian drops as a function of the size ratio for various viscosity ratios without interparticle forces. (Redrawn from X. Zhang and R.H. Davis, *J. Fluid Mech.* 230: 479 (1991).)

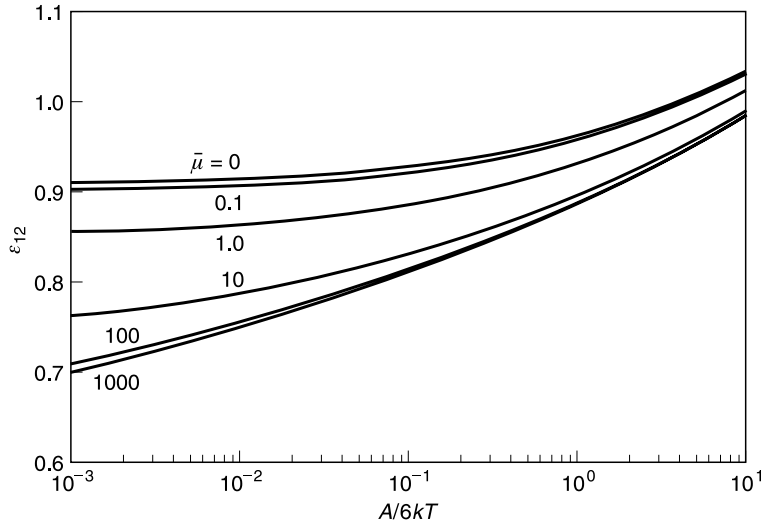

FIGURE 1.3 The collision efficiency for Brownian drops as a function of the Hamaker group for $\lambda = 1.0$ and various ratios with unretarded van der Waals attraction. (Redrawn from X. Zhang and R.H. Davis, *J. Fluid Mech.* 230: 479 (1991).)

Moreover, the van der Waals attraction plays an increasingly important role as μ increases. In particular, the collision efficiency for $\hat{\mu} \gg 1$ is independent of $\hat{\mu}$ at large values of $A/6kT$ but not for small values of $A/6kT$. This is because van der Waals forces are too weak when $A \ll 6kT$ to become important until after the viscous drops have become sufficiently close that the squeeze flow in the gap between them causes their interfaces to become mobile so that the internal flow and viscosity affect the collision process. In contrast, if both $\hat{\mu}$ and $A/6kT$ are large, then the drops are pulled into contact rapidly by the attractive forces they approach within this range and so the interface mobility and internal flow do not affect the process and the drops behave as rigid spheres. In this limit, results [74] agree to within 0.2% with the earlier calculations of Spielman [63], which are shown as filled circles in Figure 1.3 for $\lambda = 1$ and $\hat{\mu} = \infty$.

Numerical results of Zhang [76] for E_{12} with retarded van der Waals attraction show no qualitative change in the effects of the van der Waals attractions on the collision efficiency.

1.3.4 Experiments

The systematic consideration of the experimental investigation is given by Sonntag [77]. The measurements [78,79] confirm the equations for singlet diffusivity and doublet diffusivity in the line of axis and perpendicular to it. In Ref. 77, several techniques are described for the measurement of the coagulation of colloid particles. Some of these give only global information on the state of the aggregation; others give a detailed picture of the particle and floc size distribution. Ideally, the monitoring technique should be suited to on-line application without a sample pretreatment such as dilution. All methods are divided into bulk techniques (turbidity, static light scattering) and single-particle techniques (Coulter counter, flow ultramicroscopy). First, quantitative experiments on rapid coagulation were performed with gold particles by slit ultramicroscopy and individual counting [80–82]. The average value of the coagulation constant of gold particles

was found to be $k_{ij} = 12 \times 10^{-18} \pm 1\ \mathrm{m^3\,s^{-1}}$ at 298 K. These are the only values described in the literature that confirm the theoretical value.

The coagulation of gold particles in different electrolytes was also investigated later with streaming ultramicroscopy with visual counting by Derjaguin and Kudravtseva [83]. For sodium chloride, $k_{ij} = 8.2 \times 10^{-18} \pm 1\ \mathrm{m^3\,s^{-1}}$; for magnesium sulfate, $k_{ij} = 8.9 \times 10^{-18} \pm 1\ \mathrm{m^3\,s^{-1}}$; and for lanthanum nitrate $k_{ij} = 6.5 \times 10^{-18} \pm 1\ \mathrm{m^3\,s^{-1}}$ was obtained. Selenium sols were investigated spectrophotometrically by Watillon et al. [84]. The rapid rate constant was $4 \times 10^{-18} \pm 1\ \mathrm{m^3\,s^{-1}}$.

Silver iodide sols were coagulated with barium nitrate and lanthanum nitrate by Ottewill and Rastogi [85]. The coagulation constants were determined to $8.78 \times 10^{-18} \pm 1$ and $10.2 \times 10^{-18} \pm 1\ \mathrm{m^3\,s^{-1}}$, respectively.

The influence of the particle size on rapid coagulation was investigated with hematite particles by Penners and Koopal [86].

In recent years, many experiments have been carried out using polystyrene lattices because of their monodispersity and their ideal spherical shape. The coagulation rate was lower than the theoretical value, even when the hydrodynamic interaction was taken into consideration.

Sonntag [77] considers two ways to explain this behavior. The first one is the introduction of reversibility into the coagulation process. This was suggested by Frens and Overbeek [51]. Under this assumption the coagulation kernel can remain constant or depend on the aggregate size.

The Smoluchowski treatment is based on the collision of spheres and this assumption is questionable in the case of aggregates. Except when coalescence occurs, aggregates cannot be truly spherical. Two colliding solid spheres must form an aggregate in the form of a dumbbell, and with higher aggregates, many different shapes become possible, as illustrated in Figure 1.4. The collision rates of such aggregates are likely to differ from those for spheres. In particular, the effects of size on the collision radius and the diffusion coefficient cannot be expected to balance each other as for spheres, which led to the very simple, size-independent form of the collision rate constant in Equation 1.16. As the size of an irregular aggregate increases, it is likely that the increase in collision radius more than compensates for the decrease in diffusion coefficient and the results of Cahill et al. [87] tend to support this conclusion. Gedan et al. [88], from their measurements of aggregate size distribution, assigned different rate constants to the various types of collision. For the collision of primary particles, k_{11} was found to be $3 \times 10^{-18} \pm 1\ \mathrm{m^3\,s^{-1}}$. For other collisions, they found $k_{12} \cong 2k_{11}$ and $k_{13}, k_{22}, k_{12}, k_{33} \cong 4k_{11}$. These values show a more pronounced effect of size on collision rate than expected. However, the value found for k_{11} is only about 25% of the Smoluchowski value and there may be some doubt about the accuracy of the value.

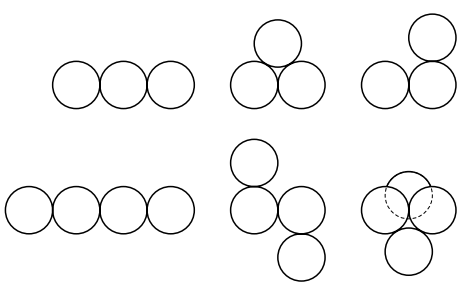

FIGURE 1.4 Possible shapes of aggregates up to four-fold.

1.4 KINETICS OF RAPID GRAVITATIONAL COAGULATION IN THE ABSENCE OF REPULSIVE SURFACE FORCES

1.4.1 Orthokinetic Coagulation and Particle Capture from Flow

The role of Brownian diffusion in the coagulation process decreases with increasing particle size, and other factors begin to dominate. The difference in particle dimension and, therefore, in their sedimentation rate play the determining role in the particle approaching a quiescent media. The "orthokinetic coagulation" term used in the case when a directed motion of particles is favorable for coagulation was initially connected just with this mechanism.

Particles of similar size also approach in a inhomogeneous hydrodynamic field. The term "orthokinetic coagulation" is now more frequently used as applied to coagulation in an inhomogeneous hydrodynamic field. Coagulation in stationary medium is often called the "gravitational coagulation," "gravity-induced coagulation," or "differential settling."

The theory is mainly developed to describe an approach of particles with largely differing dimensions. The coordinate system is related to the larger particle, and the trajectory of the smaller particle is considered in the hydrodynamic field of the larger one. The hydrodynamic field arises at the cost of the motion of the larger particle with respect to the medium, which in the laboratory coordinate system is considered to be stationary. But in the coordinate system related to the particle a liquid flow runs on the latter, which is homogeneous at infinity and carries particles of small size. In this problem, the large particle is called the collector because small particles settling from the flow accumulate in it. Only the relative velocity of the medium and collector is substantial for the settling mechanism.

The situation is fully identical to the following: A liquid comprised of small particles is at rest as a whole (in the laboratory coordinate system) and the collector moves with respect to it, for example, under the effect of gravity, electric, or centrifugal field; the collector rests (in the laboratory coordinate system) and liquid flow is present. It is precisely the setting of the experiment aimed at the study of the elementary orthokinetic coagulation act. Similar to that is the elementary act of particle capture from the flow in filtering with the use of porous media, for example of granular filters. A particle from the flow is settled on individual elements of the filtering medium (on a granule of a granular filter or on fibers of a fibrous filter). Thus, considering the process of particle sedimentation from the flow on collector, we obtain, at the same time, information about the elementary act of orthokinetic coagulation.

Processes controlling the formation of cloud drop spectrum or emulsion drop spectrum are more complex, as it is much more difficult to describe coagulation of drops of almost equal size.

It is natural to first consider the gravitational coagulation of drops strongly differing in size (Sections 1.4.1–1.4.8), which will facilitate the understanding of the more complex process of coagulation of drops of close dimensions (Sections 1.4.9 and 1.4.10).

Investigations of coagulation in aqueous aerosols [16,17,89] at flotation [18,19] and filtration [90,91] were started earlier and have been conducted on a front wider than in the case of emulsions. Therefore, in studying gravitational coagulation in emulsions, one should not ignore the experience accumulated in adjacent scientific leads. In addition, the specific nature of emulsions can be taken into consideration.

The first gravitational coagulation model was proposed by Smoluchowski [4]. The next important step was the investigation by Langmuir and Blodgett [92] in which the role of inertial and hydrodynamic forces was demonstrated apparently for the first time. Then investigations have been conducted mainly applied to aerosols and flotation. A systematic consideration of orthokinetic coagulation was given in Refs. 15 and 91.

1.4.2 Primitive Model of Gravitational Flocculation and its Specification for Emulsions

Particles of different size or density will settle at different rates and the resulting relative motion can cause particle collisions and, hence, flocculation. The first attempts to estimate the rate of gravity-induced coagulation of a dispersion were made by Smoluchowski [4].

The collision frequency can be calculated very simply, assuming that the Stokes or the Hadamard–Rybczynski law [93,94] applies and that particle motion is linear up to contact with another particle. The resulting single-particle collision rate was found to be

$$J_{\mathrm{Gr}}^{0} = \pi (u_{02} - u_{01})(a_1 + a_{02})^2 n_1 \tag{1.39}$$

where u_{01} is Stokes creaming velocity for particles of radius a_1. Because all resistances are ignored in this analysis, the Smoluchowski flocculation rate provides a useful scale on which other flocculation rates can be compared. The ratio of Smoluchowski flocculation rate to the actual flocculation rate in a system undergoing gravity-induced flocculation, G_{Gr}, is known as the stability ratio,

$$W_{\mathrm{Gr}} = \frac{J_{\mathrm{Gr}}^{0}}{J_{\mathrm{Gr}}} \tag{1.40}$$

The gravity-induced capture efficiency is defined as the reciprocal of the stability ratio:

$$E_{\mathrm{Gr}} = \frac{1}{W_{\mathrm{Gr}}} \tag{1.41}$$

Some authors assume erroneously that this first primitive model of gravity-induced coagulation was proposed by Saffman and Turner [95].

Zhang and Davis [75] specified the Smoluchowski model for emulsions, taking into account that the drag coefficient of a drop is described by the Hadamard–Rybczynski equation [93,94].

In distinguishing this from the Stokes equation, the sedimentation velocity of a droplet expressed according to the Hadamard–Rybczynski theory is given by

$$\bar{u}_0 = \frac{2}{3}\frac{\Delta\rho g a^2}{\mu}\frac{1+\hat{\mu}}{2+3\hat{\mu}} \tag{1.42}$$

where g is the gravitational acceleration vector and $\Delta\rho = \rho' - \rho$, where ρ' and ρ are densities of oil and water, respectively. The internal circulation in a drop and the mobility of its surface reduces the media hydrodynamic resistance to a drop movement that causes the increase in its creaming velocity in comparison with a solid sphere. The relative velocity due to gravity for widely separated drops is given by

$$u_{12}^{(0)} = u_0^1(\hat{\mu}) - u_0^2(\mu) = \frac{2(\hat{\mu}+1)\Delta\rho a_1^2(1-\lambda^2)g}{3(3\hat{\mu}+2)\mu} \tag{1.43}$$

It is seen that when $\hat{\mu} \to \infty$, Equation 1.42 transforms into the equation for the Stokes settling velocity, and when $\hat{\mu} \ll 1$, the settling velocity increases 3/2 times.

In Ref. 96, the experimental data concerning the droplet settling velocity are analyzed. Some experimental data confirm the Stokes equation, whereas others are in agreement with the Hadamard–Rybczynski theory. The systematic experimental theoretical investigations of Frumkin and Levich described in Ref. 97 proved that the transition from the Hadamard–Rybczynski regime to Stokesian behavior of a droplet occurs due to the retardation coefficient χ_r. The Hadamard–Rybczynski equation (1.42) was generalized by Levich and Frumkin by incorporation of the retardation coefficient χ_r:

$$u_0(\hat{\mu}) = \frac{2}{3}\frac{\Delta g a^2}{\mu}\frac{\mu + \mu' + \chi_r}{2\mu + 3\mu' + 3\chi_r} \tag{1.44}$$

where

$$\chi_r = \frac{2}{3}\frac{RT}{D_i}\frac{\Gamma_0^2}{c_0} \tag{1.45}$$

D_i is a surfactant molecule diffusion coefficient and c_0 and Γ_0 are its bulk and surface equilibrium concentration, respectively.

At a very low surfactant concentration, χ_r is small and Equation 1.44 transforms into the Hadamard–Rybczynski equation (1.42). The surfactant concentration growth leads to the surface retardation and the decrease of settling velocity. For $\chi_r \to \infty$, Equation 1.44 transforms into the Stokes equation.

The different equations for χ_r corresponding to the different types of the adsorption kinetics are given in Refs. 96 and 98. The level of impurities in water and their adsorption usually is sufficiently high to cause a strong or even complete retardation of droplet surface mobility in emulsions. The larger the droplet, the lower the retardation. The surface movement is possible for sufficiently large drops and by the special purification of water and oil. Thus, at $\mathrm{Re} \ll 1$, the deviation from the Stokesian drag coefficient is weak even under special experimental conditions. At the same dimension of a drop and a bubble the gravity force and correspondingly the viscous stresses which cause the surface movement are weaker in emulsions than in foams. Thus, neglecting the droplet surface mobility in the differential settling in emulsions is justified even in higher degrees than for bubbles in foam.

One underlying restriction is that the flow in and around the drops is sufficiently slow that inertia is small relative to viscous forces. This requires that the Reynolds number

$$\mathrm{Re} = \frac{\rho \mu_0 a_2}{\mu} \tag{1.46}$$

is small compared to unity for all phases, where a_2 is the larger drop radius and μ_0 is its sedimentation velocity. Typical conditions are $\mu = 0.01\ \mathrm{g\,cm^{-1}\,s^{-1}}$, $\rho = 1\ \mathrm{g\,cm^{-3}}$, $\Delta\rho = 0.1\ \mathrm{g\,cm^{-3}}$, and $g = 10^3\ \mathrm{cm\,s^{-2}}$; this requires that $a_2 < 50\ \mu\mathrm{m}$.

As seen from Equations 1.44 and 1.46, Re is proportional to a_2^3. It means that condition 1.46 is strongly violated for $a_2 > 50\ \mu\mathrm{m}$. In addition, the experimental investigations of the collision efficiency are simplified for large drops.

The droplet velocity in centrifugal field can increase up to hundred times, which leads to a similar growth of Reynolds number. Meanwhile, the ultracentrifugation is important in the investigations of emulsion stability [99–101]. Hence, the case $\mathrm{Re} \gg 1$ becomes interesting as well. For this condition, the empirical dependence of the settling velocity on the radius of a

solid particle or a droplet with the retarded surface is known. It follows from the expression for the resistance coefficient for the spherical particle which is a function of the Reynolds number [102,103].

The relative motion of different sized particles can be induced in other ways. In this respect, one important method is the acoustic method, in which ultrasonic waves induce vibrations of suspended particles. The smaller particles are better able to respond to the inducing frequency and to vibrate with greater amplitude than larger particles, facilitating collisions between particles of different size [104].

1.4.3 Long-Range and Short-Range Hydrodynamic Interaction

The process when two droplets of different size approach each other undergoes qualitative changes as the distance between their surfaces diminishes. At larger distances, this process is determined by two parameters: forces of inertia and the long-range hydrodynamic interaction (LRHI).

A sufficiently large drop moves linearly under the effect of the forces of interia until it collides with the bigger one, which takes place if the target distance $b < a_2 + a_1$ (Figure 1.5), where R is the radius of the bubble.

The liquid flow envelops the surface of the big drop, and the small drops are entrained to a greater or a lesser extent by the liquid. The smaller the drops and their difference in density relative to the medium, the weaker the inertial forces acting on them and the more closely the

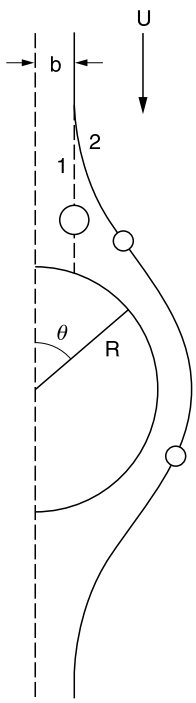

FIGURE 1.5 The influence of the inertia of particles on their trajectory in the vicinity of the floating bubble. Trajectories of the great (inertial) (line 1) and the small (inertia-free) (line 2) particles at the same target distance b.

drop trajectory coincides with the liquid streamlines. Thus, at the same target distance, fairly large drops move almost linearly (Figure 1.5, line 1), whereas fairly small drops move essentially along the corresponding liquid flow line (line 2). The trajectories of drops of intermediate size are distributed within lines 1 and 2; as the size of drops decreases, the trajectories shift from line 1 to line 2 and the probability of collision thus decreases.

The deviation of trajectory of small droplets from the rectilinear path to the surface of the biggest drop at distances of the same order as the biggest drop is caused by LRHI. The biggest drop causes a curving of liquid streamlines and thereby bends the trajectory of small drops (i.e., acts on them hydrodynamically due to the liquid velocity field). In the case of large drops, the forces of inertia considerably exceed the LRHI which is, therefore, not clearly manifested. In the case of small drops, the forces of inertia are small compared with the LRHI.

Thus, the process of the approach of large drops to the biggest drop is ensured by forces of inertia, whereas in the case of small drops, this process occurs in an inertia-free manner and is strongly hindered by the LRHI [105,106].

In addition, the hydrodynamic interaction at distances comparable to the drop radius has to be taken into account; the latter causes the drop's trajectory to deviate from the liquid flow line and should naturally be called the short-range hydrodynamic interaction (SRHI). Using Taylor's solution of the hydrodynamic problem involving the squeezing out of liquid from the gap as spherical particles approach the flat surface, Derjaguin and Dukhin [106] have shown that the SRHI may prevent drops from coming into contact.

The process of the approach of particles to the bubble surface can be described quantitatively by taking into account both LRHI and the SRHI. One introduces a dimensionless parameter of the collision efficiency,

$$E = \frac{b^2}{a^2} \tag{1.47}$$

where b is the maximum radius of the cylinder of flow around the bigger drop encompassing all particles deposited on the small droplets surface (Figure 1.6). The particles moving along the streamline at a target distance b are deposited on the surface of a bigger drop (Figure 1.6, as indicated by a dashed line). Otherwise the particle is carried off by the flow. From Figure 1.6 it is evident that the calculation is essentially reduced to the so-called "limiting (grazing) trajectory" (continuous curve) and, correspondingly, the target distance.

According to Taylor, at a gap thickness h, which is much smaller than a_1, the hydrodynamic resistance of the film to the thinning process is

$$F_h = \frac{u(h)\mu a_1^2}{h} \tag{1.48}$$

where $u(h)$ is the velocity at which the drops approach a certain surface area of the biggest drop, which may be considered to be flat because $a_2 \gg a_1$. If a constant force F_h is applied to the smaller drop, then according to Equation 1.48,

$$u(h) \equiv \frac{dh}{dt} = \frac{F_h h}{a_1^2 \mu}$$

It may be inferred that complete removal of the liquid from the gap requires an infinitely long time:

$$t \sim -\int_h \frac{\mu a_1^2 dy}{F_h y} \sim -\frac{a_1^2 \mu}{F_h} \ln y\,|_h \to \infty$$

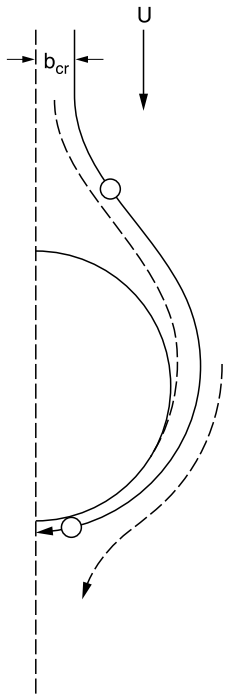

FIGURE 1.6 Continuous line illustrating the concept of the limiting trajectory of particles. Dashed line indicates the trajectories of the particle at $b < b_{cr}$ and $b > b_{cr}$.

In the area above the equatorial plane, the liquid flow lines approach the surface of the biggest drop, which means that the radial component of the liquid velocity is directed toward the surface of the biggest drop. Because the motion of the particle toward the surface is obstructed within the zone of the SRHI, the radial velocity of the liquid is higher than that of the small drop. Thus, at a small gap thickness where the viscous resistance is high, the radial velocity of the liquid will be even higher. The radial flow of liquid envelops the small drop whose approach to the biggest drop has been retarded and presses it against the latter. As a first approximation, this hydrodynamic force can be estimated from the Stokes formula by substituting into it the radius of the small drop and the difference in the local values between the velocity of the liquid and that of the small droplet.

1.4.4 The Effect of Droplet Inertia

In order to understand the mechanism of inertial deposition of smaller drops on the biggest drop, one must introduce the notion of the particle inertial path, l. The latter is defined as the distance the particle with an initial velocity u_0 is able to cover in the presence of the viscous resistance of the liquid due to the initial velocity

$$l = \frac{2}{9}\frac{u_0 a_1^2 \rho'}{\mu} \tag{1.49}$$

This result follows from the linear differential equation of the particle hydrodynamic relaxation which consists of two terms. The first term describes the inertial force and the second one the hydrodynamic resistance.

Because the drop surface is impermeable to liquid, the normal component of the liquid velocity on the surface is zero. As the distance from the drop surface increases, the normal component of the liquid velocity also increases. The thickness of the liquid layer, in which the normal component of the liquid velocity decreases because of the effect of the drop, is of the order of a_2. The particle traverses this liquid layer due to the inertial path whereby the deposition of a smaller drop depends on the dimensionless parameter:

$$\tilde{l} = \frac{l}{a_2} \tag{1.50}$$

When $\tilde{l} > 1$, deposition is obviously possible; yet, calculations have shown that it can also take place at $\tilde{l} < 1$ as long as this value is not too small. This conclusion becomes apparent if it is considered that in a layer of thickness a_2, the smaller drop moves toward the surface not only due to inertia but also together with the liquid of the biggest drop. The motion component of the latter normal to the surface of the biggest drop becomes zero at its surface. Inertial depositions prove to be impossible if $\tilde{l}$ is smaller than some critical value $\tilde{l}_{cr}$. Neglecting the size of the smaller drop, Levin [107] obtained

$$\tilde{l}_{cr} = \frac{1}{24} \tag{1.51}$$

This is taken into account in the equation describing the hydrodynamic relaxation in the hydrodynamic field if the biggest droplet. The one-dimensional equation describes the small droplet movement along the symmetry axis crossing the centers of both droplets:

$$\mathrm{St}\frac{d^2x}{dt^2} + \left(\frac{dx}{dt} - u(x)\right) = 0 \tag{1.52}$$

where the Stokes number $\mathrm{St} = \tilde{l}$ characterizes the ratio of inertial and viscous forces when the Stokes mobility is valid for smaller droplets. It means its Reynolds number is less than 1. x is the distance to the surface of biggest droplet and $u(x)$ is the liquid velocity distribution along the symmetry axis. It is described by the Stokes equation for the hydrodynamic field if the Reynolds number for the biggest droplet is less than 1 also. The characteristic equation $\mathrm{St}m^2 + m + 2 = 0$ has one real (negative) root and separation between the droplet surface decreases exponentially with time. However, the (point) particle never reaches the surface because the particle velocity and fluid velocity coincide. This conclusion holds for nonzero St values if St is smaller than a critical value,

$$\mathrm{St} < \mathrm{St}_{cr} \tag{1.53}$$

Considerable attention was paid to the calculation of St_{cr}. The numerical calculations of Natanson [108] are in good agreement with the original Langmuir data [92] for E. Later, the general solution of the problem for St_{cr} was given by Levin [107] who derived the equation for St_{cr} for any hydrodynamic field. It is important because condition 1.53 is often violated for the biggest drop.

The dependence $E(\mathrm{St})$ can be obtained by the solution of a set of two differential equations for two components of particle velocity. The results of the numerical calculation of Fonda and Herne [109] for the potential and the Stokes flow are given in Ref. 110. These results and the analytical results of Natanson [108] and Levine [107] are in good agreement [89].

The differential equation (1.53) describes the movement of a spherical particle center. Inertial deposition proves to be possible even at $\mathrm{St} < \mathrm{St}_{cr}$ if it is considered that at a distance equal to $a_1 + a_2$ between the smaller droplet center and the biggest droplet surface, the surfaces touch each other.

The possibility of the inertialess collision due to interception and the importance of the particle dimension was proved by Sutherland [105]. During some decades, there was no coupling between two directions in the theory of the collision efficiency. At $\mathrm{St} < \mathrm{St}_{cr}$, the collision efficiency was considered to be caused by the interception. The inertial forces were neglected and the dimension of a particle was important. At $\mathrm{St} > \mathrm{St}_{cr}$, the inertial forces were taken into account. However, the role of a particle dimension was neglected. These simplifications can be verified at extreme cases of

$$\mathrm{St} \ll \mathrm{St}_{cr} \text{ and } \mathrm{St} \gg \mathrm{St}_{cr} \tag{1.54}$$

In Ref. 111, it is emphasized that in the intermediate range of Stokes values [i.e., at the violation of conditions 1.54], both the interception mechanism and inertial forces are important.

Condition 1.46 is violated at the conditions which are necessary for the manifestation of inertial forces. It is violated even at smaller droplet dimensions when the inertial forces can be neglected. Thus, the extension of the droplet range in the theory of the collision efficiency can be achieved by the refusal of condition 1.46. The next and more difficult task is the incorporation of inertial forces in the theory of macroemulsions. The inertialess collision at the intermediate Reynolds number will be considered in the next section. Some additional remarks concerning the inertial collision in emulsion will be given in Section 1.4.6.

1.4.5 Collision Efficiency Caused by Long-Range Hydrodynamic Interaction

1.4.5.1 The Grazing Trajectory Method

Collision efficiency calculations were presented for the first time in Ref. 105. They were based on the consideration of liquid streamlines and of the finite size of spherical particles. Functions characterizing liquid streamline are related to the velocity field by well-known differential relations, and in the Stokes case

$$\Psi = a_2^2 U \left(\frac{1}{2}\rho^2 + \frac{1}{4}\rho^{-1} \right) \sin^2 \theta \tag{1.55}$$

where ρ denotes the radial position scaled on a_2 and θ denotes the angle from the front stagnation point. As can be seen from Equation 1.55, streamline $\rho(\theta)$ is symmetrical with respect to equatorial plane of bubble: $\theta = \pi/2$. This means that the droplet moving along the liquid streamline approaches the drop surface most closely at $\theta = \pi/2$. Because the center of a droplet moves along the liquid streamline, it will touch the surface of bigger drops only in the case when the distance between the streamline and the droplet is equal to the droplet radius. According to Ref. 105, liquid streamline passing through a point with coordinates

$$r = a_2 + a_1 \text{ and } \theta = \frac{\pi}{2} \tag{1.56}$$

represents the limiting trajectory of the droplet ($\Delta\rho = 0$). Under conditions 1.56, the droplet touches the drop. But if we increase the tangent distance, then even the nearest distance between the streamline and the drop surface ($\theta = \pi/2$) proves to be larger than the droplet radius. By substituting values of r and θ according to Equations 1.56 into Equation 1.55, Ψ_c which characterizes grazing streamline giving the basis for the collision efficiency E_{0c} can be determined:

$$\lim_{\rho\to\infty}(\rho^2\sin^2\theta) = \frac{1}{a_2^2}\lim_{r\to\infty}(r^2\sin^2\theta) = \frac{b^2}{a_2^2} = E_{0c} = \Psi_p$$

After substitution of the expression for Ψ_p in which at $a_1/a_2 \ll 1$, only the term linear in small parameters is considered, we obtain

$$E_{0s} = \frac{3}{2}\frac{a_1^2}{a_2^2} \tag{1.57}$$

We introduced the subscript zero to denote that SHRI and surface forces are not taken into account. According to it, when the size of particles decreases, LRHI retards coagulation kinetics by a factor hundreds and even thousands.

1.4.5.2 Equation for the Smaller Drop Flux on the Surface of a Larger Drop

In the case of non-inertia collisions and without regard for SHRI, the velocity of a smaller drop is well known at any distance from the bigger one:

$$\mathbf{u} = \mathbf{u}(r,\theta) + \mathbf{u}_g \tag{1.58}$$

so that it is advisable to derive an expression for the radial component of smaller drop flux density

$$J_r = n(r,\theta)u_r \tag{1.59}$$

where $n(r, \theta)$ is the smaller drop number concentration next to the surface of a bigger drop. Integrating the flux density over that part of the surface on which sedimentation takes place, we obtain the number of smaller drops colliding with the bigger one in unit time N, which relates to E_0 as

$$N = 4\pi a_2^2 E_0 u_0 \tag{1.60}$$

Earlier [112], a theorem was proven that the particle concentration remains constant if the velocity field is solenoidal. From this, it follows that

$$E_0 = \frac{1}{\pi a_1^2 u_0 n_1}\int_0^{\theta_c} n_1(u_r + u_g)2\pi a_1^2\sin\theta d\theta \tag{1.61}$$

where θ_c characterizes the boundary of the region of deposition of smaller drops at the surface of the bigger drop. To consider the effect of a finite size of a smaller drop, integration over a

concentric sphere of radius $a_1 + a_2$ has to be performed. From this condition, θ_c can be derived:

$$u_r(a_1 + a_2, \theta_c) = 0 \tag{1.62}$$

Substituting the Stokes velocity field into Equation 1.61 and using Equation 1.44 at $\hat{\mu} \to \infty$, we obtain [112]

$$E_{0s} = \frac{3}{2}\left(\frac{a_1}{a_2}\right)^2 - \frac{\Delta\rho}{\rho}\left(\frac{a_1}{a_2}\right)^2 \tag{1.63}$$

This method of calculation was provided almost a quarter of a century later by Weber [113], who, probably, was not aware of the work of Dukhin and Derjaguin [112]. The usefulness of the method was well demonstrated, although the discussion was restricted by the consideration of systems in which the particle density differs only slightly from water density and allows one to ignore the role of sedimentation. A more general approach was demonstrated in the recent work of Nguen Van and Kmet [114].

It is important that Equation 1.61 is applicable not only under Stokes and potential flow but also at any solenoidal hydrodynamic field, which ensures its wide application.

1.4.5.3 Long-Range Hydrodynamic Interaction at Intermediate Reynolds Numbers

The important equation (1.63) is valid for condition 1.46. At higher Reynolds numbers, the hydrodynamic flow pattern around a drop changes and causes the change in the equation for collision efficiency. Flow conditions representative of very high Reynolds numbers can be approximated by the potential flow. It is not valid in the surface vicinity within the so-called hydrodynamic boundary layer. This case of very high Reynolds numbers will not be considered here because it corresponds to very big drop dimensions and the deviation of shape from sphericity.

The hydrodynamic at intermediate Reynolds numbers with respect to spherical particles is considered in Ref. 115. There is a large qualitative distinction in flow pattern around a drop, depending on the ratio $\hat{\mu}$. If an oil viscosity strongly exceeds water viscosity, the flow pattern is similar to that of a solid sphere.

According to experimental investigations and numerical solutions (cf. Clift et al. [115]) qualitatively different hydrodynamic regimes exist at different Reynolds numbers. At $7 < \mathrm{Re} < 20$, a so-called unseparated flow is observed. Flow separation is indicated by a change in the sign of the vorticity and first occurs at the rear stagnation point, approximately at $\mathrm{Re} = 20$.

If Re increases beyond 20, the separation ring moves forward so that the attached recirculation wake widens and lengthens. A steady wake region appears at 20. The onset of wake instability corresponds to separation angle

$$Q_s = 180 - 42.5(\ln \mathrm{Re}/20)^{0.48}$$

To generalize Equation 1.63, the theories of flow pattern around the bubble at intermediate Re can be used [114,116,117].

If an oil viscosity is less than water viscosity, the theory in Ref. 118 predicts the disappearance of flow separation. For this case, the solution of the Navier–Stokes equation can be accomplished according to numerical methods only [119].

Investigations of droplet collisions in emulsions at intermediate Reynolds numbers seem to be lacking. However, the emulsion specificity disappears in the presence of even traces of a

surfactant with respect to long-range hydrodynamic interactions. This statement cannot be valid with respect to short-range hydrodynamic interaction, which will be discussed in the next section.

1.4.5.3.1 Complete Surface Retardation

As discussed in Section 1.4.1, a droplet surface can be substantially retarded even in distilled water due to the presence of surfactants. Weber and Paddock [120] applied a curve-fitting technique to the numerical solutions of the Navier–Stokes equations obtained by Masliyah [121] and Woo [122] and derived the expression for the interceptional collision efficiency:

$$E_0 = \frac{3}{2}\lambda^2 \left(1 + \frac{(3/16)\mathrm{Re}}{1 + 0.25\mathrm{Re}^{0.56}}\right) \tag{1.64}$$

Yoon and Luttrel [116] empirically developed an analytical expression for the streamline function at intermediate Reynolds number by combination of the stream function for creeping and potential flow regimes and derived the equation for the interceptional collision efficiency. As can be seen from Figure 1.4 of their article [116], the difference of their results from Equation 1.64 is small.

The complete Navier–Stokes equation was solved numerically again by Nguen Van and Kmet [114] who obtained the interceptional collision efficiency. Its first term coincides with Equation 1.64; the second one characterizes the particle sedimentation on the bubble surface. It is important in the condition of mineral flotation and can be neglected in emulsions. Thus, the theoretical results of Refs. 114 and 116 do not contradict Equation 1.64.

1.4.5.3.2 Incomplete Surface Retardation

The term "emulsion" usually relates to the dispersion with drops less than 100 μm in diameter. At these dimensions, the droplet surface mobility is retarded completely or very strongly by the traces of surfactants. At strong retardation, a small residual surface mobility is possible. However, under some special conditions, the participation of the droplet of bigger dimensions in collisions can be of interest. In this extreme case, the interceptional collision efficiency can be described by means of the theory [123] elaborated for the description of the flotation kinetics at intermediate Reynolds number and unretarded bubble surface. As surface retardation decreases, both the tangential liquid velocity and its normal component at the distance of order a_1 from the surface increased. Thus, the smaller drop flux increases, and this increase can be described by the Sutherland equation as the surface retardation decreases. Thus, the interceptional collision efficiency for free surface E_{0c} is less sensitive to the small value of the radius ratio λ than that for immobile surface E_{0r}. For the intermediate Reynolds number, Rulyov and Leshchov [123] used Hamieloe theory [124] and obtained

$$E_{0c} \sim \frac{a_1}{a_2^{0.9}}, E_{0r} \sim \frac{a_1^2}{a_2^{1.8}} \tag{1.65}$$

For small values of the radius ratio surface retardation reduces the interceptional efficiency by magnitudes of hundred or thousand. Experimental investigation is easier for big drops and the discussed theory [123] can be useful for this purpose.

1.4.5.3.3 Experiments

Experimental investigations of the droplet collisions in emulsions at intermediate Reynolds numbers are not reported. However, some information can be extracted from the experiments

accomplished for the investigation of particle collisions with a small bubble at an intermediate Reynolds number. In experiments [114], a single bubble is generated and captured on a needle. Afterwards, the small particles' trajectories in the vicinity of the captive bubble were observed and the grazing trajectory was determined. In these experiments [114], the size of a captive bubble was in the range 0.5 to 2 mm, the Reynolds number in the range 30 to 300, and the particle size in the range 10 to 35 μm. In other experiments [116], the bubble size was in range 100 to 500 μm and the particle size in the range 1 to 40 μm. The experiments [114,116] confirmed the theoretical prediction of collision efficiency dependence on particle and bubble dimensions.

In these experiments, the influence of solid-particle sedimentation on the bubble surface predominated due to the large difference of densities of solid particles and water. It means that the manifestation of a second component of the particle transport to the bubble surface, caused by the normal component of liquid velocity, was weak. Thus, the exactness of the verification of the theory of the convective transport in these experiments was low. Meanwhile, the convective transport predominates in emulsions due to small differences in densities of water and oil.

Thus, Equation 1.64 can be used for the description of the interceptional collision efficiency in emulsions to a first approximation. However, the exactness of its experimental verification with respect to emulsions is limited.

The experimental methods and the experimental installations, described in Ref. 114, can be applied for the experimental investigations of the collision efficiency in emulsions. It is sufficient to replace the captive bubble by a big captive oil drop.

If a particle shape is isometric, its behavior in the long-range hydrodynamic interaction is similar to the spherical particle with the same dimension. However, their behavior in short-range hydrodynamic interaction will be different. The drainage in the gap between a bubble (drop) and particle (small drop) is very sensitive to the microrelief on the surface. The resistance to thinning of the interfacial film can be drastically reduced if the angles between the facets are sufficiently sharp so that "intrusion" of the interface film by a sharpened section of a particle surface may take place. Anfruns and Kitchener [125] determined the efficiency of the accumulation of glass spheres and broken quartz particles and established that the manifestation of SRHI is weakened in the case of quartz particles.

Thus, the discrimination between LRHI and SRHI contributes to measured particle accumulation by a big bubble (drop) is possible. The broken particle accumulation yields information concerning LRHI. The decrease of small droplet accumulation yields information concerning SRHI. The exactness of this procedure can be decreased if SRHI preserves in some degree for the broken particle also.

1.4.6 Flocculation in a Centrifugal Field and Dynamic Adsorption Layer

Centrifugal fields are used for demulsification [126] and in the investigation of emulsion stability [99,100]. The increase of a droplet velocity in a centrifugal field (for example, 100-fold) led to the corresponding increase of Reynolds and Stokes numbers. Thus, the movement of not very small droplets in the centrifugal field occurs in the intermediate range of Reynolds number (Section 1.4.5.3) and their flocculation can be complicated by the action of the inertial force (Section 1.4.4).

Larger drop velocities create stronger viscous stresses in the vicinity of its surface. Thus, the residual surface mobility increases as the Reynolds number increases and has to be taken into account in the theory of orthokinetic coagulation. Probably this question was not considered with respect to drops. Thus, the experience of the flotation theory can be used [18,19].

Steady-state motion of a drop induces adsorption–desorption exchange with the subsurface, with the amount of substance adsorbed on one part of its surface being equal to the amount desorbed from another part. Obviously, the surface concentration is lower on the part where adsorption takes place and it is higher on the part where desorption occurs. Thus, surface concentration varies along the surface of a moving drop, taking a maximum value at the rear pole and a minimum one at the front pole [97]. The adsorption difference between the poles of a drop causes the surface tension drop and Marangoni–Gibbs phenomena; that is, the surface movement in the direction of the surface tension decreases. This secondary surface flow is directed opposite to the primary surface and flow; consequently, the surface velocity retards.

Therefore, the state of adsorption layer on a moving drop surface is qualitatively different from that on a resting one. Such an adsorption layer was called a dynamic adsorption layer [127].

With respect to the large Reynolds numbers, the retardation coefficient can be evaluated at the strong surface retardation by using the concept of the hydrodynamic and diffusion layers [97,127] having a thickness δ_G and δ_D, respectively, independent of angle θ. It follows from the boundary condition expressing the interconnection between adsorption–desorption flux and the surface divergence of the surface convective flux of the adsorbates [127]

$$\chi_b = \frac{RT\Gamma_0^2}{Dc_0}\frac{\delta_D}{a}\frac{\delta_G}{a} = \frac{RT\Gamma_0^2}{Dc_0}\frac{D}{\nu \mathrm{Re}} \tag{1.66}$$

because

$$\frac{\delta_c}{a} \sim Re^{-1/2}, \frac{\delta_\delta}{a} \sim \mathrm{Pe}^{-1/2} \tag{1.67}$$

and the Peclet number $\mathrm{Pe} = \dfrac{ua}{D}$,

$$\mathrm{Pe} = \frac{\nu}{D}\mathrm{Re} \tag{1.68}$$

Comparing Equations 1.66 and 1.45, one concludes that the decrease of the retardation coefficient is

$$\frac{\chi_B|_{\mathrm{Re}\gg 1}}{\chi_B|_{\mathrm{Re}\ll 1}} = \frac{D}{\nu \mathrm{Re}} \tag{1.69}$$

Taking into account that $\nu/D \sim 10^3$, one concludes that the transition from a small Reynolds number to a larger one is accompanied by a reduction in the retardation coefficient by a factor of 10^4–10^5. Thus, for big drops or under the action of centrifugal force, the state of the mobile surface is possible even at noticeable surfactant concentrations.

The dynamic state of the adsorption layer causes the change in all stages of the flocculation. It influences the degree of the drop surface retardation, its velocity and the relative velocity for two widely separated drops, the hydrodynamic velocity distribution around a drop, and, consequently, the LRHI. It modifies surface forces because they depend on the surface concentration. Thus, it is important at the last stage of flocculation too.

1.4.7 Incorporation of Short-Range Hydrodynamic Interaction and Attractive Surface Forces in the Theory of Inertialess Collision

In the process involving an inertialess approach of a smaller drop to a bigger one, the size of the latter plays an important role. It is in the equatorial plane that the closest approach of a streamline of the surface of a bigger drop is attained. In Figure 1.7, the broken line (curve 1) represents the liquid streamline whose distance from the surface of the bigger drop in the equatorial plane is equal to the radius of the smaller drop. Some authors erroneously believe that this liquid streamline is limiting for the drops of that radius. The error consists in that the SRHI is disregarded in this case. Under the influence of the SRHI, the drop is displaced from liquid streamline 1 so that its trajectory (curve 2) in the equatorial plane is shifted from the surface by a separation larger than its radius. Therefore, no contact with the surface occurs and, correspondingly, $b(a_1)$ is not a critical target distance.

Due to the SRHI, the distance from the smaller drop to the surface in the equatorial plane is larger than the distance from the surface to the liquid streamline with which the trajectory of the smaller drop coincides at large distances from the bigger drop. It may thus be concluded that $b_{cr} < b(a_1)$. The limiting liquid streamline (curve 3) is characterized by the drop trajectory (curve 4),

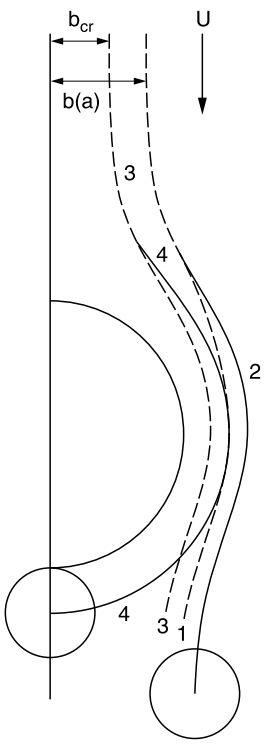

FIGURE 1.7 The influence of the finite dimension of particles in the inertial-free flotation on their trajectory in the vicinity of the floating bubble. The liquid flow lines corresponding to target distances $b(a)$ and b_{cr} are indicated by dashed lines. The continuous lines are characteristic for the deviation of the trajectory of particles from the liquid flow lines under the influence of short-range hydrodynamic interaction.

which, branching off under the influence of the SRHI, runs in the equatorial plane at a distance a_1 from the surface of the bigger drop.

The value of b_{cr} decreases, first due to the deflection of the liquid streamlines under the influence of the LRHI and, second, due to the deflection of the small drop trajectory from the liquid streamline under the influence of SRHI. Therefore, the collision efficiency is expressed as the product of two factors, E_0 and f, both smaller than unity. The first one represents the influence of the LRHI and the second, the influence of the SRHI.

It is evident that SRHI, like LRHI, manifests itself in the gravitational coagulation of drops, solid particles of suspensions, bubbles, and in their sedimentation from a flow on large-size surfaces, with the SRHI mechanism being common in these systems. In essence, identical SRHI theories are created as applied to flotation, aerosols, and suspension purification from particles by filtration. Only lately has the problem received further development as applied to emulsions [26,27].

The mechanism of SRHI is the same under conditions of perikinetic and orthokinetic coagulation. Derjaguin and Dukhin [106] formulated the problem of SRHI as applied to orthokinetic coagulation or, more properly, to the elementary act of flotation of a small spherical particle by a bubble.

> When the mineral particle comes closer than its own radius to the bubble viscous resistance forces should develop retarding thinning of the intervening layer ... assuming the trajectory of the particle center to be independent of its radius it is easier for a particle of larger radius to contact the bubble surface. It can be easily shown that it is impossible to predict the outcome of the competition between two opposite effects without considering the forces of interaction between particle and bubble surfaces. When the radius of action of the attraction forces acting in zone 3 is much smaller than the particle radius the influence of viscous deflection of the particle trajectory will always outweigh the other effect and contact ... will not occur [106].

If we replace "bubble" with "a big drop" and "particle" with "small drops" in this quote, then we obtain the statement of the problem of the role of SRHI in emulsions. As can be seen from the quote, the main features of this stage of coagulation process were already clear at that time. When the size of the particle increase, the effect of LRHI on collision efficiency decreases and the negative effect of the SRHI increases. It is shown in the further development of quantitative theory that the effect of particle size prevails of LRHI. Along with this, the remark about flocculation of large particles not taking place even in the presence of attractive forces is not always correct, as seen below.

1.4.7.1 Quantitative Theory of Short-Range Hydrodynamic Interaction Given Attractive Surface Forces

A more general approach to the problem of small-particle deposition from laminar flow on the surface of a big particle (collector) was elaborated by Spielman [128] and Goren [129,130]. They introduce a local coordinate system for the description of a local hydrodynamic field around the small particle and in the interlayer between it and the collector. They presented the equations for the short-range hydrodynamic forces caused by the field. Their results form an important component of the Derjaguin–Dukhin–Rulyov (DDR) theory of SRHI in flotation [19]. The particles move along a bubble surface and the condition for particle–bubble interactions changes (i.e., the short-range interaction is unsteady). However, in the local coordinate system which is bound to the particle and moves with it, the interaction can be considered as a quasi-steady one.

The cylindrical system of coordinates is introduced. Its center is lying on the bubble surface with the z-axis crossing the center of the moving particle.

Cylindrical symmetry in the chosen coordinate system simplifies the description of hydrodynamic interaction. Separate equations for the normal component $u_r = dh/dt$ and tangential component $u_\theta = a_2(d\theta/dt)$ of a particle velocity are written respectively

$$\frac{dh}{dt} = \frac{F_n f_1(h)}{6\pi\mu a_1} \tag{1.70}$$

$$a_2\frac{d\theta}{dt} = u_\theta f_2(h) \tag{1.71}$$

The equations describe the stage of a particle movement when the liquid interlayer is thin and the distance between the centers of a particle and the bubble equal to $a_1 + a_2$.

The rates of interlayer thinning and particle movement to the bubble surface coincide and are determined by the action of pressing force F_n and the resistance source which is characterized by the product of the Stokes drag coefficient and the dimensionless function $f_1(H)$.

The particle trajectory equation follows from the set of Equations 1.70 and 1.71 after the introduction of H instead of h and the time exclusion

$$\frac{dH}{d\theta} = \frac{a_2 F_n(\theta, H) f_1(H)}{6\pi\eta a_1^2 u_\theta(\theta, H) f_2(H)} \tag{1.72}$$

In the general case, the pressing force is a superposition of many forces:

$$F_n = F_A + F_\Psi + F_V + F_g \tag{1.73}$$

where F_A, F_Ψ, F_V, and F_g are the attractive surface force, the repulsive surface forces, the hydrodynamic pressing force, and the gravity force, respectively. The semianalytical solution of Equation 1.72 is possible if the radius of action of surface forces is small in comparison with the particle dimension.

The hydrodynamic pressing force is proportional to the local value of the normal component of the hydrodynamic velocity:

$$F_n = F_H = 6\pi a\eta u_r(H, \theta) f_3(H) \tag{1.74}$$

The function $f_3(H)$ yields its dependence of the film thickness. After the substitution of Equation 1.74 into Equation 1.73, one obtains

$$\frac{dH}{d\theta} = \frac{Ru_r(\theta, H) f_1(H) f_3(H)}{au_\theta(\theta, H) f_2(H)} \tag{1.75}$$

The functions f_1, f_2, and f_3 were determined in the work of Goren [130], Goren and O'Neil [129], Goldman et al. [131], and Spielman and Fitzpatrick [90]. At a distance which is comparable with the dimension (i.e., at $H \geq 1$), a simplification occurs:

$$\frac{f_1 f_2}{f_3} \sim 1 \tag{1.76}$$

It means that at this distance, Equation 1.72 transforms into an equation for the liquid streamline. Consequently, at this distance, the particle trajectory coincides with the specific streamline.

The theory specifies how surfaces of the two models influence the drainage [19].

1. A critical thickness h_{cr} exists. Naturally, there is a correlation between h_{cr} and DL thickness. This is not taken into account and the surface forces action beyond h_{cr} is neglected. In this model, a particle is attached after the film thinning is culminated, satisfying the boundary condition

$$H\left(\frac{\pi}{2}\right) = H_{cr}\left(H_{cr} = \frac{h_{cr}}{a_1}\right) \tag{1.77}$$

   Naturally, a particle is attached when $h(\theta) = h_{cr}$ at any θ. However, condition 1.77 separates the grazing trajectory. The result for creeping flow is

$$f_s = 1.5(1 - 0.3 \ln H_{cr})^{-2} \tag{1.78}$$

2. The notion of h_{cr} is neglected. The attachment is caused due to a predominating attraction [132]. In the case of the first model, neglecting the molecular attractive force we could not consider the particle attachment on the lower surface of a bubble because any particle departs there from the bubble surface under the gravity action. Neglecting h_{cr}, we considered the particle almost on the bubble surface under the action of the predominating attractive force which can exceed the gravity. Thus, the model enables one to consider the particle attachment on the lower surface of a bubble. The grazing trajectory finishes at the rear stagnant pole of the bubble. Due to cylindrical symmetry,

$$\left(\frac{dH}{d\theta}\right)_{\theta=\pi} = 0 \tag{1.79}$$

Comparing condition 1.39 and Equation 1.72, one concludes that the final coordinates of the grazing trajectory satisfy conditions

$$\theta_0 = \pi,\ F_n(\pi, H_0) = 0 \tag{1.80}$$

1.4.7.2 Theory Specification for Different Models

First, the function (1.78) was calculated. At all values under consideration, this function is smaller than unity; it decreases with H_{cr} and becomes zero at $H_{cr} = 0$. This confirms the aforementioned representation of the mechanism based on the influence of the SRHI on the particle deposition process.

As H_{cr} decreases from 10^{-1} to 10^{-3}, f decreases from 0.5 to 0.15; that is, the dependence of f (and of E) on the absolute value of h_{cr} is weak. Thus, the inclusion of the SRHI is important not only in considering the problem of flotation. This effect reduces the number of collisions by several times.

Rulyov [132] has developed the SRHI theory without considering the phenomenological parameter, h_{cr}, by directly taking into account the dependence of molecular forces on h, and obtained

$$E = E_0 f(W), \quad W = \frac{Aa_2^2}{27u_s\pi\mu a_1^4} \tag{1.81}$$

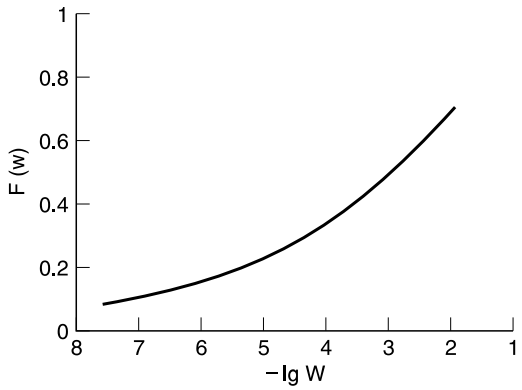

FIGURE 1.8 The multiplier in Equation 1.81 expressing the influence of hydrodynamic and molecular interaction between particle and bubble at inertialess flotation. (After V. Shubin and P. Kekicheff, *J. Colloid Interface Sci.* 155: 108 (1993).)

The function $f(W)$ is plotted in Figure 1.8 and can be approximated [133] to

$$f = 1.2W^{0.15} = \frac{1.2A^{0.15}}{(2\Delta\rho g/9)^{1/6}a_1^{0.7}} \tag{1.82}$$

The first model can be applied to unstable emulsions. The interdroplet lamellae is unstable and its critical thickness is h_{cr}. The second model corresponds to emulsions which are unstable with respect to flocculation and stable with respect to coalescence. The drop doublet forms under the action of attractive molecular forces. However, the coalescence is prevented due to the presence of a stable adsorption layer.

The second model was used by Spielman and Fitzpatric [90,91] who earlier considered the same problem as Rulyov [132]. It is interesting to compare the results of these investigations. The dimensionless number N_A introduced in Ref. 90 differs from W by a factor of 4/3 only. In Ref. 90, the dependence E/E_0 is presented as a function of N_A (Figure 1.9). Taking into account that $E/E_0 = f$, one concludes that the ordinates in Figures 1.8 and 1.9 coincide. Neglecting the difference in abscissas caused by the multiplier 4/3, one concludes that the functions $f(W)$ and $f(N_A)$ practically coincide. In Ref. 90, N_A is called the attraction number. Its physical sense is explained in Ref. 91.

Different velocity and time scales are appropriately close to the particle surface where viscous and colloidal forces become important. The characteristic fluid velocity is smaller [i.e., $O(a_1u_0/a_2)$] due to the proximity of the surface, so the time spent in the neighborhood of collector, the dwell time, is $O(a_2^2/u_0a_1)$. The importance of interparticle attraction is assessed by calculating the time required to capture a particle once it has been moved close to the surface and comparing this to the dwell time. A particle mobility of $O((\mu a_1)^{-1})$ and a dispersion force of A/a (see Section 1.2.1) produce a velocity toward the surface of $O(A/\mu a_1^2)$. Therefore, a representative capture time, the time required to move a distance $O(a_1)$, is $O(\mu a_1^3/A)$. The ratio of the dwell time to the capture time is called the attraction or adhesion number, N_A.

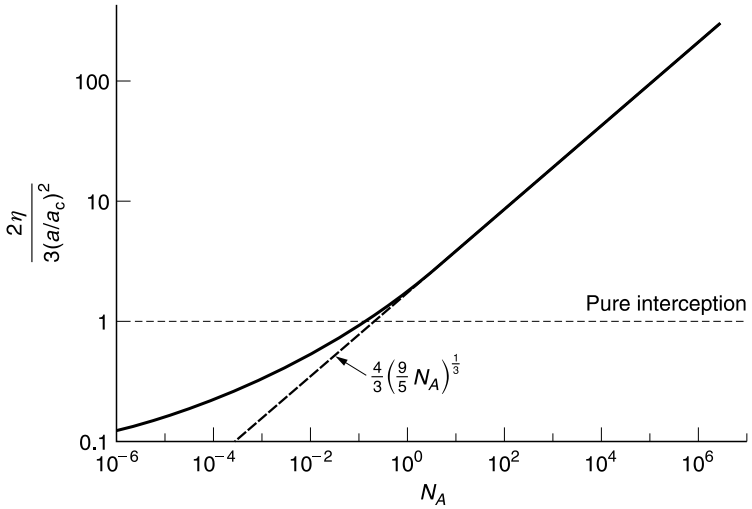

FIGURE 1.9 Capture efficiencies for a spherical collector. Solid line from a numerical solution. (From L.A. Spielman and J.A. Fitzpatrick, *J. Colloid Interface Sci*. 42: 607 (1973).)

As the dwell time exceeds the capture time, that is,

$$N_A > 1, \tag{1.83}$$

the smaller drop moves along the surface of the bigger drop during a sufficiently long time and can be attracted to the surface from a distance of the order of its dimensions. It means that in condition 1.83, the collision efficiency can increase due to attraction forces in comparison with its value caused by the interception. It explains why at condition 1.83, $f > 1$; as can be seen from Figure 1.9, the smaller the N_A, the shorter the distance from the grazing trajectory to the surface of the bigger drop; that is, the smaller the collision efficiency and f.

1.4.7.3 Peculiarities of Gravitational Coagulation at Small Aggregation Numbers

An interesting peculiarity of short-range hydrodynamic interaction is the fact that according to Equation 1.82, it depends to a larger degree on the size of the smaller particle (power 0.7) than on the Hamaker constant (power 1.6). As can be seen from this formula and from Figure 1.8, a decrease in the Hamaker constant is accompanied by a decrease in collision efficiency. But this dependence is very weak; and so, the impression arises that coagulation is possible at any small (but finite) value of the Hamaker constant.

This impression is most likely incorrect. With an increasing size of the smaller drop, the stability of the doublet is attained at the cost of the closest separation between two droplet surfaces, h. In this case, it is assumed that the attractive force infinitely increases. The infinite growth of attractive force with decreasing h cannot be proved due to difficulties in measuring surface forces at very small distances [134].

The initial model of surface forces with an infinitely deep primary energy minimum in DLVO theory was replaced by a model with the potential well of a finite depth in the works by Frens and Overbeek [51] and Martinov and Muller [135]. This has resulted in the abandonment of the notion

of completely irreversible coagulation and in the development of important notions of reversible coagulation. In this context, the paradoxical result can be discussed, which points to the possibility of gravitational coagulation at an arbitrarily small but finite value of the Hamaker constant. Hydration effects and/or structural components of disjoining pressure (Section 1.2.4) which will further restrict the possibility of gravitational coagulation should be taken into consideration in the future.

The mentioned factors restricting gravitational coagulation manifest themselves when we consider conditions 1.73 and 1.80, which in the absence of the repulsive force can take the form

$$\frac{aa_1}{6}h_m^2 = 6\pi\mu a_1\left(4.8V_2\frac{a_a^2}{a_2^2} - V_1\right) = (3.8)6\pi\eta a_1 V_2\frac{a_1^2}{a_2^2} = 2.2\pi\Delta\rho g a_1^3 \tag{1.84}$$

The first term on the right-hand side of the equation is the detaching hydrodynamic force and the second one is the gravity force.

Equations for the absolute values of the detaching force and the pressing force are identical. The normal component of liquid flow has different directions in the vicinity of the leading and rear hemispheres and causes the pressing force on the leading hemisphere and the detaching force on the rear hemisphere. Consequences of Equation 1.84 on emulsions will be discussed in the next section.

1.4.7.4 Estimation of the Size of Emulsion Drops Stable Against Flocculation with Larger Drops

As was pointed out in Section 1.4.7.2, the value of the Hamaker constant in oil–water (o/w) emulsions is approximately known. In the case of emulsion-stabilized surfactants, we obtain the lower bound of h also, i.e., h_m. In this case, h_m exceeds the double thickness of the adsorption layer h_a. Then for the critical radius act of the smaller of the drops it follows from Equation 1.84 that

$$a_{1cr} \leq \left(\frac{A}{2.2\pi\Delta\rho g}\right)^{1/2}(2h_a)^{-2} \tag{1.85}$$

Drops with a radius exceeding a_{1cr} cannot flocculate with drops of a much larger radius, $a_2 \gg a_{1cr}$. Substituting the values $A = (3 \times 10^{-21} \div 10^{-20})$, $\Delta\rho = 0.1\ \mathrm{g\,cm^{-3}}$, $2h_a \cong 2 \times 10^{-7}$ cm into Equation 1.85, we obtain $a_{1cr} \leq 100$ to 300 μm.

It is that h_a can be both larger and smaller than the estimated value when using emulsifiers of different nature. The condition of a small Reynolds number is poorly fulfilled at this value of a_{1cr} and is completely violated for a larger drop with a radius $a_2 \gg a_{1cr}$. This limits the accuracy to estimate according to Equation 1.85. Nevertheless, it is clear that the detaching force cannot prevent gravitational coagulation in emulsions for drops of Stokesian size if additional repulsion forces are absent because of the small value of $\Delta\rho$. In suspensions, $\Delta\rho$ can be 10 to 70 times higher and a_{1cr} can be 3 to 8 times smaller. Thus, the statement [106] cited in Section 1.4.7.1 that molecular attractive forces cannot result in coagulation of particles of a larger size is to some extent confirmed. But at a radius $a_1 < a_{1cr}$ even very small molecular forces provide coagulation which was underestimated in Ref. 106.

1.4.8 Experiments

There is a lack of systematic experimental investigations of coagulation kinetics in emulsions. This drawback can be compensated in some degree by the consideration of the capture efficiency in adhesion experiments with packed beds and in flotation, because the mechanism of the collision is the same.

1.4.8.1 Experiments with Packed Beds

Experiments with beds of solid spheres have been carried out to establish the applicability of theories based on single collector-to-collector arrays where several transport processes operate and the flow field is not known in detail. Here, filter coefficients are measured instead of single-particle capture efficiencies and a flow structure parameter is used.

An extensive study of nonBrownian particles was carried out by Spielman and Fitzpatrick [90,91] to test theories for attraction-dominated capture. Several hundred experiments were done wherein latex particles were filtered from aqueous suspensions using beds of glass particles. Particle diameters ranged from 0.7 μm to 21 μm, bead diameters from 0.1 mm to 4 mm, and velocities between 0.01 and 0.1 cm s^{-1}. Electrolyte type and ionic strength were varied in order to control electrostatic repulsion and to avoid interference from particle deposits. Filter coefficients were calculated from particle concentrations measured with a Coulter counter.

In Ref. 91, data are shown for conditions in which the electrostatic repulsion and sedimentation are negligible. Although there is a fair amount of uncertainty in the data, the data cluster about the line derived from the theory given by Spielman and Fitzpatrick [90].

At low ionic strengths, where repulsion is strongest, agreement between theory and experiment was poor. This was attributed to the acute sensitivity of the capture rate to small adjustments (~1 mV) to the values of the ζ-potential of the film used in theory; the agreement has improved.

1.4.8.2 Experimental Investigation of Collision Efficiency at a Small Radius Ratio

Equation 1.63, which can be recommended for the collision efficiency in emulsions, was confirmed in systematic investigations devoted to microflotation kinetics. The monodisperse latex or glass spherical particles were used in the experiments. The radius ratio was very small. Thus, in Equations 1.63 and 1.82, a_1 corresponds to the latex particle dimension and a_2 to the bubble dimension. The dependence $E \sim a_2^{-2}$ was confirmed in Refs. 136 and 137. The dependence $E \sim a_1^{1.5}$ was established in Refs. 138 and 139. The combination of Equation 1.63 describing LRHI and Equation 1.82 describing the SRHI influence leads to the dependence $E \sim a_1^{1.4}$. Thus, the theory of short-range hydrodynamic interaction is confirmed by the investigations [134,136–139].

Recently, the direct observation of the grazing trajectory of latex particles (0.9 μm) in the vicinity of the rising bubble with radius 15 μm was accomplished [140,141]. The cell was attached to the microscope stage which is capable of moving vertically in the same velocity as that of the rising bubbles in the cell.

The similar experiments in emulsion can be very important. The predicted particle trajectory agreed well with those obtained experimentally. It was found that the collision efficiency values obtained experimentally were at maximum when the absolute values of ζ-potentials of both the bubbles and particles were at minimum.

1.4.9 Long- and Short-Range Hydrodynamic Interaction and Collision Efficiency at Any Radius Ratio

If the difference between particle dimensions is not large, the dynamics of the interacting spheres have to be represented in terms of the relative and center of mass motion by defining $dr/dt = u_2 - u_1$ and $d\bar{x}/dt = u_{12} = (u_1 + u_2)/2$, where u_1 and u_2 (see Figure 1.10) are the velocities of particles 1 and 2. Every particle moves under the action of the external field and the interaction with the neighboring particle. Thus, its velocity can be represented by the sum

$$u_i = \sum_{i=1}^{2} \omega_{ij} F_j \tag{1.86}$$

with $i = 1,2$. The mobility tensors ω_{ij} express the response of the ith sphere to a force acting on the jth and depend on the separation. The superposition (1.86) is justified by the linearity of the Stokes equation. The set of equations (1.86) can be transformed in the expression for the relative velocity of two sphere centers. Batchelor and colleagues [65,142,143] accomplished this transformation:

$$\mathbf{u}_{12}(\mathbf{r}) = \mathbf{u}_{12}^{(0)}\left[\frac{\mathbf{rr}}{\mathbf{r}^2} L(s) + \left(\mathbf{I} - \frac{\mathbf{rr}}{\mathbf{r}^2}\right) M(s)\right] \tag{1.87}$$

The relative mobility functions for motion along the line of centers (L) and motion normal to the line of centers (M) describe the effects of hydrodynamic interactions between the two drops. These functions depend on λ, $\hat{\mu}$, and s.

When the spheres are very close ($\xi = s - 2 \ll \lambda, \xi \ll 1$) the mobility functions have the asymptotic forms given by Jeffrey and Onishi [144]. Using these asymptotic forms, Davis [145] incorporated them in the equation for the particles' trajectories. Its solution with the boundary condition 1.80 enabled one to determine the grazing trajectory and accomplished the numerical calculations of the collision efficiency. At $\lambda \ll 1$, his results agree with Rulyov's results (Section 1.4.7). Davis' data are plotted in Figure 1.13 for $\hat{\mu} = 1000$.

The kinetics of the doublet formation were also analyzed in Ref. 142 by another method. Authors note the agreements with Ref. 145.

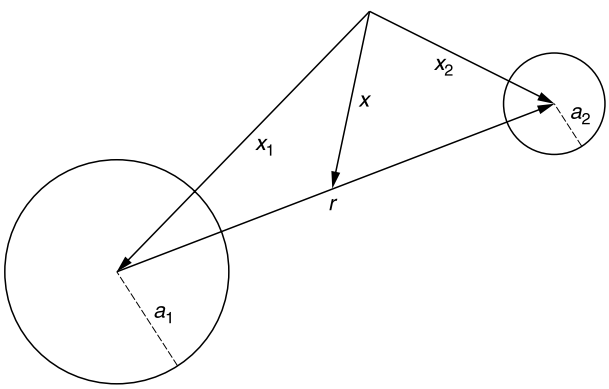

FIGURE 1.10 Two interacting spheres.

1.4.10 Collision Efficiency for Interacting Drops

Zhang and Davis [28] use the Batchelor expression (Equation 1.87) for u_{12} and modify it for spherical drops.

1.4.10.1 Mobility Functions for the Relative Motion of Two Drops

Their derivation [28] of expressions for the function L is based on the equation for the lubrication force on drops in the direction along their line of centers. The force balance enables one to obtain the functions L(s) and M(s) in Equation 1.87. They consider two unequal drops which are nearly touching and which move together as a pair due to gravity. Superimposed on this is a small relative velocity of the larger drop approaching the smaller one. A force balance on each drop yields

$$F_{g,i} + F_{d,i} + F_{l,i} = 0 \tag{1.88}$$

where $F_{g,i}$ is the gravity force acting on the drop i, which can be described by the Hadamard–Rybczynski result, Equation 1.42:

$$F_{g,i} = 6\pi\mu a_i U_i^{(0)} \frac{3\hat{\mu}+2}{3\hat{\mu}+3} \tag{1.89}$$

$F_{d,i}$ is the drag force exerted on the drop i by the surrounding fluid and is defined as the total hydrodynamic force minus the lubrication force. According to the analysis of Reed and Morrison [146] for two touching drops, it can be expressed as

$$F_{d,i} = -6\pi\mu a_i U_p \frac{3\hat{\mu}+2}{3\hat{\mu}+3}\beta_i \tag{1.90}$$

where β_i is a correction factor of the Hadamard–Rybczynski formula for drop i to account for the presence of the second drop.

Equations 1.88 to 1.90 for $i = 1$ and $i = 2$ may be solved for the pair velocity U_p and the lubrication force, $F_{11} = -F_{12}$. It enables the determination of the coefficients L_1, M_0, and M_1 in asymptotic equations:

$$L\xi = L_1\xi, \quad M(\xi) = M_0 + M_1(\xi) \tag{1.91}$$

The coefficient dependence on $\hat{\mu}$ and λ are given numerically in Table 1 of Ref. 28.

The trajectory equation follows from the definition of functions L and M,

$$\frac{ds}{d\theta} = s\frac{-L(s)\cos\theta}{\mathrm{M(s)}\sin\theta} \tag{1.92}$$

In the absence of interparticle forces, the limiting trajectory is one with the final condition $s = 2$ (contact) when $\theta = \pi/2$, because by symmetry, the point of closest approach occurs at $\theta = \pi/2$. Using the result of the integration of Equation 1.92, the collision efficiency is [28]

$$E_{12} = \exp\left(-2\int_2^1 \frac{M-L}{sL}ds\right) \tag{1.93}$$

With interparticle forces considered, the trajectory equation can no longer solve L analytically for an explicit formula for the dimensionless critical impact parameter, and hence the collision efficiency. Instead, the determination of the collision efficiency has to be performed by integrating Equation 1.92 numerically along the limiting trajectory from the infinite separation of two drops to the termination point.

The dimensionless critical impact parameter may be determined by integrating Equation 1.92 backward along the limiting trajectory from the termination point $\theta = \pi$ and $\xi = \delta$, to a position $s = s_1$ and $\theta = \theta_f$, beyond which the van der Waals forces are negligible. This numerical solution may be matched with the solution in the outer region ($s > s_f$). Setting $s > s_f$ and $\theta = \theta_f$ as the matching condition reveals that

$$E_{12} = \left\{ 4 \left[s_f \sin\theta_f \exp\left(\int_{s_f}^{\infty} \frac{L - M}{sL} ds \right) \right]^2 \right\}^{-1} \tag{1.94}$$

Figure 1.11 shows the results for E changing with λ for several different $\hat{\mu}$ [28]. The results for the collision efficiencies predicted by Zinchenko [68] are presented as solid circles for comparison. There is a very good agreement between the present results and Zinchenko's, with the relative difference between them being smaller than 3%. The *collision efficiency* approaches a finite value as the drops become equi-sized ($\lambda \to 1$). However, the *collision rate* goes to zero in this limit because the relative velocity of the two drops approaches zero. The collision rate may be nondimensionalized with a quantity not involving the size ratio: $J_{12}/J_{12}/(n_1 n_2 u_{01} \cdot \pi a_1^2) J_{12}/(n_1 n_2 u_{01} \pi a_1^2) = E_{12}(1 - \lambda^2)(1 + \lambda)^2$. This quantity is shown in Figure 1.12.

The collision rate is small for small size ratios because of the reduced collision cross section and collision efficiency (as discussed previously) achieves a maximum at moderate size ratios, and then decreases as the size ratio approaches unity because of the reduced relative velocity.

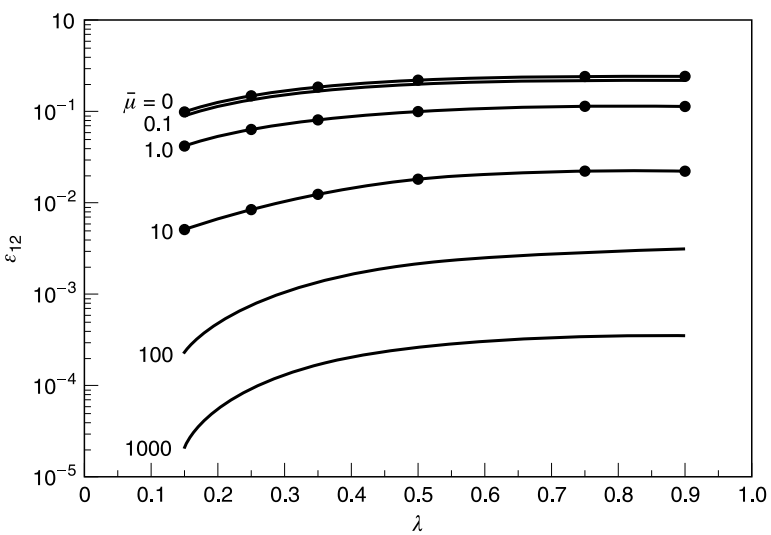

FIGURE 1.11 The dimensionless collision rate, $J_{12}/(n_1 n_2 u_{01} \pi a_1^2) = E_{12}(1 - \lambda^2)(1 + \lambda^2)$, for gravity sedimentation of drops as a function of the size ratio for various viscosity ratios without interparticle forces. (After X. Zhang and R. Davis, *J. Fluid Mech.* 230: 479 (1991).)

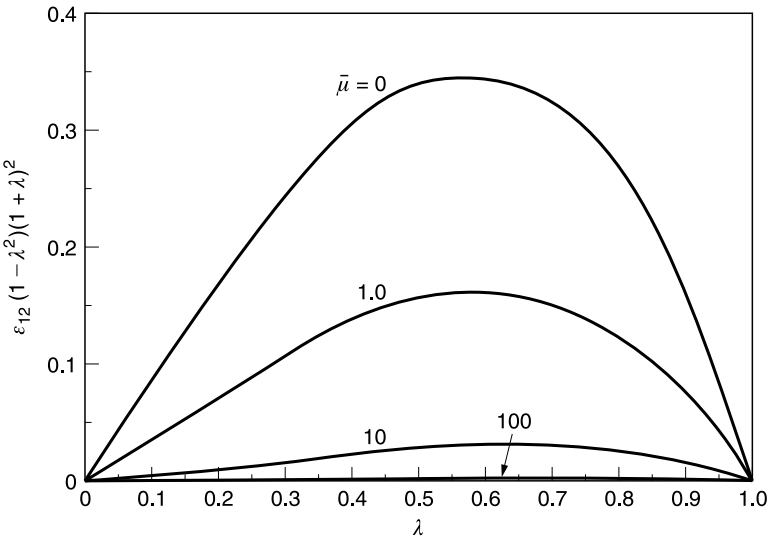

FIGURE 1.12 The collision efficiency for gravity sedimentation of drops as a function of the size ratio of various viscosity ratios without interparticle forces. (After X. Zhang and R. Davis, *J. Fluid Mech*. 230: 479 (1991).)

The unique peculiarity of results characterized by Figure 1.12 is that the nonzero collision efficiency occurs in the absence of attractive molecular forces. This is possible due to the mobility of droplet surfaces. The mobility decrease caused by liquid viscosity increase leads to a drastic decrease in the collision efficiency. As $\hat{\mu}$ increases, E decreases and its value is unusually low for $\hat{\mu} = 100$ and 1000. The increase in the unrestricted $\hat{\mu}$ corresponds to the transition to the solid particle and to the transition to $E_{12} = 0$ in the absence of attractive surface forces.

Typical results for the collision efficiency as a function of the parameter Q_{12} are shown in Figure 1.13 for $\lambda = 0.9$ for various $\hat{\mu}$, where the corresponding results of Davis [145] for rigid spheres are shown as solid circles. In the limit of $\hat{\mu} \to \infty$, there is an excellent agreement between our new results [28] and those of Davis [145]. As expected, the collision efficiency increases with increasing values of the Hamaker constant. The collision rate is more sensitive to the van der Waals attraction for drops with high viscosities relative to the surrounding fluid than for drops with moderate or low viscosities. Drops with high viscosities offer considerable resistance to near-contact relative motion. For collisions to occur, this resistance must be overcome by the van der Waals attraction. The internal flow for drops with low viscosities allows them to collide with relatively little resistance and without the aid of attractive forces.

1.5 GRAVITATIONAL COAGULATION IN SECONDARY MINIMUM

1.5.1 Secondary Minimum of Interaction Energy in Emulsions

Thermal motion energy of a colloidal particle has a value proportional to kT. The particle will easily escape a potential well whose depth has the same order of magnitude. An energy of the order of 10 kT is seldom acquired by a particle. Hence, a particle will stay rather long in a potential well of this magnitude. The depth of the secondary minimum can be fairly large (i.e., of the order of 10 kT and more) if two conditions are fulfilled simultaneously. The thickness of

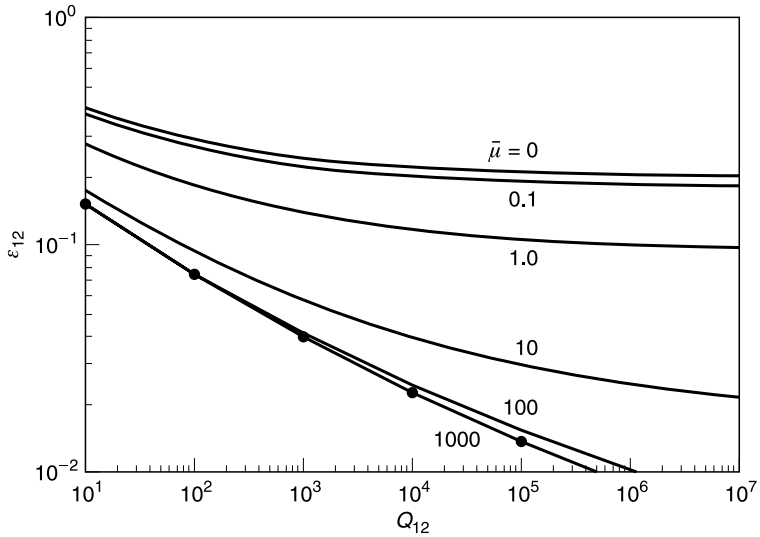

FIGURE 1.13 The collision efficiency for gravity sedimentation of drops as a function of the interparticle force parameter for $\lambda = 0.90$ and various viscosity ratios with unretarded van der Waals attractions. The solid circles are the rigid sphere results of Davis (1984). (After L. Spielman, *J Colloid Interface Sci.* 33: 562 (1970).)

the double layer is small (of the order of nanometers) and the size of the particles is rather large. The necessity of these conditions is clear without further calculations. The secondary minimum appears at the periphery of DL where electrostatic repulsive forces are weakened and molecular attractive forces prevail. Therefore, the thinner the DL, the closer the secondary minimum is to the surface; but the closer the secondary minimum to the surface, the higher the molecular attractive forces. A calculation shows that the secondary minimum is localized at a distance of several Debye radii (Figure 1.14). Then its distance to the surface is of the order of 10 nm as applied to conditions of interest to us. These conditions are realized rather often in natural colloidal and technological processes. Indeed, electrolyte concentration usually is fairly high under technological conditions and it can be equal to several centimols in 1 liter, which corresponds to a DL thickness of 3 nm and more.

The depth of the minimum strongly depends on the value of the Hamaker constant and on the size of particle. The energy due to attractive forces and electrostatic energy (and therefore energy as a whole) is proportional to particle size. As can be seen from Figure 1.15, the depth of the secondary minimum expressed in kilotesla units quickly decreases with the size of particles. Long-range aggregation is possible for particles in colloidal dispersions only for very high values of the Hamaker constant (i.e., for metal particles). On the other hand, long-range aggregation for large particles in microheterogeneous systems ($a > 1$ μm) is carried out over a wide range of Hamaker constants.

When the charge increases, the electrostatic energy of repulsive forces increases, the primary minimum disappears, and the height of the repulsion barrier grows. The electrical contribution to primary coagulation is very substantial. It is practically impossible to prevent long-range coagulation by increasing electrostatic repulsion (at real high electrolyte concentrations). The electrostatic factor of stability is strong with respect to short-range aggregation and is weak with respect to the long-range one. In colloidal systems, it dominates over other factors because

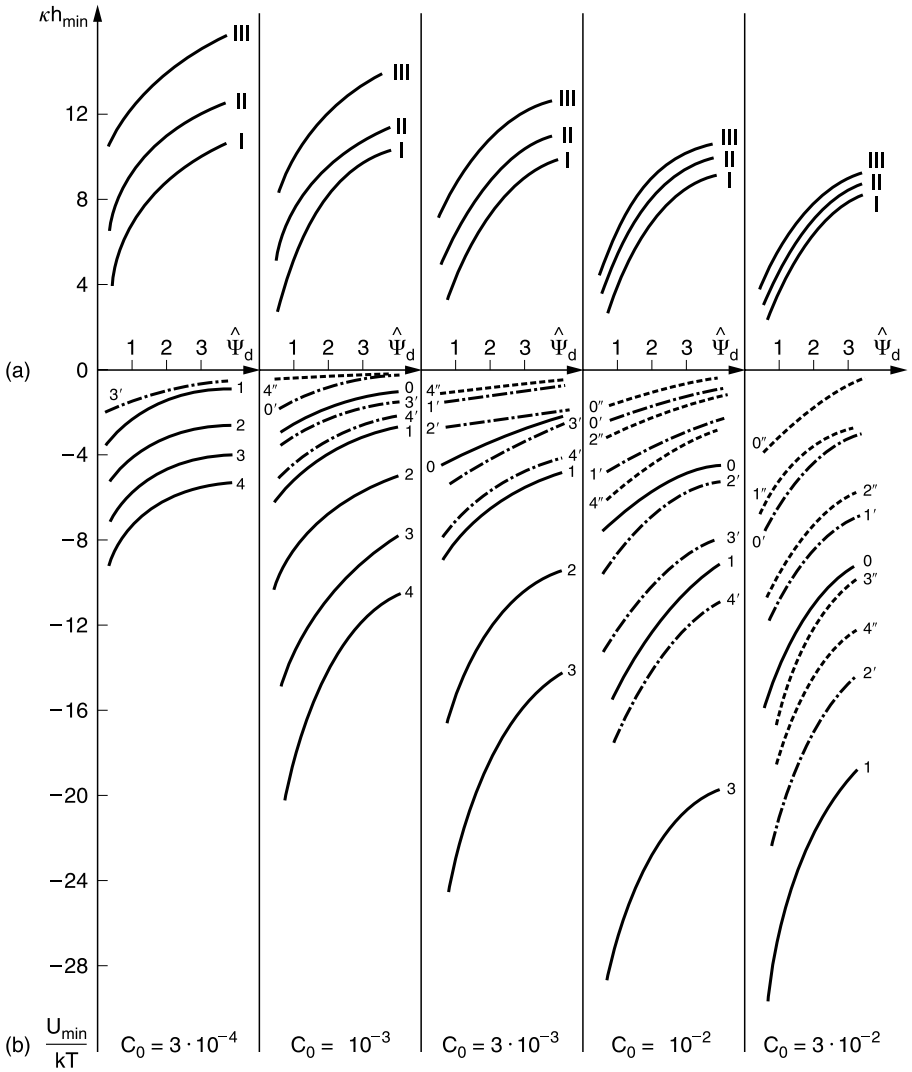

FIGURE 1.14 Dependence on the Stern potential for the coordinate (a) and the depth (b) of the secondary minimum: I, 0–4 without the retardation of screening; II, 0′–4′ with account for retardation; III, 0″–4″ with account for retardation and screening (0-a = 0.5 μm; 1-a = 1 μm; 2-a = 2 μm; 3-a = 3 μm; 4-a = 4 μm). The electrolyte concentrations [M] are shown at the bottom.

the depth of the secondary minimum is small and long-range aggregation is impossible. The electrostatic factor appears as a weak one in microheterogeneous systems when the depth of the secondary minimum is large and slightly depends on particle charge so that it does not prevent the long-range aggregation.

The depth of the secondary minimum was calculated from the expression for the total interaction energy between a spherical particle and a planar surface or (what is the same) with a

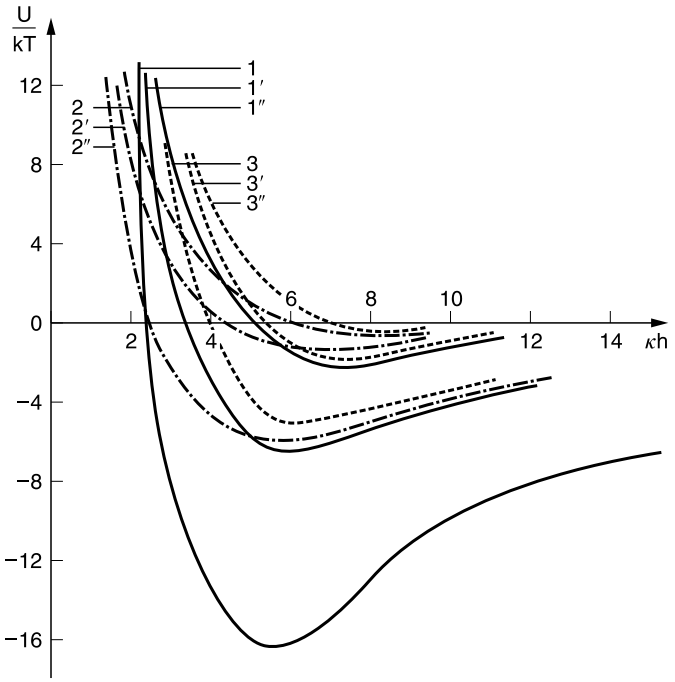

FIGURE 1.15 Pair interaction energy versus κh: 1, 1′, 1″ — $\tilde{\Psi}_d = 1$; $c_0 = 10^{-2}$ mol l^{-1}, 2, 2′, 2″ — $\tilde{\Psi}_d = 0.5$; $c_0 = 10^{-3}$ mol l^{-1}, 3, 3′, 3″ — $\tilde{\Psi}_d = 1$; $c_0 = 10^{-3}$ mol l^{-1}, 1, 2, 3: without retardation and screening; 1′, 2′, 3′: with account of retardation; 1″, 2″, 3″: both screening and retardation are taken into account.

particle of a much larger size. With regard to Equations 1.1 and 1.7, this expression has the form

$$y = de^{-\kappa h} - B\frac{\kappa a}{\kappa h} \tag{1.95}$$

where

$$y = \frac{U}{kT}, \quad U = U_A + U_\Psi, \quad B = \frac{A}{6kT}, \quad d = \frac{\varepsilon\Psi^2 a}{kT} \tag{1.96}$$

From $y = 0$ we can find the equation for κh_m:

$$(\kappa h_{\min})^2 \exp(-\kappa h_{\min})^2 = \frac{B\kappa a}{d} = \beta \tag{1.97}$$

This equation has two solutions, one of which corresponds to the "bottom" of the distant well and the other to the "top" of the barrier. The expression for the depth $U_{\min}$ of the secondary minimum follows from Equations 1.95 and 1.96:

$$-\frac{U_{\min}}{kT} = \frac{A\kappa a(\kappa h_{\min} - 1)}{6kT(\kappa h_{\min})^2} \tag{1.98}$$

1.5.1.1 Secondary Minimum in Potential Curve of Charged Emulsions

The dimensionless parameter on the right-hand side of Equation 1.97 characterizes the balance between the attractive and repulsive forces:

$$\beta = \frac{1}{96\varepsilon}\left(\frac{e}{kT}\right)^2 \frac{A\kappa}{\tanh^2\left(\frac{\tilde{\Psi}_d}{4}\right)} \tag{1.99}$$

The left-hand side of Equation 1.97 has a maximum at $\kappa h_m = 2$. Its height is $2^2 e^{-2} = 0.54$. It is convenient to introduce the boundary value $\beta_b = 0.54$. There is no solution of Equation 1.97 for $\beta > \beta_b$. This corresponds to the predomination of the attractive forces and the absence of the energetic barrier. Accordingly, the barrier and the secondary minimum exist at

$$\beta < \beta_b \tag{1.100}$$

Equation 1.100 is a necessary condition for secondary flocculation. The second condition is a sufficient depth of the secondary minimum. Note that Equation 1.11 is valid for $\kappa h > 2$. This condition is always satisfied at the secondary flocculation.

The dependence of the depth of the secondary pit on the droplet dimension is plotted in Figure 1.14. One can see that it is impossible to remove the secondary pit by the potential increase.

According to Equations 1.1 and 1.7, the influence of the droplet dimensions is identical. Thus, Equation 1.95 can be generalized by multiplying by $\lambda/(1+\lambda)$. The localization of the secondary minimum does not depend on λ. However, the equation for its depth of minimum has to be generalized:

$$\tilde{U}(\lambda) = \frac{\lambda}{1+\lambda} U|_{\lambda=0} \tag{1.101}$$

where $U|_{\lambda=0}$ is given by Equation 1.95. Note that the depth of the potential pit is a factor of 2 smaller for identical droplets in comparison with the case $\lambda \ll 1$.

At lower electrolyte concentrations and higher potentials, the distance of the secondary minimum from the surface is larger by 5 to 10 nm. Thus, the retardation of the dispersion forces (Section 1.2) influences the localization of the secondary minimum and the depth of the potential pit (Figures 1.14 and 1.15).

1.5.1.2 Repulsive Hydration Forces and the Secondary Minimum

Similar to the electrostatic energy, hydration forces decline (Section 1.2) exponentially with the distance. Thus, the conditions for the formation of the secondary potential pit are identical. This identity exists even on the quantitative level because the same function describes the dependence on the distance for electrostatic and hydration forces. Due to this similarity, the introduction of the dimensionless ratio h/h_s, instead of κh, enables one to derive an equation similar to Equation 1.98:

$$\tilde{U}_{\min} = A\frac{a}{h_s}\frac{h_{\min}/h_s - 1}{6kT(h_{\min}/h_s)^2} \tag{1.102}$$

where $h_{\min}$ satisfies the equation similar to Equation 1.97:

$$\left(\frac{h_{\min}}{h_s}\right)^2 e^{-(h_{\min}/h_s)} = \beta_s = \frac{A}{6\pi h_s^3 K_s} \tag{1.103}$$

β_s characterizes the balance between the attractive and the hydration repulsive forces. Because Equations 1.97 and 1.103 are identical, we can conclude that the hydration forces can produce the barrier and the secondary minimum at the condition

$$\beta_s < \beta_{sb} \tag{1.104}$$

which is identical with condition 1.100.

If K_s and h_s are not sufficiently large, the hydration forces cannot give rise to the barrier and the secondary minimum. The manifestation of the hydration repulsive forces was found in the investigation of emulsion stability in Ref. 147. The substitution of the values of K_s and A determined in Ref. 147 and $h_s = 1$ nm, assumed by the authors, into Equation 1.103 yields β_s value exceeding β_{sb}. However, Equation 1.103 for β_s is written for an interaction at small λ, whereas the equation for any λ is used in Ref. 147. For $\lambda \ll 1$, the multiplier 0.5 has to be introduced into Equation 1.103. After this correction, it turns out that the experimental data in Ref. 147 agree with condition 1.104. The information concerning K_s and h_s values in Ref. 147 agrees with condition 1.104. The data cited in Ref. 31 confirm the importance of repulsive hydration forces in the formation of the energy barrier and secondary potential pit. These forces were introduced to explain the forces observed between bilayers in lamellar phases [148,149]. In Ref. 31, the data concerning h_s for different phospholipids, lipids, and a few surfactants are summarized in Table 14 of Ref. 31. The table shows that $h_s = 2$ to 3 nm for phosphatidylcholins [150], about 2 nm for phosphatidylethanolamine, and approximately 1.5 nm for glycerol groups on alkoxyglycerol surfaces. The K_s values change in broad range.

In Ref. 31, the authors emphasize that the surface charge in food emulsions is low, electrolyte concentration is high, and, hence, the DL is not responsible for the emulsion stability. The stabilization can be caused by the repulsive hydration forces. However, the secondary flocculation preserves.

1.5.2 Estimation of the Size of Drops Not Coagulating in the Secondary Minimum. Sedimentation–Hydrodynamic Stability Mechanism of Microheterogeneous Dispersed Systems

The important question of a critical size of drops not undergoing a coagulation in the secondary minimum can be considered to be very simply based on the balance of forces at the rear stagnant pole of a larger drop (Section 1.4.7.4). Most likely, this effect was considered for the first time when applied to flotation [19].

It was shown in Ref. 19 that only particles of a rather small size can float, at the cost of coagulation in the secondary minimum. The larger the particle, the deeper the secondary minimum and the larger the gravity force. Gravity forces increase with increasing particle size faster than the depth of the secondary minimum. Therefore, coagulation of rather large particles in the secondary minimum is impossible. The failure of long-range aggregation for rather large

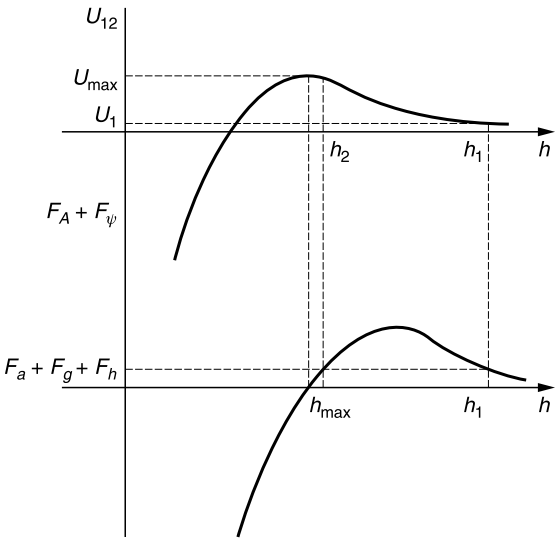

FIGURE 1.16 Illustrative curves representing the dependencies of surface forces $F_A + F_\Psi$ and corresponding energy U_{12} on h. The points h_1 and h_2 are characterized by the equality of the surface forces and the bulk forces $F_a + F_h + F_g$. (After A.S. Dukhin, *Kolloidn. Zh.* 50: 441 (1988).)

particles (microheterogeneous disperse systems) is an experimentally established fact considered by Kruyt [151], although he provided no explanation for the phenomenon.

The notion of a sedimentation–hydrodynamic mechanism of aggregate stability (SHAS) of microheterogeneous systems was introduced in Ref. 152. The importance of this phenomenon for classification of powders is shown in Ref. 153.

The dependence of particle interaction force on h is obtained by differentiating the known curve of total interaction energy (Figure 1.16). The decrease in the curve to the right of the minimum of total interaction force F is caused by the decrease of each of the forces with distance. The decrease at the left is caused by the faster increase in repulsive forces than in the attractive forces. The minimum size of the particle is determined from the condition of equilibrium between the pull force and the maximum force of attraction between particles in the floc:

$$F_A(h_{f\,\min}) + F_\Psi(h_{f\,\min}) = F_h + F_g + F_a \tag{1.105}$$

As mentioned in Section 1.5.1, energy due to molecular attractive forces predominates in the secondary energy minimum. This is true to a still larger extent in the secondary force minimum because $\kappa h_{f\,\min} > \kappa h_{\min}$ (see Figure 1.16). Therefore, the electrostatic repulsive force in Equation 1.95 can be omitted. In view of a large distance from the surface, the molecular attractive force in the region of the secondary force minimum should be calculated with regard to electromagnetic delay, that is, by Equation 1.4. F_g and F_a in Equation 1.105 are the gravity and the Archimed force, respectively, for the smaller of the particles; F_h is the detaching hydrodynamic force. Taking into consideration the aforementioned, the formula follows from

Equation 1.105 [152]:

$$a_{1cr} = \sqrt{\frac{B}{2\Delta\rho g(h_{f\min})^3}F(\lambda)},$$
$$F(\lambda) = \sqrt{\frac{\lambda^2\left[\lambda\Lambda(\lambda) + \Lambda(\lambda^{-1})\right]}{(1+\lambda)\left[\Lambda(\lambda) - \lambda^2\Lambda(\lambda^{-1})\right]}} \tag{1.106}$$

where $\kappa h_{f\min}$ is the greater of two possible positive roots of the analogue to Equation 1.97,

$$(\kappa h_{0\min})^4 e^{-\kappa h_{0\min}} = \frac{2\pi\kappa^2 B}{\Psi^2\varepsilon} \tag{1.107}$$

and $B = \lim(A(h))_{h\to\infty}$.

A very complicated function $\Lambda(\lambda)$ was obtained in Ref. 154. Its graphical and asymptotic representations are given in Ref. 155. The plot of the function $F(\lambda)$ is given in Ref. 155. The calculation is performed for the values $B = 2.5 \times 10^{-20}$ J m, $\Psi = 25$ mV, $c = 10^{-3}$ M, and $\lambda = 0$ (i.e., approximately at $a_2 \gg a_1$; $a_{1cr} = 1$ μm corresponds to this case). If we increase λ to 0.9 and make it very close to a_2, $a_{1cr} = 4.2$ μm at $a_2 = 4.2$ μm. These calculations have been performed for titanium carbide powder.

Using formula 1.106, the graphical representation of function $F(\lambda)$, and the calculated value of $a_{1cr}|_{a_{1cr}\ll a_2}$ we obtain curve $a_{1cr}(a_2)$ as presented in Figure 1.17. At any fixed a_2 particles with radius $a_1 > a_{1cr}(a_2)$ cannot aggregate with particles with radius a_2. Only for particles with radius $a_1 < a_{1cr}(a_2)$ is this possible.

Let us consider a region in Figure 1.17 bounded below by curve $a_{1cr}(a_2)$ and by bisectors $a_1 = a_2$. Each point corresponds to a pair of particles with radii a_1 and a_2. For a pair of particles belonging to this region, secondary flocculation is impossible due to the sedimentation–hydrodynamic mechanism of stability. The position of the boundary of this region [i.e., of curve

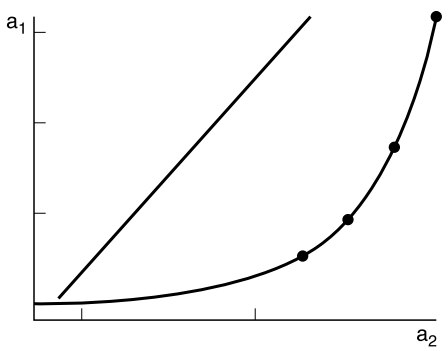

FIGURE 1.17 Flocculation in the secondary minimum is impossible for a pair of particles belonging to the region between bisectors $a_1 = a_2$ and curve $a_{1cr}(a_2)$.

$a_{1cr}(a_2)$ depends on values of $B]\Delta\rho$, electrolyte concentration, and Stern potential according to Equations 1.106 and 1.107.

1.5.3 Wet Fractionation Method and Sedimentation–Hydrodynamic Mechanism of Aggregate Stability

It is apparent that aggregation prevents powders from separation. The sedimentation–hydrodynamic aggregative stability mechanism (SHAS) prevents particles of rather large size from aggregation and thus creates necessary conditions for separation of narrow fractions. This explains the substantial success in the classification of wet powders [156]. The difference in sedimentation rate for particles of different size is used in wet classification. In the light of results obtained in the preceding section, pairs of particles belonging to region I (Figure 1.17) can be separated in principle using this method. We will divide the region under curve $a_{1cr}(a_2)$ into two zones. Zone 2 in which either a_1 or a_2 is reasonably small is characterized by a small depth of the remote potential well. Flocculation does not occur in zone 2. The boundary between zones 2 and 3 is fuzzy because the lifetime of a doublet due to secondary flocculation depends on the size of particles.

Pairs of particles corresponding to points in zone 2 are subjected to secondary aggregation. Liquid classification according to the method above is difficult. This difficulty is overcome by centrifuging. As can be seen from Equation 1.106, an ordinate of curve $a_{1cr}(a_2)$ decreases by a factor of 10 when we apply centrifugal acceleration of $100 \times \mathbf{g}$.

1.5.4 Peculiarities of Secondary Flocculation in Emulsion and Their Fractionation

According to Equation 1.106, a_{1cr} for the emulsion is $\sqrt{\Delta\rho_{TiO_2}/\Delta\rho_{em}}$ times higher than in the case of titanium carbide (i.e., approximately 7 μm at $a_1 \ll a_2$. At $\lambda = 0.9$, $a_{1c} \sim 30\,\mu m$ and $a_2 = 33\,\mu m$). Thus, due to the small $\Delta\rho$, emulsions are subjected to secondary flocculation to a substantially larger extent than microheterogeneous solid suspensions.

Nevertheless, the SHAS mechanism can presumably have a strong effect on secondary flocculation in emulsions and creaming and deserves systematic studies.

Considerations set forth in Sections 1.5.1–1.5.3 relate to the initial stage of flocculation. In going from doublets to multiparticle aggregates, the mechanism behind SHAS becomes more complicated.

In accordance with the analysis of Figure 1.17, after a lapse of time, the rear stagnant part of the surfaces of the big droplet will be covered by small droplets. It is apparent that applicability of Equation 1.106 needs a revision as applied to paired hydrodynamic interaction of such large particle aggregates.

Differing from powders, a substantial difficulty arises in fractioning micron-size drops as applied to emulsions because they are aggregated so that SHAS does not function in this case. It is likely that fractioning can be achieved by applying a centrifugal field. A change to the regime of fairly large Reynolds numbers (Section 1.4.5.3) and supercritical Stokes numbers (Section 1.4.4) is possible in this case. DAL can have an effect on interaction of drops in this situation (Section 1.4.6). Theoretical analysis of emulsion fractioning in a centrifugal field is thereby substantially complicated.

This range of questions is of fundamental interest for the emulsion stability problem, because in this way, it will most likely be possible to obtain narrow fractions of drops. This will allow us to apply the flocculation investigation methods to emulsions which have proved to be advantageous in studying flocculation kinetics of monodispersed systems (Section 1.3.4).

1.5.5 Gravitational Coagulation Kinetics in the Secondary Minimum

1.5.5.1 General

Flocculation of coarse emulsions in the secondary minimum proceeds at any electrokinetic potential and at fairly high electrolyte concentrations or even at low electrolyte concentrations when combined with thicker DL and small surface charge density (Section 1.5.1). In other words, secondary coagulation of coarse emulsions is more a rule than an exception. Because of the large drop size, this process is mainly a gravitational coagulation. For some intermediate drop size, Brownian coagulation might not be excluded; but gravity coagulation predominates for large drop sizes.

If we consider a general case of emulsion containing also small drops, the posed question has great importance. Secondary flocculation will be of minor importance for small drops because the depth of the secondary potential well is small. But the coarse part of drops will be involved in the secondary coagulation process, and after a period of time, the system will be represented by doublets rather than by singlets.

The formulated problem, in fact, defines concretely the problem of the initial stage of flocculation. Of course, this problem is presented in the general formulation and in general equations considered in articles and in the review by Melik and Fogler [15], but it is not treated as a separate problem. In a series of studies by Batchelor and Wen [143], the effect of surface forces on gravity coagulation was restricted to attractive forces. The same holds for works by Zhang and Davis [28] and Davis [145]. However, Spielman and Cukor [157] pay attention to the gravitational coagulation in the secondary minimum.

Derjaguin et al. [19], Rulyov [132,133], and Rulyov, Dukhin, and Semenov [155] raise the question about the importance of gravity coagulation in the secondary minimum. The necessary condition imposed on drop size is formulated [28]. The equation and the boundary condition are derived for finding the limiting trajectory but the equation is solved under the assumption of lack of repulsive forces, that is, in accordance with Refs. 28 and 143. Omitting the electrostatic component, Rulyov [133] was able to obtain an exact analytical solution of the equation. The inclusion of this term along with attractive forces excludes the possibility of an exact solution. However, an approximate method for analytical consideration of the problem can be proposed.

1.5.5.2 Similarity in Collision Efficiencies of Primary and Secondary Gravitational Coagulation

Secondary gravitational coagulation occurs in the force well of a larger drop and is correspondingly caused by the transport of the smaller droplet.

The larger the drops, the smaller the part of the well occupied by them. The drops of a finite dimension distribute symmetrically with respect to the maximum of the surface force h_{fm}. The maximum distance for the droplet of a finite dimension corresponds to the balance of the attaching surface force and detaching hydrodynamic force (see Equation 1.105).

The boundary condition for the grazing trajectory of the droplet is expressed by Equations 1.79 and 1.80, in which h_0 has to be substituted. The equation for the grazing trajectory in the case of the secondary flocculation differs from the treatment in Section 1.4.7 due to the additional repulsive electrostatic force. However, the electrostatic force can be neglected, as seen below.

Take into account that the electrostatic force is κh_m times smaller at the force maximum than the attraction force and that $\kappa h_{fm} \gg 1$ (Section 1.5.1). The distance to the surface increases along the grazing trajectory when the angle θ decreases. Thus, the maximum error in neglecting the electrostatic force corresponds to the point $\theta = \pi, h = h_0(a_1)$. Neglecting the electrostatic force

corresponds to an increase in the molecular force or in the Hamaker constant by the multiplier $(1 - \kappa h_{fm}^{-1})$. This approximation causes a negligible error in the collision efficiency because its dependence on the Hamaker constant is very weak. Taking into account Equation 1.98, one concludes that neglecting the electrostatic force is equivalent to omitting the multiplier $(1 - \kappa h_{fm}^{-1})^{0.15}$. This estimation concerns the drop of the critical dimension a_{1cr} (Section 1.5.2) which occupies only one point in the well corresponding to force maximum. At $a_1 < a_{1cr}$, $h_0(a_1)$ exceeds h_{fm}. It means that the ratio of the electrostatic force to the attraction force for $a_1 < a_{1cr}$ is less than for a_{1cr}. Thus, for drops with radius less than a_{1cr}, the error decreases.

One concludes that Equation 1.94 (and, correspondingly, Figure 1.13) describes the collision efficiency of the gravitational coagulation in the remote well too. However, there is a large difference in the application of Equation 1.94 to the collision efficiency in the case of uncharged droplets (Section 1.4) and charged droplets (Section 1.5). This concerns the boundaries of the application of the equation. For the uncharged droplets, Equation 1.94 is valid for any $a_1 \ll a_2$. For the charged droplets, Equation 1.94 is valid for the case

$$a_1 < a_{1cr}(a_2) \tag{1.108}$$

1.6 GRAVITATIONAL COAGULATION IN THE PRIMARY MINIMUM

The pressing hydrodynamic force (Section 1.4.7) produces the pressure excess in the gap between sedimenting drops and causes the liquid to flow from the gap between them. The hydrodynamic pressing force can exceed the force barrier of the disjoining pressure, thereby allowing the possibility of coagulation in the primary minimum. This problem may be examined when considering the drop motion along their symmetry axis [19]. Under this condition, the hydrodynamic pressing force is a maximum; hence, one can obtain the necessary and sufficient condition for the primary gravitational coagulation of drops.

Along the axis of a drop pair, the tangential flow velocity is equal to zero. Thus, the duration of the deposition process can be indefinitely long. This means, in turn, that the viscous resistance of the interface film can be neglected in the balance of acting forces. It leads to an equation similar to Equation 1.105. The difference concerns the pressure hydrodynamic force instead of the detaching hydrodynamic force. Both forces are expressed by the same equation but of different sign.

Equation 1.105 indicates that for all values of h, the smaller droplet is subjected to a force directed toward the surface of bigger drop (front pole). Otherwise, the deposition and coagulation cannot occur. The same expression imposes limitations in the values of the parameters at which the disjoining pressure can be overcome. We represent it as the critical radius of the small drop for the gravitational primary coagulation. It occurs at

$$a_1 > a_{1cr}^{pc}(a_2) \tag{1.109}$$

where a_{1cr}^{pc} is the smaller root of Equation 1.107. Instead of only electrostatic forces, the repulsive hydration forces have to be considered too (Section 1.5.1.2).

1.7 CLASSIFICATION OF REGIMES OF GRAVITATIONAL COAGULATION

There are two regimes in the absence of repulsive forces. At condition 1.109,

$$a_1 < a_{1cr},$$

coagulation occurs. Due to SHAS (Section 1.4.7.4), there will be no repulsive forces in the opposite case.

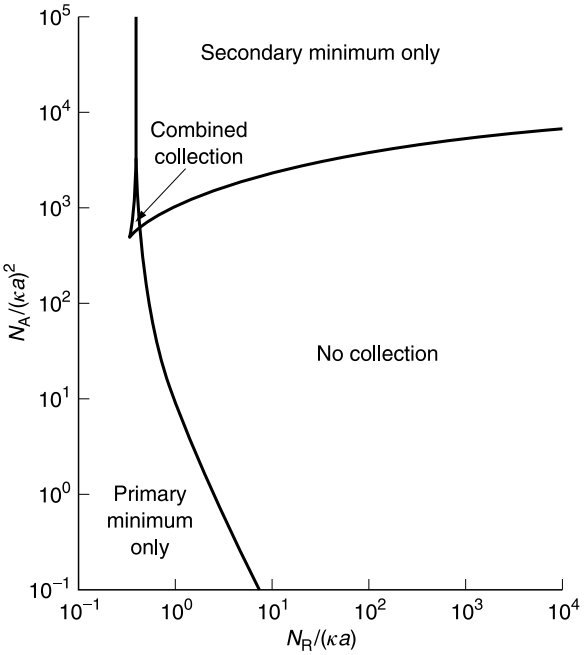

FIGURE 1.18 Stability diagram for a spherical collector showing the influence of electrostatic repulsion at constant potential. (After W.R. Russel, D.A. Saville, and W.R. Schowalter, *Colloidal Dispersions*, Cambridge University Press, Cambridge, 1989, Chap. 11.)

There are three regimes in the presence of repulsive forces: the primary coagulation, the secondary coagulation, and lack of coagulation. One can see in Figure 1.18 that at $a_1 > a_{1c}^{\text{det}}(a_2)$ detachment occurs, at $a_1 < a_{1cr}^{pc}$ primary coagulation occurs, and the condition of the secondary coagulation is

$$a_{1cr}^{pc}(a_2) < a_1 < a_{1cr}^{\text{det}}(a_2) \tag{1.110}$$

Again, Spielman and his co-workers [129,157] were first to classify the regimes of gravitational coagulation in systems of dimensionless criteria. In order to characterize the role of the attractive and the repulsive forces, they used the attraction Equation 1.99 and the repulsion numbers:

$$N_R = \frac{6\varepsilon\Psi^2 a}{A} = \frac{\kappa a}{16\beta}\left(\frac{\tilde{\Psi}}{th\tilde{\Psi}/4}\right)^2 \tag{1.111}$$

where β is given by Equation 1.99. The result is displayed in Figure 1.18 which is also presented in Ref. 110 (Figure 11.8 in that reference).

Naturally, the primary coagulation occurs at a sufficiently low Ψ potential when the electrostatic barrier is absent. It corresponds to low values of the repulsive number and to the left domain in Figure 1.18. The growth in Ψ and N_R leads to a growth in electrostatic barrier and

excludes the possibility of primary coagulation. However, at any high value of the repulsive number, the secondary coagulation is possible, corresponding to the domain in the higher right corner of Figure 1.18. The second alternative at high repulsive numbers is the absence of coagulation, which corresponds to the third domain in Figure 1.18. Which alternative is realized depends on the value of attractive number. At a fixed N_R value (i.e., at fixed Ψ and a values), N_A increases the mean molecular force growth, and the relative velocity of droplet decreases. Drop coagulation in the secondary minimum results from a flow too weak to carry the droplet through the secondary well. It corresponds to high values of attractive numbers and to the domain in the upper right corner of Figure 1.18.

The boundary between the domain of stability and of secondary coagulation is given by the curve of the critical condition of the sedimentation–hydrodynamic aggregative stability [SHAS (Section 1.5.4) and Equation 1.106].

The slope of the boundary curve can be explained. At fixed values of the drop dimensions, the Hamaker constant, and the Ψ-potential, the relative velocity only changes along the boundary curve. The decrease in velocity corresponds to an increase in the attraction number and to a decrease in the pressing hydrodynamic force. Thus, the increase in the attraction number corresponds to the decrease in the pressing hydrodynamic force which causes the shrinkage of the domain of the primary coagulation in Figure 1.18.

For an interpretation of the slope of the boundary curve of SHAS, fixed droplet dimension, relative velocity, and Hamaker constant can be assumed. For these conditions, N_A is invariant and the growth in $N_R(\kappa a)^{-1}$ corresponds to the growth in Ψ-potential and the decrease in attraction force between the droplets in a doublet. Thus, the increase in $N_R(\kappa a)^{-1}$ is favorable for the sedimentation–hydrodynamic stability; it explains the shrinkage of the secondary coagulation domain in Figure 1.18 upon growing $N_R(\kappa a)^{-1}$ values.

The evaluation of the coagulation kinetics for a specific emulsion starts with the determination of the stability diagram, that is, the calculation of the boundary curves for the primary and secondary coagulation. The attraction number for emulsions can be specified by expressing the relative velocity by means of the Stokes equation and using the known value of the density difference $\Delta\rho$, that is,

$$N_A = \frac{A}{2\pi g \Delta\rho a^4}, \tag{1.112}$$

$$N_A(\kappa a)^2 = \frac{A\kappa^2}{2\pi g \Delta\rho a^2}, \qquad N'_R = N_R(\kappa a)^{-1} = \frac{3\varepsilon\Psi^2}{4\pi A\kappa} \tag{1.113}$$

In emulsions, the value of A changes in a narrow range and the information concerning $\Delta\rho, \kappa$, and $\Psi \cong \varsigma$ is usually available too. For a specific emulsion, $\Delta\rho$, κ, Ψ, and A are invariants. However, a can vary over a broad range.

The evaluation of N'_R enables one to discriminate between the gravitational stability and the gravitational coagulation. For sufficiently high ς-potentials and sufficiently low electrolyte concentrations, the gravitational stability or secondary coagulation will take place. These two regimes can be discriminated by the N'_R evaluation. As the electrolytic concentration increases, the secondary minimum approaches the surface, which is accompanied by an increase in the molecular attraction. Thus, experimental evaluation of the N_R and N_A criteria enables one to

determine both boundary curves and identify the coagulation regime. Depending on the values of the parameters, the regimes of primary or secondary coagulation or gravitational stability can be identified. However, these simple regimes exist for emulsions with narrow drop size distributions. Due to the strong dependence of N'_R on real emulsions with a broad droplet distribution, mixed regimes will occur. For the largest droplets, SHAS becomes of increasing importance and droplets satisfying condition 1.110 participate in secondary coagulation.

The stability diagram (Figure 1.18) does not account for Brownian coagulation. In principle, Brownian coagulation manifests itself at any value of the repulsion number.

For an application of the kinetic theory of emulsion stability, the stability diagram is extremely important. Unfortunately, the exactness of the boundary curves plotted in Figure 1.18 is rather low. The boundary curve of primary coagulation reflects the interaction constant of both charge and constant potential. The curve in Figure 1.18 is plotted for an invariant potential. General criteria for the discrimination between the two cases are known (Section 1.2) and formulated on the basis of the Debora number. However, a quantitative determination is difficult due to the lack of information concerning the charge relaxation.

The exactness of the boundary curve of SHAS is limited due to the restriction in knowledge concerning the retardation of the van der Waals attraction (Sections 1.2 and 1.5.4).

The boundary curve in Figure 1.18 is calculated for the extreme case of $\lambda = 0$. The incorporation of the multiplier $\Lambda(\lambda)$ (Sections 1.4.9 and 1.5.2) into the equation for the balance of the hydrodynamic detaching force and attractive surface force equation (1.110) enables a generalization of the theory. It leads to a splitting of the boundary curve into a family of curves.

1.8 DELINEATION OF DIFFERENT PARTICLE LOSS MECHANISMS. RAPID COAGULATION

In emulsions, flocculation will be significant for smaller particles and creaming will be significant for larger particles. However, it is extremely important to have quantitative relationships that can predict the state of an emulsion or suspension; that is, whether the particles are creaming or flocculating, and if both are occurring, determine the predominant one. If they are flocculating, what type of flocculation dominates, if any? This information can be used to predict the behavior of the colloidal system from the solution of the convective–diffusion equation and population balance equations by including only those destabilizing factors which dominate the particle breakdown process. This type of analysis has the potential of greatly simplifying the process of predicting the stability of a given emulsion or suspension. Melik and Fogler [15] accomplished this for both uncharged and charged emulsions. Taking into account the results of the preceding section, a specification is necessary. In this section, the delineation concerns a weakly charged emulsion where the role of the electrostatic component of disjoining pressure can be neglected. As to emulsions stabilized by electrostatic interaction, the delineation procedure as a whole cannot be realistic due to the large discrepancy between theory of slow coagulation and experiment.

1.8.1 Gravity-Induced Flocculation versus Brownian Flocculation

This section is primarily based on the review by Melik and Fogler [15]. As a first approximation, the relative strength of gravity-induced flocculation as compared to Brownian flocculation is given

by the gravity number

$$\mathrm{Gr} = \frac{(u_{02} - u_{01})(a_1 + a_2)}{2D_0} = \frac{2\pi g \Delta\rho a_2^4}{3kT}\lambda(1-\lambda)^2 \tag{1.114}$$

and represents the relative strength of gravitational to Brownian forces.

In Figure 1.19, the gravity number Gr is shown as a function of the particle size ratio λ for the case $\Delta\rho = 0.1$ g cm^{-3} at $T = 298$ K under normal gravity. As λ deviates from unity, the difference in particle size causes the differential creaming contribution to Gr to be enhanced at a rate faster than the increase of the Brownian motion of the smaller particle. A further decrease in λ only results in a small increase in differential creaming, whereas the diffusivity of the smaller particle starts becoming quite vigorous. The maximum value of Gr at $\lambda = (1/3)^{1/2}$ reflects the balance point between these two competing effects. That is, one can estimate the relative importance of gravity-induced flocculation and Brownian flocculation from a plot similar to Figure 1.19. For example, if the colloidal particles are about 1.0 μm in diameter with $\Delta\rho =$ 0.1 g cm^{-3} and $T = 298$ K, Brownian flocculation will be approximately 100 times more

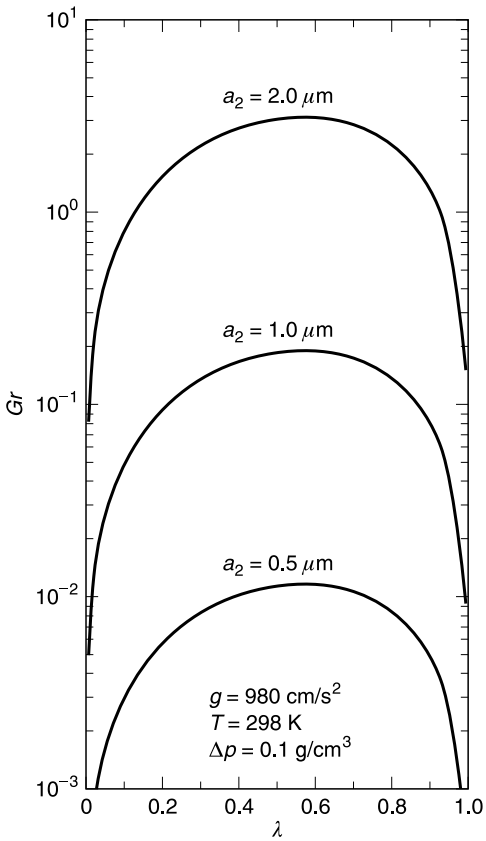

FIGURE 1.19 Effect of particle size ratio on the gravity number Gr for various type 2 particle sizes. (After D.H. Melik and H.S. Fogler, in *Encyclopedia of Emulsion Technology*, Vol 3, Marcel Dekker, Inc., New York, 1988, pp. 3–78.)

important than gravity-induced flocculation. On the other hand, for particles about 4.0 μm in diameter, gravity-induced flocculation will be about three times larger than Brownian flocculation. A plot of this type can provide useful qualitative information on the stability of a colloidal dispersion. This approach was used by Melik and Fogler [15] to delineate the various particle loss mechanisms in quiescent media.

However, an underlying assumption that is invoked when using the parameter Gr is that the stability factor for the loss mechanism of each particle is identical. The gravity number implies that the particle loss mechanisms due to differential creaming and Brownian motion can be quantified independently. Although there are regimes for which the assumption of linear independence is quite good, one should be careful because we can only account for the differences in the gravity-induced and Brownian flocculation stability factors. The ratio of the particle loss due to gravity-induced flocculation to the particle loss due to Brownian flocculation is given by

$$R_{GB} = \frac{J_{Gr}}{J_{Br}} = \frac{Gr}{2}\frac{W_{Br}}{W_{Gr}} \tag{1.115}$$

where J_{Br} is given by Equations 1.13 or 1.14. As shown by Melik and Fogler [15] for $Gr \ll 1.0$, additivity is justified only in the absence of electrostatic repulsion. Consequently, we will restrict our discussion to conditions of rapid flocculation.

The effect of gravitational forces on the flocculation ratio R_{GB} is shown in Figure 1.20 for various strengths of interparticle attraction. As expected, the effect of gravity-induced flocculation

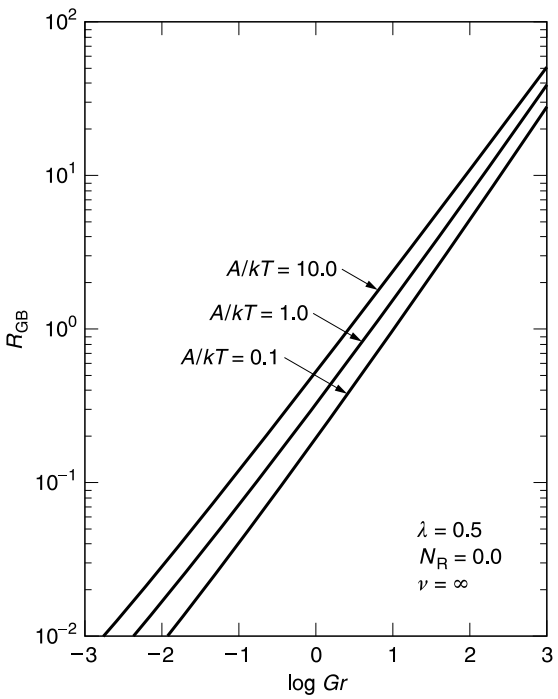

FIGURE 1.20 The importance of gravity-induced flocculation and Brownian flocculation. (After D.H. Melik and H.S. Fogler, in *Encyclopedia of Emulsion Technology*, Vol 3, Marcel Dekker, Inc., New York, 1988, pp. 3–78.)

becomes more pronounced as the gravitational force is increased. It is interesting to note that the gravity number Gr does not give a good estimate of the relative importance of gravity-induced flocculation as compared to Brownian flocculation. For example, if Gr = 10.0, one would probably assume that the rate of particle loss due to gravity-induced flocculation is approximately 10 times higher than the particle loss due to Brownian flocculation. However, as can be seen from Figure 1.20 for Gr 10.0, the particle loss ratio is only approximately 1.5 for a dimensionless Hamaker constant of $A/kT = 1.0$, typical of colloidal dispersions. This result clearly shows that hydrodynamic interactions reduce the rate of gravity-induced flocculation more than the rate of Brownian flocculation. This effect is absent when using the gravity number to delineate the mechanisms of gravity-induced and Brownian flocculation.

1.8.2 Gravity-Induced Flocculation versus Creaming

Whenever a colloidal system is destabilized due to gravity-induced flocculation, a breakdown due to particle creaming occurs simultaneously. The ratio of the total rate of particle loss due to creaming to the net rate of particle loss as a result of gravity-induced flocculation R_{CG} was determined by Melik and Fogler [15]. Their result is given by the following analytical expression:

$$R_{CG} = \frac{f(a_2, N_{02}, \lambda, R_N)}{\pi H E_{1,2}(1-\lambda^2)(1+\lambda)^2 R_N} \tag{1.116}$$

where $f(a_2, N_{02}, \lambda, R_N)$ with $H = h/a_2$ is the dimensionless container height and $R_N = N_{01}/N_{02}$ is the particle concentration ratio.

Under conditions of negligible electrostatic repulsion, the particle loss ratio R_{CG} is most sensitive to changes in the total initial particle concentration N_{TOT} (where $N_{TOT} = N_{01} + N_{02}$), the size of the larger particle a_2, and the particle size ratio λ. The effect of each of these parameters is discussed next.

Figure 1.21 shows the effect of the total particle concentration N_{TOT} on the relative rates of creaming to gravity-induced flocculation. As expected, the higher the particle concentration, the more significant the process of gravity-induced flocculation becomes. The presence of a minimum in Figure 1.20 is to be expected. For small values of R_N, $N_{02} \gg N_{01}$ and for large values of R_N, $N_{02} \ll N_{01}$. In each of these extreme cases, the effect of gravity-induced flocculation is reduced because there are either not enough collectors (a_1) for the given number of particles (a_2) or there are too many collectors. In either case, creaming begins to dominate the colloidal breakdown process. When $N_{02} \cong N_{01}$, the effect of gravity-induced flocculation is at a maximum in the breaking process.

Figure 1.22 shows the effect of increasing particle size on the relative rates of creaming to gravity-induced flocculation. As the particle size increases, the rate of flocculation increases faster than the creaming rate of the particles.

Figure 1.23 shows how changes in the particle size ratio affect the relative rates of creaming and gravity-induced flocculation. When the concentration of smaller particles is less than the concentration of larger particles ($R_N < 1$), the larger particle size ratio reduces the rate of gravity-induced flocculation as compared to the creaming rate of the particles. On the other hand, when the concentration of the smaller particles is slightly higher than that of the larger particles ($R_N \geq\sim 3.2$), the situation is reversed. Smaller particle size ratios favor gravity-induced flocculation over creaming more than the larger particle size ratios.

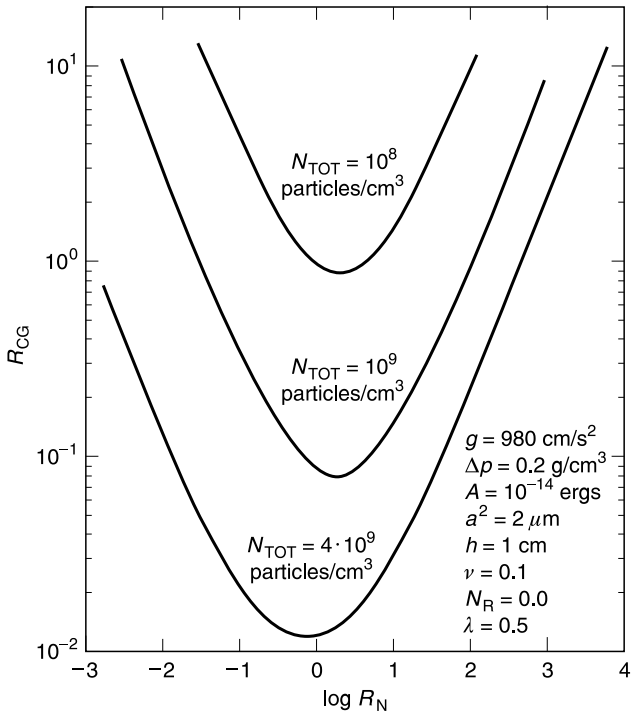

FIGURE 1.21 Effect of particle concentration ratio on the relative particle loss rates of creaming and gravity-induced flocculation for various total particle concentrations. (After D.H. Melik and H.S. Fogler, in *Encyclopedia of Emulsion Technology*, Vol 3, Marcel Dekker, Inc., New York, 1988, pp. 3–78.)

1.8.3 Domains of Dominant Particle Loss Mechanisms

Regimes of the various limiting cases of particle loss can be delineated quantitatively by manipulating the equations for the creaming rate and the Brownian and gravity-induced flocculation rates. For a given fluid, the creaming rate is strongly depending on particle size. For very small particles, the creaming velocity will be negligible as compared to the Brownian motion of the particles. It is generally accepted that the gravitational forces acting on a particle can be neglected for creaming velocities of 1.0 mm per day or less [15] and the case of negligible interactions (surface and hydrodynamic):

$$u_{0i} = \frac{2g\Delta\rho a_i^2}{9\mu_f} < 1.0 \ \text{mm/day} \tag{1.117}$$

or

$$a_c = \left(\frac{(1.0\ \text{mm/day})9\mu_f}{2g\Delta\rho}\right)^{1/2} \tag{1.118}$$

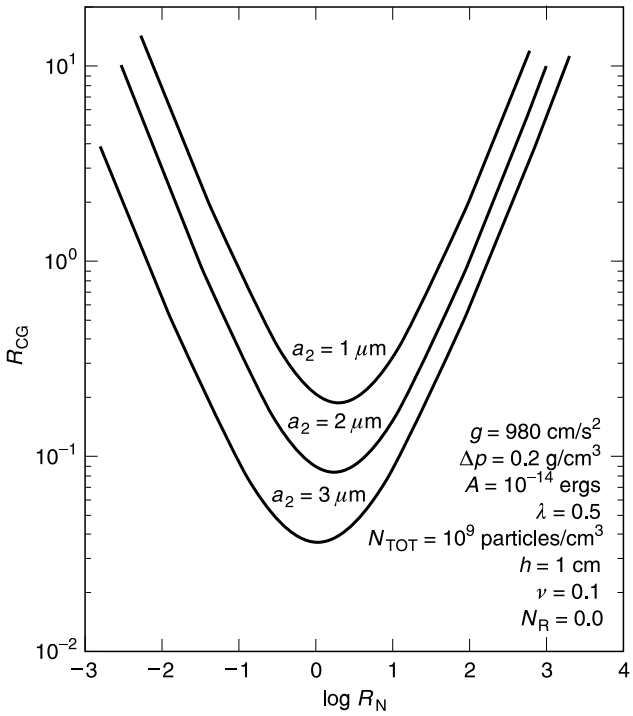

FIGURE 1.22 Effect of particle concentration ratio on the relative particle loss rates of creaming and gravity-induced flocculation for various type 2 particle sizes. (After D.H. Melik and H.S. Fogler, in *Encyclopedia of Emulsion Technology*, Vol 3, Marcel Dekker, Inc., New York, 1988, pp. 3–78.)

Particles with a radius smaller than a_c will disappear from the system primarily due to Brownian flocculation. For values larger than a_c particles can disappear by any of the three particle loss mechanisms.

Brownian flocculation will be negligible for large values of the flocculation ratio R_{GB}, whereas gravity-induced flocculation will be negligible for small values of R_{GB}. Consequently, Equation 1.115 can be used to define quantitatively the regions where only one mechanism will be predominant. Melik and Fogler [15] define Brownian flocculation as predominant if the flocculation ratio R_{GB} is less than 0.1, and gravity-induced flocculation as predominant if R_{GB} is higher than 10.0. As discussed in Section 1.8.1, this rationale does not account for any possible coupling between differential creaming and Brownian motion:

$$\frac{\mathrm{Gr}}{2}\frac{W_{\mathrm{Br}}}{W_{\mathrm{Gr}}} \leq 0.1 \text{ (Brownian flocculation)}, \tag{1.119}$$

$$\frac{\mathrm{Gr}}{2}\frac{W_{\mathrm{Br}}}{W_{\mathrm{Gr}}} \geq 10.0 \text{ (gravity-induced flocculation)} \tag{1.120}$$

The key parameters in Equations 1.118 to 1.120 are the particle radius a_2, the net gravitational force $g\Delta\rho$, and the particle size ratio λ. Consequently, these parameters can be used to map the various domains for the particle loss mechanisms.

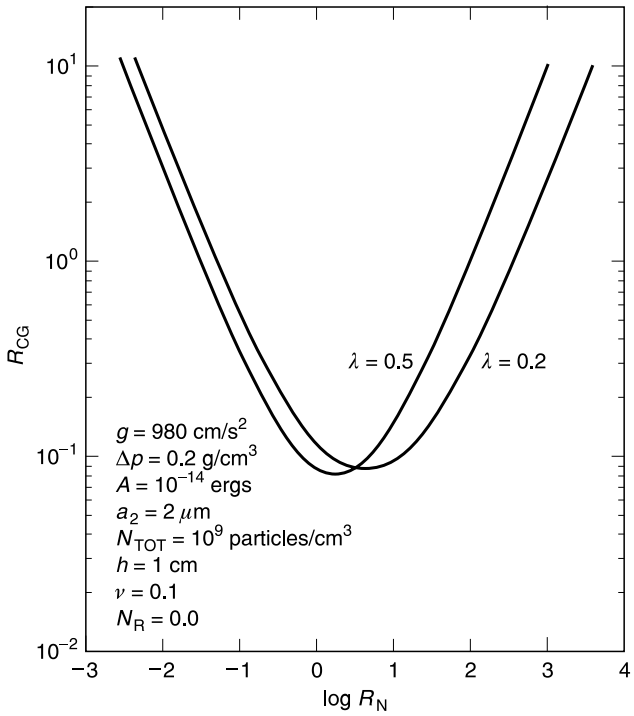

FIGURE 1.23 Effect of particle concentration ratio on the relative particle loss rates of creaming and gravity-induced flocculation for various particle size ratios. (After D.H. Melik and H.S. Fogler, in *Encyclopedia of Emulsion Technology*, Vol 3, Marcel Dekker, Inc., New York, 1988, pp. 3–78.)

In a fairly general manner, plots of a_2 versus λ for a constant value of $g\Delta\rho$ can be prepared by using Equations 1.118 to 1.120. An example of this analysis is shown in Figure 1.24 for the case of negligible electrostatic repulsion ($N_R = 0$) and for a Hamaker constant $A/kT = 1.0$. Equation 1.118 was used to obtain the upper boundary of region I, and Equations 1.119 and 1.120 to obtain the lower and upper boundaries of region III. A plot of this type can also be used for centrifugal creaming instead of gravitational creaming. For centrifugal creaming, g is simply replaced with $\omega^2 X$, where ω is the angular velocity of the centrifuge rotor and X is the distance from the axis of rotation.

Various regions in Figure 1.24 represent the possible dominant particle loss processes in quiescent media. For example, in region I, creaming and gravity-induced flocculation will be negligible and particles disappear primarily by Brownian flocculation. Brownian flocculation in region I will depend on the electrostatic properties of the particles and also the total particle concentration. If the colloidal system is very dilute, Brownian flocculation will also be negligible.

For colloidal systems in region II, gravity-induced flocculation will be negligible as compared to Brownian flocculation. In region III, creaming is bound to occur and the rate of Brownian and gravitational flocculation will depend on the total particle concentration. Similarly, in region IV, Brownian flocculation will be negligible as compared to gravity-induced flocculation. Creaming will also occur in this region and the rate of gravity-induced flocculation will depend on particle concentration, and even on the polydispersity of the colloidal system. Figure 1.24 is useful in

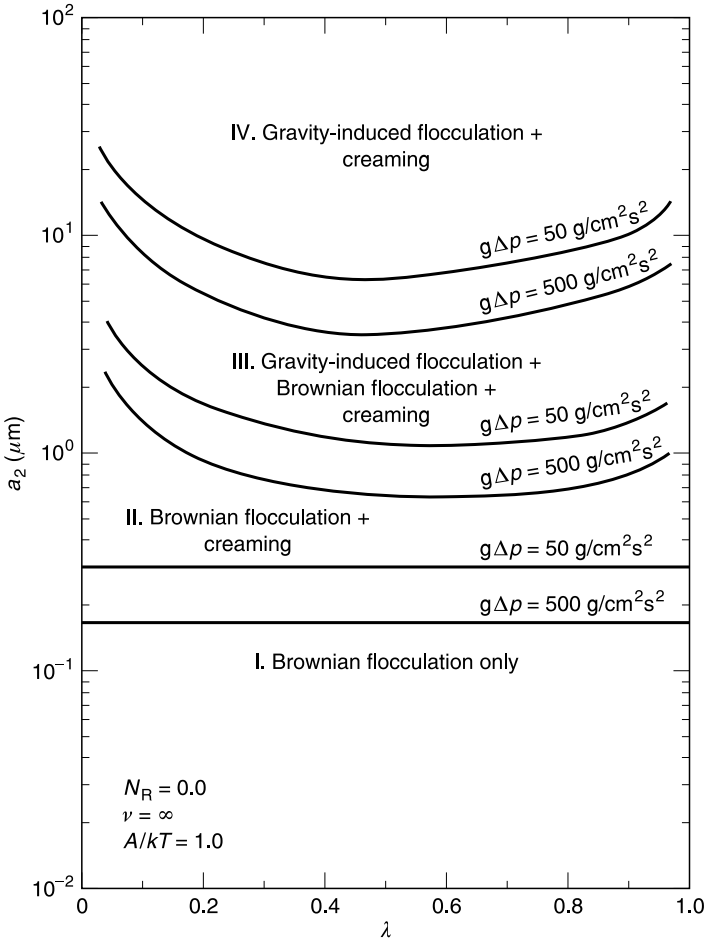

FIGURE 1.24 Regimes of dominant particle loss mechanisms in quiescent media. (After D.H. Melik and H.S. Fogler, in *Encyclopedia of Emulsion Technology*, Vol 3, Marcel Dekker, Inc., New York, 1988, pp. 3–78.)

determining the state of a colloidal system; that is, whether the colloidal particles are creaming or flocculating.

1.8.4 Experiment

A methodology of experimental investigation of the kinetic and aggregative instability of mini-emulsions is elaborated by Ostrovsky and Good [158]. The methodology is illustrated by Figures 1.25A and 1.25B. The invariant slope of section c of the experimental curve characterizes the rate of coalescence. Its value depends only on the composition of the system and is called the coalescence time parameter. More than 50 different compositions were studied.

By means of the linear extrapolation, as shown in Figure 1.25B, the authors introduced the notion of τ_{sed}. The authors neglect the flocculation and coalescence during stages b and c and

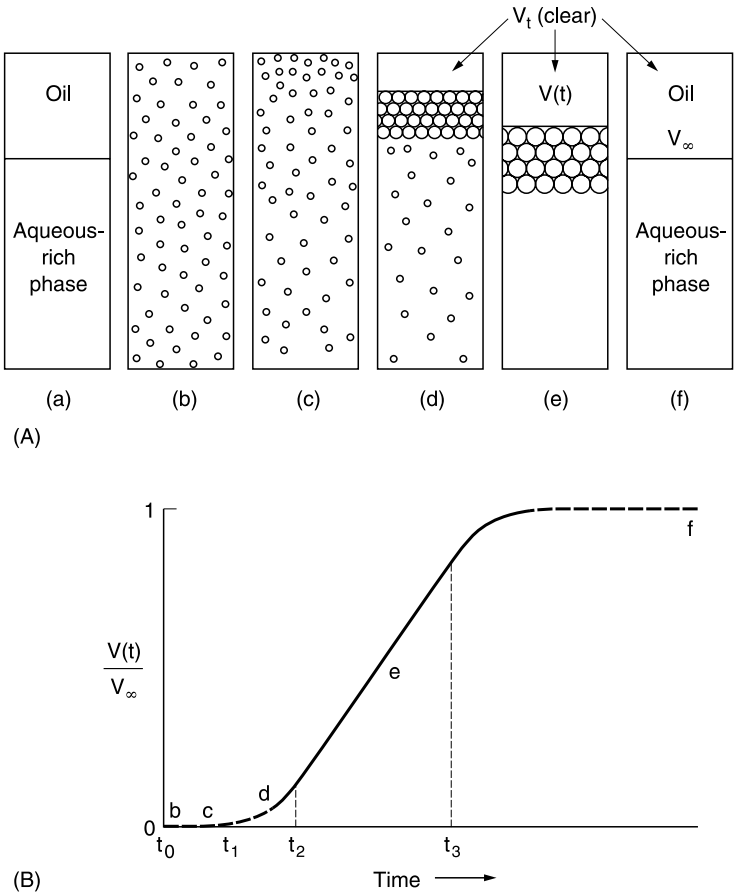

FIGURE 1.25 (A) Commonly observed sequence of events in separation processes. Schematic sequence of direct observations: (a) Before shaking: equilibrated volumes. (b) Just after stopping shaking: $t = 0$. Macroemulsion of oil phase in aqueous phase. (c) Droplets of oil have migrated toward top of aqueous phase, but no appreciable coalescence is detectable. $t_0 < t < t_1$. (d) Appreciable coalescence of oil droplets; V_t increasing. Note larger droplet size just below clear layer, and sedimentation from lower part of aqueous phase still in progress. $t_1 < t < t_2$. (e) Sedimentation effectively complete. Coalescence of droplets continues in layer at top of aqueous phase. $t_2 < t < t_3$. (f) Separation complete. $t \gg t_3$. (B) Schematic kinetic curve of separation, corresponding to conditions in (A). (Parts A and B after I.B. Ivanov, R.K. Jain, P. Somasundaran, and T.T. Traykov, in *Solution Behavior of Surfactants*, Vol 2 (K.L. Mittal, ed.), Plenum Press, New York, 1979, p. 817.)

at $t < \tau_{sed}$. They interpret the time $t < \tau_{sed}$ as being determined by the mean velocity of the translating droplet and identify averaged velocity with the velocity corresponding to averaged radius $\bar{r}$.

For the droplet velocity characterization, the radius, the density difference $\Delta\rho$, and the viscosity of the external phase μ were varied and measured in a wide range. For τ_{min} a rather good correlation between the measured and calculated values is established. It means that the flocculation influence on the droplet dimension and velocity was weak.

Comparing this result with the delineation procedure characterized in Figure 1.24, one concludes that the droplet dimensions in the experiment in Ref. 158 were large. They corresponded to the higher domain in Figure 1.24.

Unfortunately, a direct measurement of the droplet dimension was not undertaken in Ref. 158. However, the conclusion can be confirmed by the comparison of the Stokesian droplet velocity and velocity from the measured effective sedimentation time $\tau_{\min}$. Substituting the measured values of μ and $\Delta\rho$ in the Stokesian expression yields $\bar{r}$. Its value exceeds 5 to 10 μm; that is, it corresponds to the highest domain in Figure 1.24. This is not surprising because the mini-emulsions were prepared by gently shaking by hand. The authors recognize the serious restrictions with respect to droplet dimensions in their investigations.

Both the investigations by Melik and Fogler [15] and by Ostrovsky and Good [158] emphasize the interdependence of the kinetic and aggregative types of emulsion instability and the importance of this topic. Melik and Fogler introduce this topic in its theoretical aspect. Ostrovsky and Good make something similar in an experimental approach. Their "two-parameter methodology" is a step forward as compared to the traditional methodology [159–161]. It is common [159–161] to report the time for the appearance of a given fractional volume (e.g., 50% of the clear phase) without any attempt to distinguish between creaming and coalescence.

The experimental system in investigations [158] was a set of surfactant–brine–oil–co-surfactant mixtures that were relevant to the optimization of composition for enhanced oil recovery [162,163].

In this system, the lower phase was a microemulsion. This choice of external phase gave opportunity to change $\Delta\rho$ and μ in a wide range of compositions. However, the buoyant droplets can interact in another way in a microemulsion environment. The closest separation between two drop surfaces h_0 can be small and approach the dimension of the microemulsion droplet. The discrete nature of the microemulsion cannot be neglected in the interlayer environment between interacting droplets of the macroemulsion.

1.9 COUPLING OF FLOCCULATION AND COALESCENCE IN DILUTE OIL-IN-WATER EMULSIONS

1.9.1 General

1.9.1.1 Kinetic and Thermodynamic Stability in Macroemulsions and Mini-Emulsions

The majority of emulsion technology problems relate to the stabilization and destabilization of emulsions [29,164–169]. Despite the existence of many fundamental studies related to the stability of emulsions, the extreme variability and complexity of the systems involved in any specific application often pushes the oil industry to achieve technologically applicable results without developing a detailed understanding of the fundamental processes. Nevertheless, since in most cases technological success requires the design of emulsions with a very delicate equilibrium between stability and instability, a better understanding of the mechanisms of stabilization and destabilization might lead to significant break-throughs in technology.

Notwithstanding their thermodynamic instability, many emulsions are kinetically stable and do not change appreciably for a prolonged period. These systems exist in the metastable state [1,2,30,34,170–173]. The fundamentals of emulsion stability (destabilization) comprise emulsion surface chemistry and physicochemical kinetics.

In contrast to the large success in industrial applications of emulsion surface chemistry the potential of physicochemical kinetics as the basis for emulsion dynamics modeling is almost not

used in emulsion technology. This situation has started to change during the last decade. Although the coupling of the subprocesses in emulsion dynamics modeling (EDM) continues to represent a large problem yet not solved, models are elaborated for (1) macroemulsions [172,174–180] and (2) mini-emulsions [181–188], for long and short lifetimes of thin emulsion films.

1. For large droplets (larger than 10 to 30 μm) in macroemulsions the rate of thinning of the emulsion film formed between two approaching droplets is rather low and, correspondingly, the entire lifetime of an emulsion need not be short, even without surfactant stabilization of the film. For this case the notion of *kinetic stability* is introduced [172, 174–177] to denote the resistance of the film against *rupture during thinning*. The droplet deformation and flattening cause this strong resistance, described by the Reynolds equation [189,190]. According to theory, the role of this deformation [165,191,192] decreases rapidly with decreasing droplet dimension.
2. For small droplets (smaller than 5 to 10 μm) in mini-emulsions droplet deformation can be neglected, because the Reynolds drainage rate increases as R_d^{-5} [172,193] (R_d, the Reynolds film radius) and because the smaller the droplets, the smaller is their deformation [165,191,192].

In distinction from macroemulsions, where the kinetic stability is the manifestation of droplet–droplet hydrodynamic interaction and droplet deformation, in mini-emulsion the kinetic stability is the manifestation of the interplay between surface forces and Brownian movement [181]. As the molecular forces of attraction decrease linearly with decreasing droplet dimension, namely approximately 10 times at the transition from macroemulsions to mini-emulsions, the potential minimum of droplet–droplet interaction (secondary minimum) decreases and for mini-emulsions thus depth can be evaluated as 1.1 to 1.5 kT [173,194]. At this low energy Brownian movement causes droplet doublet disaggregation after a short time (the doublet fragmentation time, τ_d). If this time is shorter than the lifetime of the thin film, rapid decrease in the total droplet concentration (t.d.c) is prevented (restricted by the coalescence time, τ_c), i.e., stability is achieved due to this kinetic mechanism [181].

1.9.1.2 Current State of Emulsion Stability Science

A large imbalance exists between knowledge concerning kinetic stability and thermodynamic stability. Main attention has been paid to *kinetic stability* for both macroemulsions [174–180] and mini-emulsions [181–188]. As a result, the droplet–droplet interaction and the collective processes in dilute emulsions are quantified [10,195] and important experimental investigations are made [185,186,196]. Some models are elaborated for the entire process of coalescence in concentrated emulsions as well [197,198]. Given thermodynamic stability, a thin interdroplet film can be metastable.

In contrast to the large achievements in investigations of kinetic stability modest attention has been paid to the fundamentals of the thermodynamic stability in emulsions, especially regarding the surfactant adsorption layer's influence on the coalescence time. There are several investigations devoted to the surface chemistry of adsorption related to emulsification and demulsification. However, the link between the chemical nature of an adsorption layer, its structure, and the coalescence time is not yet quantified.

A premise for such quantification is the theory of a foam bilayer lifetime [199]. The main notions of this theory is similar to the theory of Derjaguin et al. [200,201]. However, the theory [199] is specified for amphiphile foam films, it is elaborated in detail, and is proven by experiment

with water soluble amphiphiles, such as sodium dodecylsulfate [202]. As the dependence of the rupture of the emulsion film on surfactant concentration is similar to that for a foam film, the modification of theory with respect to emulsions may be possible. Although this modification is desirable the specification of theory for a given surfactant will not be trivial, since the parameters in the equation for the lifetime [201] are unknown and their determination not easy. As the theory [199,203] is proposed for amphiphiles and since a wider class of chemical compounds can stabilize emulsions, the film rupture mechanism [200] is not universal regarding emulsions.

Thus, in contrast to the quantification of kinetic stability, the empirical approach continues to predominate regarding thermodynamic stability. Meanwhile, thermodynamic stability provides greater opportunity for long-term stabilization of emulsions, than does kinetic. This means that the experimental characterization of thermodynamic stability, i.e., the measurement of coalescence time, is of major importance.

1.9.1.3 The Specificity of Emulsion Characterization

Generalized emulsion characterization, i.e., measurement of droplet size distribution, electrokinetic potential, Hamaker constant, etc., is not always sufficient. Thermodynamic stability with respect to bilayer rupture cannot be quantified with such a characterization procedure alone. Consequently, measurement of the coalescence time τ_c is of major importance for an evaluation of emulsion stability; it is an important and specific parameter of emulsion characterization.

The current state of mini-emulsion characterization neglects the importance of τ_c measurement. A practice for τ_c measurement is practically absent with the exception of only a few papers, considered in this chapter. Meanwhile, many papers devoted to issues more or less related to emulsion stability do not discuss τ_c measurement. One reason for this scientifically and technologically unfavorable situation in which emulsions are incompletely characterized may originate from a lack of devices enabling τ_c measurement.

1.9.1.4 Scope of Section 9

This section is focused on kinetic stability in mini-emulsions with emphasis on the coupled destabilizing subprocesses. In general there are three coupled subprocesses that will influence the rate of destabilization and phase separation in emulsions. These are aggregation, coalescence, and floc fragmentation. Often, irreversible aggregation is called coagulation and the term flocculation is used for reversible aggregation [199,204]. Ostwald ripening [205,206] coupled [182] with aggregation and fragmentation is a separate topic which will be not considered here.

A simplified theory is available for the coupling of coalescence and flocculation in emulsions void of larger flocs. This theory is considered in Section 1.9.2 and will assist in the consideration of the more complicated theory of coupling of coalescence and coagulation (Section 1.9.3). The experimental investigations are described in parallel. Section 1.9.4 is devoted to the theory of doublet fragmentation time and its measurement, as this characterizes an emulsion regarding fragmentation and because its measurement is an important source of information about surface forces and the pair interaction potential. The discrimination between conditions for coupling of coalescence with coagulation or with flocculation is considered in Section 1.9.5. The quantification of kinetic stability creates new opportunities for long-term prediction of mini-emulsion stability, for stability optimization, and for characterization with the standardization of τ_c and τ_d measurements. This forms the base for emulsion dynamics modeling (Section 1.9.6).

1.9.2 Coupling of Coalescence and Flocculation

1.9.2.1 Singlet–Doublet Quasi-Equilibrium

Each process among the three processes under consideration is characterized by a characteristic time, namely τ_{Sm}, τ_d, and τ_c. The Smoluchowski time [3], τ_{Sm}, gives the average time between droplet collisions. If the time between two collisions is shorter than τ_d a doublet can transform into a triplet before it spontaneously disrupts. In the opposite case, i.e., at

$$\tau_{Sm} \gg \tau_d \tag{1.121}$$

the probability for a doublet to transform into a triplet is very low because the disruption of the doublet occurs much earlier than its collision with a singlet. The rate of multiplet formation is very low for

$$\mathrm{Rev} = \frac{\tau_d}{\tau_{Sm}} \ll 1 \tag{1.122}$$

where we introduce the notation Rev for small values of the ratio corresponding to the reversibility of aggregation and a singlet–doublet quasi-equilibrium.

The kinetic equation for reversible flocculation in a dilute monodisperse o/w emulsion when neglecting coalescence is [14,207,208]

$$\frac{dn_2}{dt} = \frac{n_1^2}{\tau_{Sm}} - \frac{n_2}{\tau_d} \tag{1.123}$$

where n_1 and n_2 are the dimensionless concentrations of doublets and singlets, $n_1 = N_1/N_{10}$, $n_2 = N_2/N_{10}$, N_1 and N_2 are the concentrations of singlets and doublets and N_{10} is the initial concentration, and

$$\tau_{Sm} = \left(\frac{4kT}{3\eta} N_{10}\right)^{-1} = \left(K_f N_{10}\right)^{-1} \tag{1.124}$$

where k is the Boltzmann constant, T is the absolute temperature, η is the viscosity of water. For aqueous dispersions at 25 °C, $K_f = \frac{4kT}{3\eta} = 6 \cdot 10^{-18}$ m^3 s^{-1}. The singlet concentration decreases with time due to doublet formation, while the doublet concentration increases. As a result, the rates of aggregation and floc fragmentation will approach each other. Correspondingly, the change in the number of doublets $dn_2/dt = 0$. Thus, a dynamic singlet–doublet equilibrium (s.d.e.) is established:

$$n_{2eq} = \frac{\tau_d}{\tau_{Sm}} n_{1eq}^2 \tag{1.125}$$

At condition 1.122 it follows from Equation 1.125 that

$$n_{1eq} \cong 1, \; N_{1eq} = N_{10} \tag{1.126}$$

$$N_2 = \mathrm{Re}\; v \cdot N_{10} \text{ or } n_2 \ll 1 \tag{1.127}$$

Thus, at small values of Rev the s.d.e. is established with only small deviations in the singlet equilibrium concentration from the initial concentration (Equation 1.126). The doublet concentration is very low compared to the singlet concentration, and the multiplet concentration is very

low compared to the doublet concentration. The last statement follows from a comparison of the production rates of doublets and triplets. The doublets appear due to singlet–singlet collisions, while the triplets appear due to singlet–doublet collisions. The latter rate is lower due to the low doublet concentration. The ratio of the number of singlet–doublet collisions to the number of singlet–singlet collisions is proportional to Rev.

1.9.2.2 Kinetic Equation for Coupling of Flocculation and Intradoublet Coalescence in Monodisperse Emulsions

Both the rate of doublet disaggregation and the rate of intradoublet coalescence are proportional to the momentary doublet concentration. This leads [181,187] to a generalization of Equation 1.123:

$$\frac{dn_2}{dt} = \frac{n_1^2}{\tau_{Sm}} - n_2\left(\frac{1}{\tau_d} + \frac{1}{\tau_c}\right) \tag{1.128}$$

There are two unknown functions in Equation 1.128, so an additional equation is needed. This equation describes the decrease in the droplet concentration caused by coalescence:

$$\frac{d}{dt}(n_1 + 2n_2) = -\frac{n_2}{\tau_c} \tag{1.129}$$

The initial conditions are

$$n_2|_{t=0} = 0 \tag{1.130}$$

$$\left.\frac{dn_2}{dt}\right|_{t=0} = \frac{n_{10}}{\tau_{Sm}} \tag{1.131}$$

Condition 1.131 follows from Equations 1.128 and 1.129. The solution of the set of Equations 1.128 and 1.129 with account for boundary conditions 1.130 and 1.131 is a superposition of two exponents [181,187]. In the case

$$\tau_c \gg \tau_d \tag{1.132}$$

the solution simplifies [181,187] to

$$n_2(t) = \frac{\tau_d}{\tau_{Sm}}\left[\exp\left(-\frac{2\tau_d t}{\tau_{Sm}\tau_c}\right) - \exp\left(-\frac{t}{\tau_d}\right)\right] \tag{1.133}$$

Equation 1.133, as compared to Equations 1.125 and 1.126, corresponds to the s.d.e. if the expression in the second brackets equals one. In the time interval

$$\tau_d < t < \tau \tag{1.134}$$

where

$$\tau = \tau_c \frac{\tau_{Sm}}{2\tau_d} \tag{1.135}$$

the first term in the second brackets approximately equals 1, while the second one decreases from 1 to a very small value. Thus, the s.d.e. is established during the time τ_d and preserves during the longer time interval (Equation 1.134).

For times longer than τ there is no reason to apply Equation 1.133 since the condition to linearize Equation 1.128 is no longer valid with the concentration decrease. At the beginning of the process the doublet concentration increases, while later coalescence predominates and the doublet concentration decreases. Thus, function 1.133 has a maximum [181,187].

1.9.2.3 Coalescence in a Singlet–Doublet System at Quasi-Equilibrium

After a time $t_{\max}$ a slow decrease in the doublet concentration takes place simultaneously with the more rapid processes of aggregation and disaggregation. Naturally, an exact singlet–doublet equilibrium is not valid due to the continuous decrease in the doublet concentration. However, the slower the coalescence, the smaller is the deviation from the momentary dynamic equilibrium with respect to the aggregation–disaggregation processes.

It is reasonable to neglect the deviation from the momentary doublet–singlet equilibrium with the condition

$$\frac{dn_2}{dt} \ll \frac{n_2}{\tau_d} \tag{1.136}$$

Indeed, for this condition the derivative in Equation 1.123 can be omitted, which corresponds to s.d.e. characterized by Equation 1.125.

It turns out [181,185–187] that the deviation from s.d.e. is negligible as the condition 1.136 is valid, i.e., for conditions 1.122 and 1.132. For these conditions the fragmentation of flocs influences the coalescence kinetics which can be represented as a three-stage process, as illustrated in Figure 1.26. During a rather short time τ_d the approach to s.d.e. takes place, i.e., a rather rapid increase in the doublet concentration (stage 1). During the next time interval $\tau_d < t < t_{\max}$ the same process continues. However, the rate of doublet formation declines due to coalescence (stage 2). The exact equilibrium between the doublet formation and their disappearance due to coalescence takes place at the time $t_{\max}$ when the doublet concentration reaches its maximum value $n_2(t_{\max})$. During the third stage, when $t > t_{\max}$, the rate of doublet fragmentation is lower than the rate of formation, because of the coalescence within doublets. This causes a slow monotonous decrease in the concentration. Taking into account the s.d.e. (Equations 1.125 and 1.127) Equation 1.129 can be expressed as

$$\frac{dn_1}{dt} = -\frac{\tau_d}{\tau_{Sm}\tau_c} n_1^2 \tag{1.137}$$

The result of the integration of Equation 1.137 can be simplified to

$$n_1(t) = \frac{n_1(t_{\max})}{1 + n_1(t_{\max})\dfrac{t}{2\tau}} \cong \left(1 + \frac{t}{2\tau}\right)^{-1} \tag{1.138}$$

with a small deviation in $n_1(t_{\max})$ from 1. Differing from the preceding stages when the decrease in the droplet concentration caused by coalescence is small, a large decrease is now possible during the third stage. Thus, this is the most important stage of the coalescence kinetics.

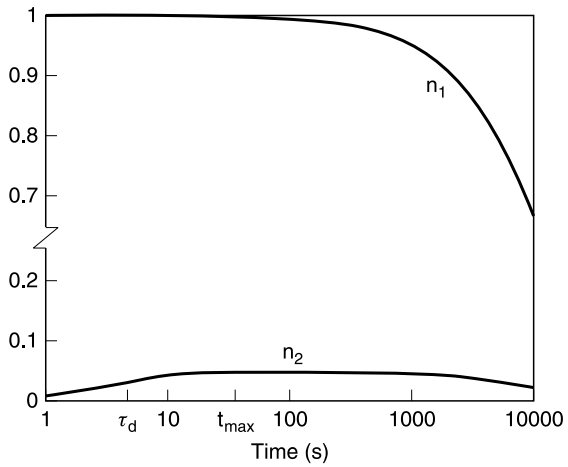

FIGURE 1.26 Three stages in the coupling of aggregation, fragmentation, and coalescence at the condition $\tau_d \ll \tau_{Sm} \ll \tau_c$. Initially, the doublet concentration n_2 is very low and the rates of doublet fragmentation and of coalescence are correspondingly low compared to the rate of aggregation (first stage, no coupling). Due to increasing n_2 the fragmentation rate increases and equals the aggregation rate at $t_{\max}$ (exact singlet–doublet equilibrium). The growth in n_2 stops at $t_{\max}$ (second stage, coupling of aggregation and fragmentation). Intradoublet coalescence causes a slight deviation from exact s.d.e. to arise at $t > t_{\max}$, and the singlet concentration n_1 and the doublet concentration decrease due to intradoublet coalescence (third stage, coupling of aggregation, fragmentation, and coalescence). n_1 and n_2 are dimensionless, $n_1 = N_1/N_{10}$, $n_2 = N_2/N_{10}$, N_{10} is the initial singlet concentration. (From S.S. Dukhin and J. Sjöblom, *J. Dispersion Sci. Technol.* 19: 311 (1998).)

1.9.2.4 Reduced Role of Fragmentation with Decreasing τ_c

With decreasing τ_c, condition 1.132 is violated and new qualitative features of the destabilization process not discussed in Refs. 185–187 arise. As the ratio τ_c/τ_d diminishes and

$$\tau_c < \tau_d \tag{1.139}$$

the s.d.e. is violated because a larger part of the doublets disappear due to coalescence. Correspondingly, the smaller the ratio τ_c/τ_d the smaller is the fragmentation rate in comparison with the aggregation rate, i.e., the larger the deviation from s.d.e. In the extreme case

$$\tau_c \ll \tau_d \tag{1.140}$$

the fragmentation role in s.d.e. can be neglected. This means that almost any act of aggregation is accompanied by coalescence after the short doublet lifetime. Neglecting this time in comparison with τ_{Sm} in agreement with condition 1.121 one concludes that any act of aggregation is accompanied by the disappearance of one singlet:

$$\frac{dn_1}{dt} = -\frac{n_1^2}{\tau_{Sm}} \tag{1.141}$$

This leads to a decrease in the singlet concentration described by an equation similar to the Smoluchowski equation for rapid coagulation:

$$n_1(t) = (1 + t/\tau_{Sm})^{-1} \tag{1.142}$$

The Smoluchowski equation describing the singlet time evolution does not coincide with Equation 1.142. The peculiarity of Equation 1.142 is that it describes the kinetics of coupled aggregation and coalescence with a negligible fragmentation rate. Due to rapid coalescence, doublet transformation into multiplets is almost impossible at condition 1.121.

The coupling of aggregation, fragmentation, and coalescence in the more general case described by condition 1.139 leads to equation

$$n_1(t) = \frac{n_1(t_{\max})}{1 + n_1(t_{\max})t/2\tau_g} \cong \left(1 + t/2\tau_g\right)^{-1} \qquad (t > \tau_d + \tau_c) \tag{1.143}$$

with a small deviation of $n_1(t_{\max})$ from 1 and

$$\tau_g = \frac{\tau_{Sm}(\tau_d + \tau_c)}{2\tau_d} \tag{1.144}$$

At conditions 1.121 and 1.132 $\tau_g \approx \tau$ and Equation 1.143 transforms into Equation 1.138. At conditions 1.121 and 1.140 $\tau_g \approx \tau_{Sm}$ and Equation 1.143 transforms into Equation 1.142. Equation 1.144 demonstrates the reduction of the role of fragmentation with decreasing τ_c. It is seen that at the transition from condition 1.139 to condition 1.140 τ_d cancels in Equation 1.141, i.e., the fragmentation role diminishes.

1.9.2.5 Experimental

1.9.2.5.1 Application of Video Enhanced Microscopy Combined with the Microslide Technique for Investigation of Singlet–Doublet Equilibrium and Intradoublet Coalescence [185–187]

Direct observation of doublets in the emulsion bulk is difficult because the doublets tend to move away from the focal plane. The microslide preparative technique can, however, be successfully applied, providing pseudo-bulk conditions. A microslide is a plane-parallel glass capillary of rectangular cross section. The bottom and top sides of the capillary are horizontal, and the gravity induced formation of a sediment or cream on one of the inner normal surfaces is rapidly completed due to the modest inner diameter of the slide. If both the volume fraction of droplets in an emulsion and the capillary height are small, the droplet coverage on the inside surface amounts to a few percent, and the analysis of results is rather simple. It can be seen through the microscope that the droplets which have sedimented onto the capillary surface participate in chaotic motion along the surface. This indicates that a thin layer of water separating the surface of the microslide from the droplets is preventing the main portion of droplets from adhering to the microslide surface, an action which would stop their Brownian motion.

During diffusion along the microslide ceiling the droplets collide. Some collisions lead to the formation of doublets. Direct visual observation enables evaluation of the doublet fragmentation time which varies in a broad range [183]. Another approach to doublet fragmentation time

determination is based on the evaluation of the average concentration of singlets and doublets and using the theory outlined above.

The application of the microslide preparative technique combined with video microscopy is promising and has enabled the measurement of the coupling of reversible flocculation and coalescence [185]. However, some experimental difficulties were encountered. Droplets could sometimes be seen sticking to the glass surface of the microslide.

1.9.2.5.2 Improving the Experimental Technique with the Use of Low Density Contrast Emulsions [186]

The sticking of droplets indicates a droplet–wall attraction and the existence of a secondary potential pit as that for the droplet–droplet attraction in a doublet. The droplet concentration within the pit is proportional to the concentration on its boundary. The latter decreases with a decrease in the density contrast.

The electrostatic barrier between the potential pit and the wall retards the rate of sticking. The lower the droplet flux through this barrier, the lower is the potential pit occupancy by droplets. Thus, an essential decrease in the rate of sticking is possible with decreasing density contrast.

O/W emulsions were prepared [186] by mixing dichlorodecane (DCD, volume fraction 1%) into a 5×10^{-5} M sodium dodecylsulfate (SDS) solution with a Silverson homogenizer. The oil phase was a 70:1 mixture of DCD, which is characterized by an extremely low density contrast to water and decane.

The droplet distribution along and across the slide was uniform [186]. This indicates that there was no gravity induced rolling either. One slide among 4 was examined for 2 weeks without any sticking being observed. The absence of the rolling and sticking phenomena allowed acquisition of rather accurate data concerning the time dependence of the droplet size distribution.

1.9.2.5.3 The Measurement of Coalescence Time and Doublet Fragmentation Time

The doublet fragmentation time was measured by direct real-time observation of the doublets on the screen and by analysis of series of images acquired with 1- to 3-min time intervals [201]. The formation and disruption/coalescence of a doublet could thus be determined.

The general form of the concentration dependence agrees with the theory. At $C \sim 3 \times 10^{-3}$ M, both theory and experiment yield times of about 1 min; at $C = 9 \times 10^{-3}$ M, these times exceed 10 min. For calculation of the doublet fragmentation time the electrokinetic potential was measured [187,202].

In experiments with different droplet concentrations it was established that the higher the initial droplet concentration, the higher the doublet concentration. This corresponds to the notion of singlet–doublet equilibrium. However, if the initial droplet concentration exceeds 200 to 300 per observed section of the microslide, multiplets predominate. Both the initial droplet concentration and size affect the rate of decrease in the droplet concentration. The larger the droplets, the smaller the concentration sufficient for the measurement of the rate of decrease in the droplet concentration. This agrees with the theory of doublet fragmentation time which increases with droplet dimension. Correspondingly, the probability for coalescence increases. These first series of experiments [185,187] were accomplished using toluene-in-water emulsions without the addition of a surfactant and decane-in-water emulsions stabilized by SDS. The obtained data concerning the influence of the electrolyte concentration and surface charge density were in agreement with the existing notions about the mechanism of coalescence. With increasing SDS concentration,

and correspondingly increasing surface potential, the rate of decrease in the droplet concentration is reduced.

Two methods were used for the measurement of the coalescence time [186,187]. Measurement of the time dependence for the concentrations of singlets and doublets and a comparison with Equation 1.129 enables an evaluation of the coalescence time. Further, information about the time dependence for singlets and the doublet fragmentation time may be used as well. These results in combination with Equations 1.138 and 1.135 determine the coalescence time. The good agreement between results obtained by these very different methods indicates that the exactness of the theory and experiments is not low.

In recent years several research groups have improved significantly the theoretical understanding of coalescence of droplet or bubbles. The new results [14,208–211] together with results of earlier investigations [212–216] have clarified the role of double-layer interaction in the elementary act of coalescence.

DLVO theory was applied [217,218] for the description of "spontaneous" and "forced" thinning of the liquid film separating the droplets. These experimental results and DLVO theory were used [217] for the interpretation of the reported visual study of coalescence of oil droplets 70 to 140 μm in diameter in water over a wide pH interval. A comparison based on DLVO theory and these experimental data led the authors to conclude [217] that "if the total interaction energy is close to zero or has a positive slope in the critical thickness range, i.e., between 30 and 50 nm, the oil drops should be expected to coalesce." In the second paper [218], where both ionic strength and pH effects were studied, coalescence was observed at constant pH values of 5.7 and 10.9, when the Debye thickness was less than 5 nm. The main trend in our experiments and in Refs. 217 and 218 are in accord, because it was difficult to establish the decrease in t.d.c. at NaCl concentrations lower than 5×10^{-3} M, i.e., DL thicknesses larger than 5 nm. An almost quantitative coincidence in the double layer influence on coalescence established in our work for micrometer-sized droplets and in Refs. 217 and 218 for almost 100 times larger droplets is important for general knowledge about coalescence.

1.9.2.6 Perspective for Generalization of the Theory for Coupling of Coalescence and Flocculation

The proposed theory for coupling of coalescence and flocculation at s.d.e. enables the proposal of some important applications (Section 1.9.6). At the same time generalized theory is necessary, since the role of multiplets increases after a long time or with a higher initial concentration. At least two approaches to this difficult task are seen.

According to our videomicroscopic observations there are large peculiarities in the structure and behavior of multiplets arising at conditions near to s.d.e. These peculiarities can be interpreted as the manifestation of quasi-equilibrium, comprising singlets, doublets, and multiplets. Similar to doublets, the lifetime of triplets, tetraplets etc. can be short due to fragmentation and coalescence. This can be valid for multiplets with an "open" structure, in distinction from another structure which can be called "closed." In open multiplets any droplet has no more than 1 to 2 contacts with other droplets, which corresponds to a linear chain-like structure. This causes easy fragmentation, especially for the extreme droplets within a chain. The "closed" aggregates have a more dense and isometric structure, in which droplets may have more than 2 contacts with neighboring droplets. As a result, fragmentation is more difficult and the frequency is lower.

The recent progress in theory of aggregation with fragmentation [219–223] for a suspension creates a premise for a theoretical extension towards emulsions. However, the necessity in accounting for coalescence makes this task a difficult one.

1.9.3 Coupling of Coalescence and Coagulation

1.9.3.1 General

For emulsion characterization the notation n_1 represents the number density of single droplets and n_i the number density of aggregates comprising i droplets ($i = 2, 3 \ldots$). The total number density of single droplets and all kinds of aggregates is given by

$$n = \sum_{i=1}^{\infty} n_i \tag{1.145}$$

This characterization corresponds with Smoluchowski theory [3]. To characterize coalescence, the total number of individual droplets moving freely, plus the number of droplets included in all kinds of aggregates, n_T

$$n_T = \sum_{i=1}^{\infty} i n_i \tag{1.146}$$

is introduced as well.

In distinction from the Smoluchowski theory for suspensions, which predicts the time dependence of the concentration of all kinds of aggregates, the time dependence for the total droplet number can be predicted at the current state of emulsion dynamics theory.

The quantification of coagulation within the theory of coupled coagulation and coalescence (CCC theory) is based on the Smoluchowski theory of perikinetic coagulation. Correspondingly, all restrictions inherent to Smoluchowski theory of Brownian coagulation preserve in the CCC theory. This means that creaming and gravitational coagulation are not accounted for. A variant of Smoluchowski theory specified with regard for gravitational coagulation is well known [4]. However, its application is very difficult because the rate constant of collisions induced by gravity depends on droplet dimension [173]. Due to the weak particle (aggregate) dimension dependence of the rate constants for Brownian collisions Smoluchowski theory is valid for polydisperse suspensions and remains valid as polydisperse aggregates arise. Unfortunately, this advantage of the Smoluchowski theory can almost disappear when combined with the coalescence theory, because the coalescence rate coefficients are sensitive to droplet dimension. Thus, droplet and aggregate polydispersity does not strongly decrease the exactness of the description of coagulation in the CCC theory, while the exactness of coalescence description can be severely reduced.

Although the coalescence influence on the Brownian coagulation rate coefficient can be neglected, its influence on the final equations of the Smoluchowski theory remains. It can be shown that Smoluchowski's equation for the total number of particles

$$n(t) = \left(1 + \frac{t}{\tau_{Sm}}\right)^{-1} \tag{1.147}$$

remains valid, while in parallel the equations for the singlet and aggregate concentrations cannot be used with account for coalescence. Regarding coupled coagulation and coalescence, the Smoluchowski equation for $n_1(t)$ is not exact because it does not take into account the singlet formation caused by coalescence within doublets.

The coalescence within an aggregate consisting of i droplet is accompanied by the aggregate transforming into an aggregate consisting of $(i-1)$ droplets. As coalescence changes the aggregate

type only, the total quantity of aggregates and singlets does not change. This means that the Smoluchowski function $n(t)$ does not change during coalescence, since Smoluchowski defined the total quantity of particles as consisting of aggregates and singlets.

1.9.3.2 Average Models

Average models do not assign rate constants to each possibility for coalescence within the aggregates, but deal with certain averaged characteristics of the process. The models in Refs. 9 and 10 introduce the average number of drops in an aggregate m, because the number of films in an aggregate n_f and m are interconnected. For a linear aggregate

$$n_f = m - 1 \tag{1.148}$$

As the coalescence rate for one film is characterized by τ_c^{-1}, the decrease in the average droplet quantity in an aggregate is n_f times larger. This is taken into account in the model by van den Tempel for simultaneous droplet quantity increase due to aggregation and decrease due to coalescence. Van den Tempel formulates the equation which describes the time dependence for the average number of droplets in an aggregate as

$$\frac{dm}{dt} = K_f N_{10} - \tau_c^{-1}(m - 1) \tag{1.149}$$

where the first term is derived using Smoluchowski theory.

The total number of droplets n_T is the sum of single droplets $n_1(t)$ and the droplets within aggregates:

$$n_T(t) = n_1(t) + n_v(t)m(t) \tag{1.150}$$

where n_v is the aggregate number. The latter can be expressed as

$$n_v(t) = n(t) - n_1(t) \tag{1.151}$$

Both terms are expressed by Smoluchowski theory. The integration of Equation 1.149 and the substitution of the result into Equation 1.150 yield the time dependence $n_T(t)$ according to the van den Tempel model.

1.9.3.2.1 The Model by Borwankar et al.

In Ref. 10 the van den Tempel model is criticized and improved through the elimination of Equation 1.149. The authors point out that the "incoming" aggregates which cause the increase in m have themselves undergone coalescence. This is not taken into account in the first term of the r.h.s. of Equation 1.149. Instead of taking a balance on each aggregate (as van den Tempel did) Borwankar et al. took an overall balance on all particles in the emulsion. For linear aggregates, the total number of films in the emulsion is given by

$$n_f n_v = (m - 1)n_v \tag{1.152}$$

Thus, instead of Equation 1.149 the differential equation for n_T follows:

$$-\frac{dn_T}{dt} = \tau_c^{-1}(m-1)n_v \tag{1.153}$$

where m can be expressed through n_T using Equation 1.150. The advantage of this equation in comparison with Equation 1.149 is obvious. However, there is a common disadvantage of both theories, caused with the use of the Smoluchowski equation for $n_1(t)$. Coalescence does not change the total particle concentration $n(t)$, but changes $n_1(t)$ and correspondingly $n_V(t)$, according to Equation 1.151.

The application of Smoluchowski theory in the quantification of the coupling of coalescence and coagulation has to be restricted with the use of the total particle concentration $n(t)$ only. The average models of van den Tempel and Borwankar et al. do not meet this demand.

The theory by Danov et al. [195] does not contradict this demand, which makes it more correct than the preceding theories. Among the Smoluchowski results the function $n(t)$ only is present in the final equations of this theory. Although the exactness of averaged models is reduced due to the violation of the restriction in the use of Smoluchowski theory, results for some limiting cases are not erroneous.

1.9.3.2.2 The Limiting Cases of Fast and Slow Coalescence

Two limiting cases can be distinguished:

1. The rate of coalescence is much greater than that of flocculation (rapid coalescence):

$$\tau_c^{-1} \gg \tau_{Sm}^{-1} \tag{1.154}$$

2. The rate of flocculation is much greater than that of coalescence (slow coalescence):

$$\tau_c^{-1} << \tau_{Sm}^{-1} \tag{1.155}$$

According to general regularities of physicochemical kinetics the slowest process is rate controlling. If the coagulation step is rate-controlling, namely when condition 1.154 is valid, then the coalescence is rapid and the general equation of the theory in Ref. 10 is reduced to second order kinetics, i.e., to Smoluchowski's equation (1.147). Flocs composed of three, four, etc. droplets cannot be formed, because of rapid coalescence within the floc. In this case the structure of the flocs becomes irrelevant.

At first glance the coagulation rate has not manifested itself in the entire destabilization process in the case of slow coalescence (condition 1.155). At any given moment the decrease in the total droplet concentration is proportional to the momentary total droplet concentration (first order kinetics), which causes an exponential decrease with time:

$$n = \exp\left(-\frac{t}{\tau_c}\right) \tag{1.156}$$

However, this equation cannot be valid for an initial short period of time, because at the initial moment there are no aggregates and their quantity continues to be low during a short time. This means that the coagulation is limiting during an initial time at any slow coalescence rate. This example illustrates the necessity of a more exact approach than that which uses average models. This was done by Danov et al. [195].

1.9.3.3 DIGB Model for the Simultaneous Processes of Coagulation and Coalescence

This kinetic model, proposed by Danov, Ivanov, Gurkov, and Borwankar, is called the DIGB model for the sake of brevity. Danov et al. [195] generalized the Smoluchowski scheme (Figure 1.27(a)) to account for droplet coalescence within flocs. Any aggregate (floc) composed of k particles can partially coalesce to become an aggregate of i particles ($1 < i < k$), with the rate constant being $K_c^{k,i}$ (Figure 1.27(b)). This aggregate is further involved in the flocculation scheme, which makes the flocculation and coalescence processes interdependent. Therefore, the system exhibiting both flocculation and coalescence is described by a combination of the schemes 1 and 2.

$$\frac{dn_k}{dt} = \sum_{i=1}^{k-1} K_f^{i,k-i} n_i n_{k-i} - 2\sum_{i=1}^{\infty} K_f^{k,i} n_k n_i + \sum_{i=k+1}^{\infty} K_c^{i,k} n_i - \sum_{i=1}^{k-1} K_c^{k,i} n_k \tag{1.157}$$

Equation 1.157 is multiplied by k and summed up for all k, that yields the equation for n_T which is expressed through double sums. The change of the operation sequence in these sums leads to the important and convenient equation

$$\frac{dn_T}{dt} = \sum_{k=1}^{\infty} k \sum_{i=k+1}^{\infty} K_c^{i,k} n_i - \sum_{i=2}^{\infty} k \sum_{i=1}^{k-1} K_c^{k,i} n_k \tag{1.158}$$

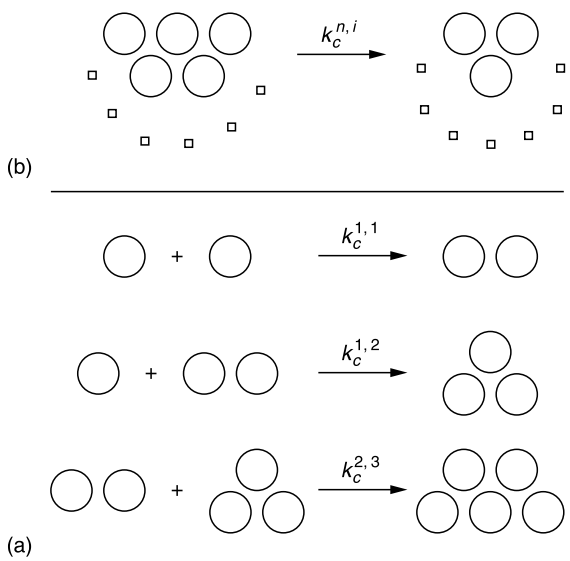

FIGURE 1.27 (a) Model of flocculation according to the Smoluchowski scheme. (b) Coalescence in an aggregate of k particles to become an aggregate of i particles, with a rate constant $K_c^{k,i}$, $1 < i < k$. (From K.D. Danov, I.B. Ivanov, T.D. Gurkov, and R.P. Borwankar, *J. Colloid Interface Sci.* 167: 8 (1994).)

Afterwards, a total rate coefficient referring to complete coalescence of the *i*th aggregate

$$K_{c,T}^{i} = \sum_{k=1}^{i-1} (i-k) K_c^{i,k} \quad i = 2, 3 \tag{1.159}$$

is introduced. For linearly built aggregates is derived

$$K_{c,T}^{i} = K_c^{2,1}(i-1) \tag{1.160}$$

With this expression for $K_{c,T}^{i}$, using also Equations 1.145 and 1.146, Equation 1.158 is transformed into

$$\frac{dn_T}{dt} = -K_c^{2,1}(n_T - n) \tag{1.161}$$

The integration result of this first order linear differential equation is well known and is represented in general form without specification of $n(t)$ (equation 1.18 in Ref. 195). An interesting peculiarity of this important derivation is the disappearance of terms, related to coagulation at the transition from the equation set 1.157 to the main equation (1.158). This corresponds to the fact that the total quantity of droplets does not change due to coagulation; it decreases due to coalescence only.

The coagulation regularity manifests itself in the $n(t)$ dependence, arising in Equation 1.161. It creates the illusion that Equation 1.161 can be specified for any $n(t)$ function corresponding to any subprocess affecting the droplet aggregate distribution. For example, the gravitational coagulation theory leads to a function $n_g(t)$ [4], but it does not create the opportunity to describe the gravitational coagulation coupling with coalescence by means of substituting $n_g(t)$ into the integral of Equation 1.161. As the coalescence influences the gravitational coagulation another function has to be substituted into Equation 1.161 instead of $n_g(t)$. This function has to be derived with account for the coupling of coalescence and coagulation. One concludes that Equation 1.161 cannot be used, because its derivation assumes that the coupling of gravitational coagulation (or another process) and coalescence is already quantified.

A happy exception is Brownian coagulation and its modeling by Smoluchowski with the coagulation rate coefficients, of which sensitivity to aggregate structure and coalescence is low. The substitution of function 1.147 into the integral of Equation 1.161 yields the equation, characterizing the coupling of coalescence and Brownian coagulation [195].

In fractal theory [224] it is established that diffusion limited aggregates and diffusion limited cluster–cluster aggregates are built up linearly. This can simplify application of the DIGB model. However, the diffusivity of fractal aggregates [225] cannot be described by simple equations and Smoluchowski theory. This will cause coagulation rate coefficient dependence on aggregate structure, decreasing the exactness of Equation 1.161 when applied to fractal aggregates. However, there is no alternative to the DIGB model, which can be used as a crude but useful approximation in this case as well. In the absence of an alternative the DIGB model can be recommended for evaluation in the case of gravitational coagulation.

Danov et al. compare their theory with the predictions of averaged models for identical conditions. It turns out that if coalescence is much faster than flocculation, the predictions of the different models coincide. Conversely, for slow coalescence the results of the averaged models deviate considerably from the exact solution. These two results of the comparison are in agreement with the qualitative considerations in Section 1.9.3.2.

Data for the relative change in the total number of droplets as a function of time are presented in Figure 1.28 (from Ref. 195). Figures a to c refer to $K_F N_{10} = 0.1\ s^{-1}$ and the coalescence constant $K_c^{2,1}$ varies between 0.1 s^{-1} (a) and 0.001 s^{-1} (c). It is seen that the agreement between the Danov et al. and Borwankar et al. models is better the faster the coalescence, as was explained qualitatively above. The van den Tempel curves deviate considerably from the other two solutions.

For very long times, and irrespective of the values of the kinetic parameters, the model by Borwankar et al. [10] is close to the numerical solution. This is probably because the longer the time, the smaller is the concentration of single droplets. In this extreme case the error caused in the average models due to the influence of coalescence on the singlet concentration (not taken into account in the equation for $n(t)$) is negligible.

The shortcomings of the averaged models [9,10] and the advantages of the DIGB model are demonstrated in Ref. 195. However, the range of applicability of this model is restricted by many simplifications and the neglect of other subprocesses (see Section 1.9.3.1). An efficient analytical approach was made possible due to the neglect of the coalescence rate coefficient's dependence on the dimensions of both interacting droplets.

The model by Borwankar et al. was examined experimentally in Ref. 196. The emulsions were oil-in-water with soybean oil as the dispersed phase, volume fraction 30%, and number concentration 10^7 to 10^{10} cm^{-3}. The emulsions were gently stirred to prevent creaming during the aging study. A sample was placed on a glass slide, all aggregates were broken up, and the size of the individual droplets was measured. A rather good agreement with the theory was established. However, the fitting of the experimental data was accomplished using two model parameters, namely the coalescence and coagulation rate coefficients. For the last coefficient the optimal values (different for two emulsions) were obtained, strongly exceeding the Smoluchowski theory value (Section 1.9.2.1). An interpretation is that orthokinetic and perikinetic coagulation took place simultaneously due to stirring. Several experiments are known (discussed in Ref. 14) which demonstrate better agreement with the value for the coagulation constant predicted in Smoluchowski theory.

1.9.4 Doublet Fragmentation Time

1.9.4.1 Theory of Doublet Fragmentation Time

A doublet fragmentation was described by Chandrasekhar [226] by the diffusion of its droplets from the potential minimum, characterizing their attraction. The time scale for this process takes the form [110]

$$\tau_d = \frac{6\pi\eta a^3}{\kappa T} \exp(-U_{\min}/\kappa T) \tag{1.162}$$

where $U_{\min}$ is the depth of the potential minimum.

To derive the formula for the average lifetime of doublets Muller [227] considered the equilibrium in a system of doublets and singlets: that is, the number of doublets decomposing and forming are equal. Both processes are described by the standard diffusion flux J of particles in the force field of the particle that is regarded as central.

Each doublet is represented as an immovable particle with the second singlet "spread" around the central one over a spherical layer, which corresponds to the region of the potential well. The diffusion flux J of "escaping" particles is described by equations used in Fuchs' theory of slow coagulation. The first boundary condition corresponds to the assumption that the escaping particles

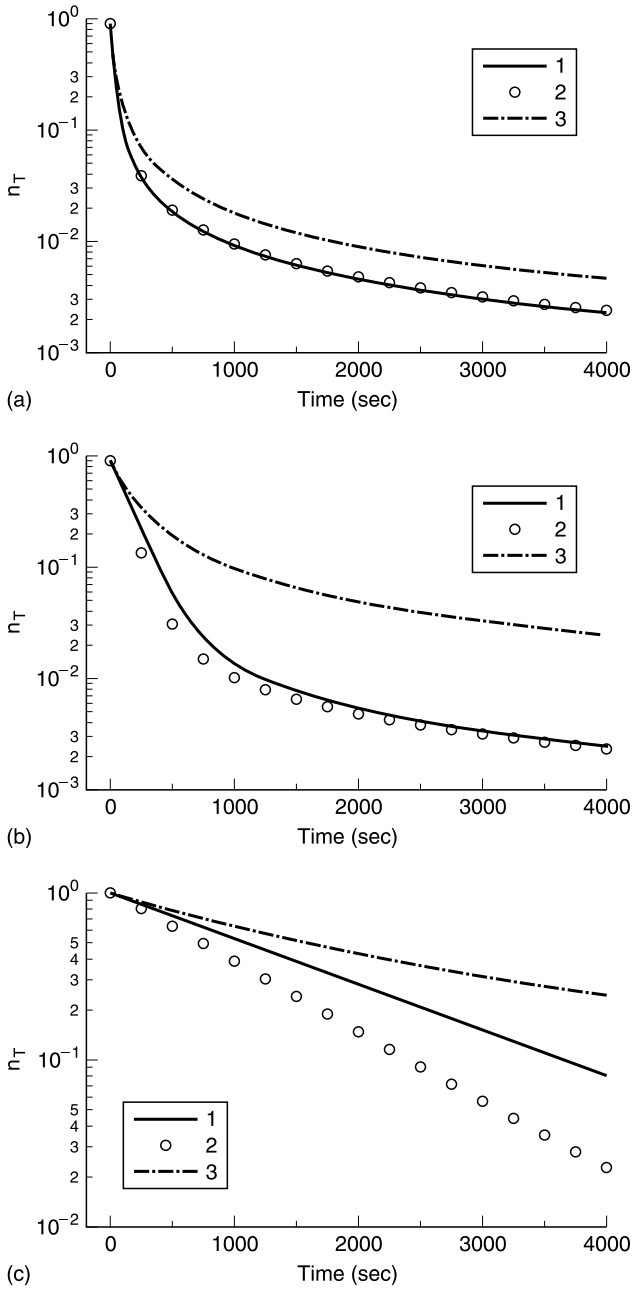

FIGURE 1.28 Relative change in the total number of droplets vs. time: initial number of primary particles $N_{10} = 1 \times 10^{10}$ cm^{-3}; curve 1, the numerical solution of the set Equation 1.157; curve 2, the model of Borwankar et al. [10] for diluted emulsions; curve 3, the model of van den Tempel [9]: (a) coalescence rate constant $K_c^{2,1} = 1 \times 10^{-1}$ s^{-1}; (b) $K_c^{2,1} = 1 \times 10^{-2}$ s^{-1}; (c) $K_c^{2,1} = 1 \times 10^{-3}$ s^{-1}. (From K.D. Danov, I.B. Ivanov, T.D. Gurkov, and R.P. Borwankar, *J. Colloid Interface Sci.* 167: 8 (1994).)

do not interact with other singlets. The second condition reflects the fact that the potential well contains exactly one particle.

At small separation between the droplets in a doublet the droplet diffusivity reduces because of the increasing hydrodynamic resistance during the droplet approach. A convenient interpolation formula was used [227] for the description of the influence of hydrodynamic interaction on the mutual diffusivity. The difference between the more exact Muller equation and Equation 1.162 is caused mainly on account of this hydrodynamic interaction.

1.9.4.2 Doublet Fragmentation Time of Uncharged Droplets

In this section we consider a doublet consisting of droplets with a nonionic adsorption layer. The closest separation between two droplet surfaces s exceeds the double thickness of the adsorption layer ($2h_a$). As a crude approximation h_0 can be identified with $2h_a$. In the case of small surfactant molecules $2h_a \approx 2$ nm.

In this case, the potential well has a sharp and deep minimum. This means that the vicinity of this minimum determines the value of the integral (Equation 1.162). For examination of this assumption Equation 1.162 was calculated numerically and according to the approximate equation [184]:

$$\int_{\alpha}^{\beta} \varphi(t) \exp[f(t)]dt = \left[\frac{2\pi}{f''(t_m)}\right]^{1/2} \varphi(t_m) \exp[f(t_m)] \tag{1.163}$$

where t_m corresponds to the potential well minimum.

The difference in results was small and enabled application of Equation 1.163 for calculation and substitution of the asymptotic expression [1,170]:

$$U(h) = -\frac{A}{12} \cdot \frac{a}{h} \tag{1.164}$$

which is valid at small distances to the surface. The result of calculations according to Equations 1.163 and 1.164 (the Hamaker constant $A = 1.3 \times 10^{-20}$ J) are shown in Figure 1.29. The chosen value of the Hamaker constant is consistent with those reported elsewhere [25,147]. In addition to the value of $A = 1.3 \times 10^{-20}$ J, we mention other values of the Hamaker constant which were employed elsewhere. For example, in food emulsions [25] the Hamaker constant lies within the range 3×10^{-21} to 10^{-20} J. The results of calculations for smaller Hamaker constants are also presented in Figure 1.29.

The influence of the adsorption layer thickness on doublet lifetime is shown in Figure 1.30 for one value of the Hamaker constant. There is high specificity in the thickness of a polymer adsorption layer. β-casein adsorbed onto polystyrene latex causes an increase in the radius of the particle of 10 to 15 nm [228]. A layer of β-lactoglobulin appears to be in the order of 1 to 2 nm thick, as compared to 10 nm for the caseins [229].

When adsorbed layers of hydrophilic nature are present the repulsive hydration forces must be taken into account. At low ionic strengths, the repulsion follows the expected exponential form for double-layer interaction:

$$U(h) = K_s e^{-(h/h_s)} \tag{1.165}$$

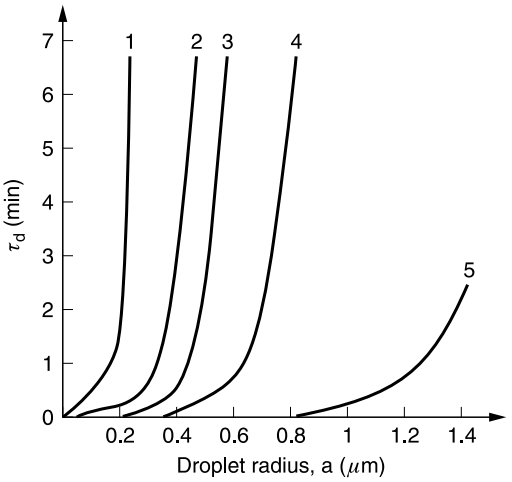

FIGURE 1.29 Dependence of doublet lifetime on droplet dimension at different values of the Hamaker constant A: 1: $A = A_1 = 1.33 \times 10^{-20}$ J; 2: $A = 0.5 \times A_1$; 3: $A = 0.35 \times A_1$; 4: $A = 0.25 \times A_1$; 5: $A = 0.1 \times A_1$. The shortest interdroplet distance 2 nm. (From S.S. Dukhin, J. Sjöblom, D.T. Wasan, and Ø. Sæther, *Colloids Surfaces*, 180: 223 (2001).)

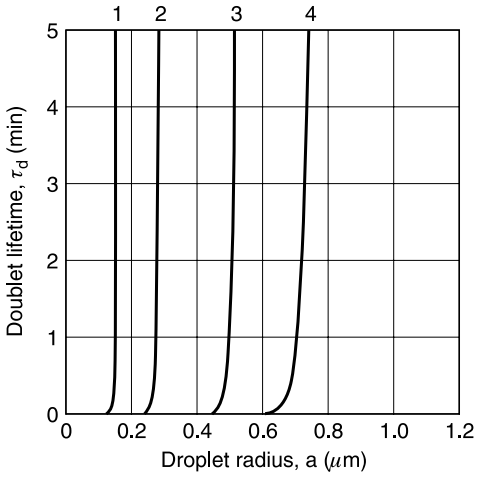

FIGURE 1.30 The adsorption layer thickness influence on the droplet lifetime of an uncharged droplet. Adsorption layer thickness: 1: $h_0 = 1$ nm; 2: $h_0 = 2$ nm; 3: $h_0 = 4$ nm; 4: $h_0 = 6$ nm. $A = 1.33 \times 10^{-20}$ J. (From S.S. Dukhin, J. Sjöblom, D.T. Wasan, and Ø. Sæther, *Colloids Surfaces*, 180: 223 (2001).)

In Ref. 31 the authors emphasize that the surface charge in food emulsions is low, electrolyte concentrations are high, and, hence, the DL is not responsible for emulsion stability. The stabilization can be caused by the hydration forces. However, the flocculation to the secondary minimum remains. Meanwhile, this conclusion must be specified with account for droplet dimension.

1.9.4.3 Lifetime of a Doublet of Charged Droplets and Coagulation/Flocculation

As seen in Figure 1 of Ref. 194 the coordinates of the secondary minimum corresponds to $\kappa h_{\min} =$ 5 to 12. Due to this rather large distance the frequency dependence of the Hamaker constant may be of importance, and the Hamaker function $A(h)$ characterizing molecular interaction should be introduced.

In Refs. 37 and 38 the distance independent interaction at zero frequency and interaction at non-zero frequency is considered separately:

$$A(h) = A_0 + [A(h) - A_0] \tag{1.166}$$

The results from 36 systems in Refs. 37 and 38 are in a rather good accordance with the calculations of other papers. According to Rabinovich and Churaev, the system polystyrene–water–polystyrene can be used to estimate the Hamaker function for oil–water systems. However, with increasing droplet separation the importance of A_0 is increasing on account of $[A(h) - A_0]$. The component A_0 is screened in electrolyte concentrations, because of dielectric dispersion [230–231]. At a distance of $h_{\min} \approx 3$ to 5 nm the authors [231] found that molecular interaction disappeared at zero frequency. Experimental evidence concerning this statement is discussed in Ref. 170. When evaluating the secondary minimum coagulation, A_0 can be omitted as illustrated in Ref. 232.

For the illustration of the influence electrolyte concentration, Stern potential, and particle dimension some calculations of doublet lifetime are made and their results are presented in Figure 1.31. The potential well depth increases and in parallel doublet lifetime increases with increasing particle dimension and electrolyte concentration and decreasing surface potential.

1.9.5 Coalescence Coupled with Either Coagulation or Flocculation in Dilute Emulsions

Limited attention is paid to the role of fragmentation in emulsion science. A comparison of the prediction of coalescence with and without accounting for fragmentation (Sections 1.9.2 and 1.9.3) enables evaluation of the fragmentation significance. This comparison will be done in Section 1.9.5.1 below.

The theories [181,195] have different areas of applicability (not specified in the papers) and are complementary. Naturally, this complicates the choice between these theories with account for concrete conditions of experiments. An approximate evaluation of the aforesaid areas of applicability is given in Section 1.9.5.2.

1.9.5.1 Fragmentation of Primary Flocs in Emulsions and the Subsequent Reduction of Coalescence

Floc fragmentation decreases the quantity of interdroplet films and correspondingly reduces the entire coalescence process. This reduction can be characterized by comparison of Equation 1.138 with theory [195], which neglects fragmentation. The longer the time, the greater the reduction which enables the use of the simpler theory [10] for comparison. The results for longer times coincide with the predictions of the more exact theory [195].

The results of theory [195] concerning slow coalescence are illustrated by curve 1 in Figure 3c in Ref. 195 which is redrawn as Figure 1.32(a). It can be seen that for a low value of the coalescence rate constant, the semilogarithmic plot is linear, indicating that the process follows a coalescence rate-controlled mechanism according to Equation 1.156. Differing from the simple

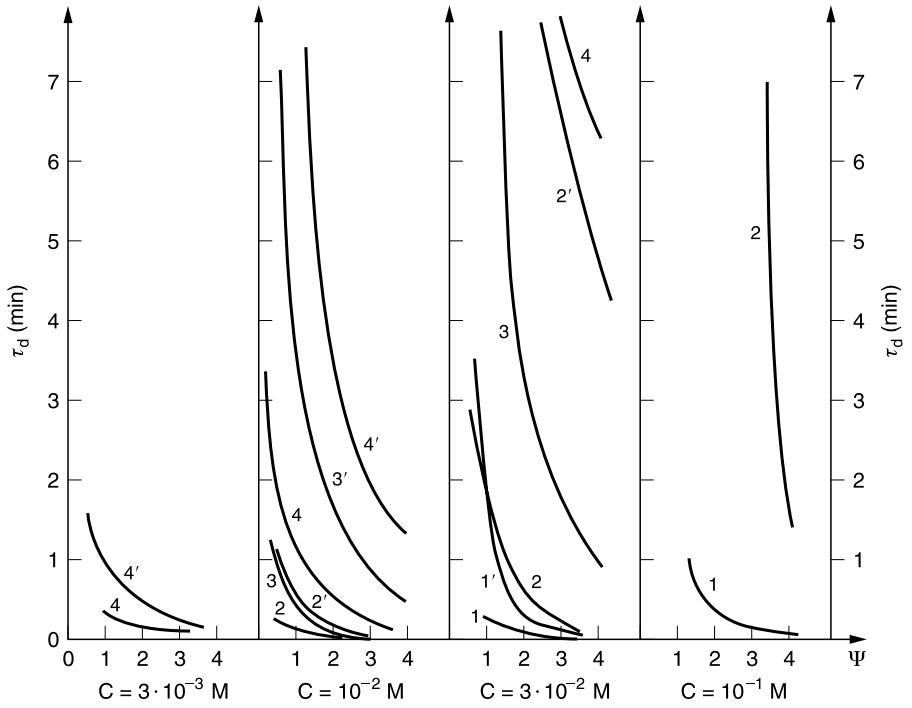

FIGURE 1.31 The dependence of doublet lifetime on the Stern potential for different electrolyte concentrations and droplet dimensions. Numbers near curves correspond to droplet radius. 1. Curves 1–4 without account for retardation of molecular forces of attraction, $\Psi = e\psi/kT$. 2. Curves $1'$–$4'$ with account for retardation. (From S.S. Dukhin, J. Sjöblom, D.T. Wasan, and Ø. Sæther, *Colloids Surfaces*, 180: 223 (2001).)

exponential time dependence in Equation 1.156, second order kinetics dominate at rapid doublet fragmentation, even if coalescence is very slow. The physical reason becomes clear when considering how Equation 1.138 is derived. As seen from Equation 1.137 the rate of decline in the droplet concentration is proportional to the doublet concentration. The latter is proportional to the square of the singlet concentration at s.d.e., which causes second order kinetics. Thus, at slow coalescence the disaggregation drastically changes the kinetic law of the coalescence, i.e., from the exponential law to second order kinetics.

In the second stage coagulation becomes the rate controlling process because of the decrease in the collision rate accompanying the decrease in the droplet concentration. Thus, at sufficiently long times second order kinetics characterize both reversible and irreversible aggregation. Nevertheless, a large difference exists even when identical functions describe the time dependence, as the characteristic times are expressed through different equations for irreversible and reversible aggregation. In the first case it is the Smoluchowski time, in the second case it is the combination of three characteristic times, i.e., Equation 1.138.

Let us now try to quantitatively characterize the reduction in coalescence caused by doublet disintegration. For this purpose the calculations are performed according to Equation 1.126 at $\tau_{Sm} = 10$ s and $\tau_c = 10^3$ s (Figure 1.32(a)), 10^2 s (Figure 1.32(b)) and 10 s (Figure 1.32(c)). For all figures the same value of the ratio $2\tau_d/\tau_{Sm} = 0.1$ is accepted, satisfying condition 1.122. In all these figures the calculations according to Equation 1.138 are illustrated by curve 2.

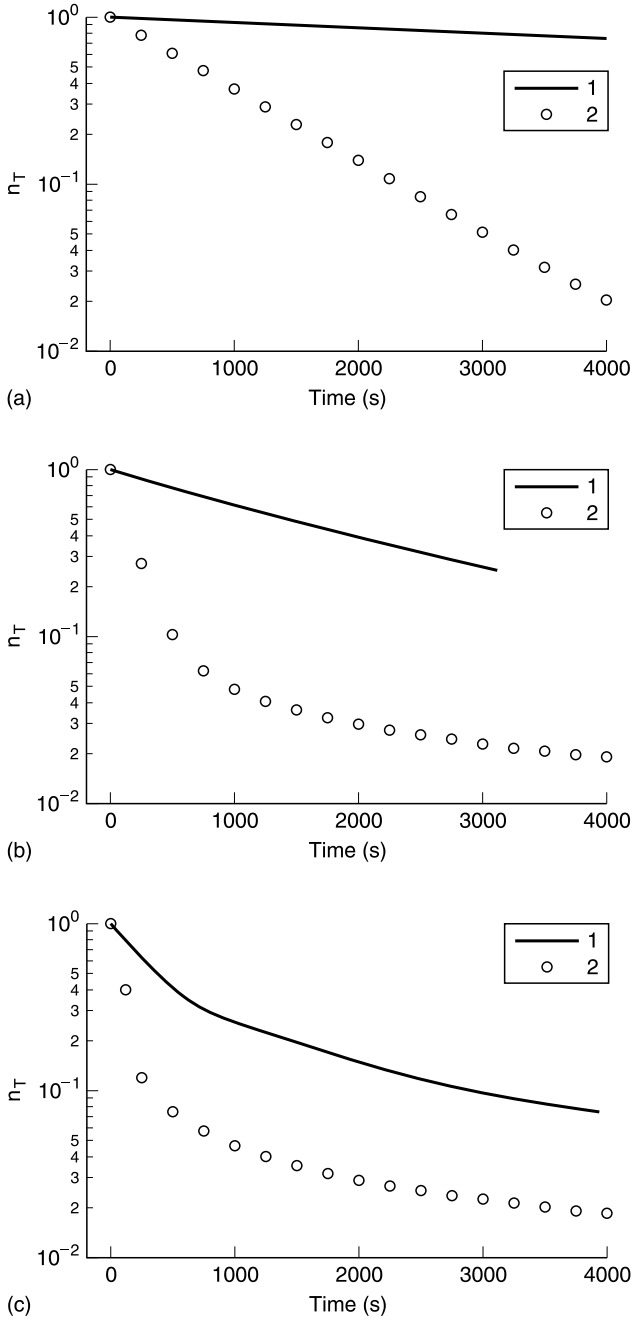

FIGURE 1.32 Relative change in the total number of droplets vs. time; initial number of droplets $N_{10} = 1 \times 10^{10}$ cm^{-3}; flocculation rate constant $K_f = 1 \times 10^{-11}$ cm^3 s^{-1}; curve 1: calculations according to Equation 1.138; curve 2: the model of Borwankar et al. [10] for dilute emulsions, coalescence rate constant (a) $K_c^{2,1} = 1 \times 10^{-1}$ s^{-1}, (b) $K_c^{2,1} = 1 \times 10^{-2}$ s^{-1}, (c) $K_c^{2,1} = 1 \times 10^{-3}$s^{-1}. Coalescence time $\tau_c = 10^3$ s (a), $\tau_c = 10^2$ s (b), $\tau_c = 10$ s (c). Smoluchowski time $\tau_{Sm} = 10$ s. Doublet lifetime $\tau_d = 0.5$ s. n_T is the dimensionless total droplet concentration, $n_T = N_T/N_{10}$. (From S.S. Dukhin and J. Sjöblom, *J. Dispersion Sci. Technol.* 19: 311 (1998).)

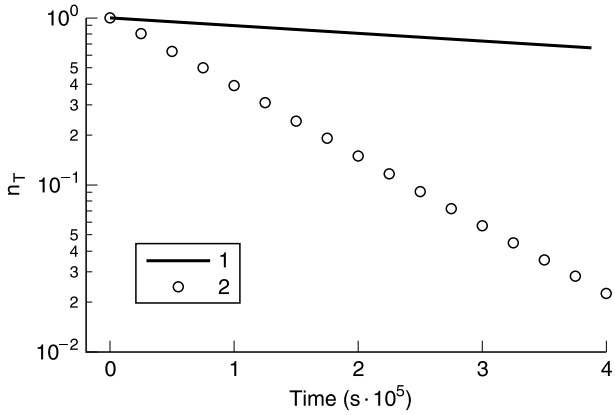

FIGURE 1.33 Similar to FIGURE 1.7, with other values for the characteristic times. Coalescence time $\tau_c = 10^5$ s. Smoluchowski time $\tau_{Sm} = 10^3$ s. Doublet fragmentation lifetime $\tau_d = 50$ s. (From S.S. Dukhin and J. Sjöblom, *J. Dispersion Sci. Technol.* 19: 311 (1998).)

The comparison of curves 1 and 2 characterizes the reduction of coalescence caused by doublet disintegration; the lower the Rev values, the stronger the reduction. The simple curve 1 in Figure 1.32(a) can be used also for higher τ_c values, because then the condition of Equation 1.156 is even better satisfied. Thus, if τ_{c1} and t_1 correspond to the data of Figure 1.32(a) and $\tau_{c2} = m\tau_{c1}$ with $m \gg 1$, the identity

$$\tau_{c2} t_2 = \tau_{c1} m \frac{t_1}{m} \tag{1.167}$$

is useful. This means that

$$\frac{n_T}{n_o}\left(\tau_{c1} m, \frac{t_1}{m}\right) = \frac{n_T}{n_o}(\tau_{c1}, t_1) \tag{1.168}$$

i.e., $t_2 = t_1/m$ where r.h.s. of Equation 1.168 is drawn in Figure 1.33. For example, Figure 1.8 is similar to Figure 1.32(a) and can be used for 100 times longer time, shown on the abscissa axis. The increase in τ_c enables us to increase τ_{Sm} without violating condition 1.155 and with Equation 1.156 valid. Thus, $\tau_{Sm} = 1000$ s or lower can be chosen as condition for Figure 1.33. Curve 2, characterizing the rate of doublet disintegration, preserves as well if the value of $2\tau_d/\tau_{Sm} = 0.1$ remains; now it corresponds to a higher τ_d value of 5 s.

1.9.5.2 Domains of Coalescence Coupled Either with Coagulation or with Flocculation

The condition

$$\text{Rev} \gg 1 \tag{1.169}$$

corresponds to coagulation. The theory for the intermediate case

$$\text{Rev} \sim 1 \tag{1.170}$$

when part of the droplets participate in flocculation and another coagulate is absent. To specify the conditions 1.122 and 1.169 the doublet lifetime must be expressed through surface force characteristics, namely through the surface electric potential and the Hamaker function, and droplet dimension, as was described in Section 1.9.4.

In the equation for the Smoluchowski time (1.124) the droplet numerical concentration N_{10} can easily be expressed through the droplet volume fraction φ and the average droplet radius a (we replace a polydisperse emulsion by an "equivalent" monodisperse emulsion). The resulting analysis respective to a and φ is easier than relating to N_{10} because the boundary of application of different regularities are usually formulated respective to a and φ. The Smoluchowski time is

$$\tau_{Sm} = \kappa_F^{-1}\varphi^{-1}\frac{4}{3}\pi a^3 \tag{1.171}$$

We exclude from consideration a special case of extremely dilute emulsions. Comparing Figure 1.31 and the results of calculations according to Equation 1.171 one concludes that condition 1.169 is mainly satisfied. It can be violated if simultaneously the droplet volume fraction and the droplet dimension are very small. This occurs if $\varphi < 10^{-2}$ and $a < (0.2 - 0.3)$ μm. Discussing this case we exclude from consideration the situation when $a \leq 0.1$ μm, corresponding to microemulsions and $\varphi \ll 10^{-2}$. With this exception one concludes that for uncharged droplets flocculation is almost impossible because condition 1.122 cannot be satisfied. A second conclusion is that at

$$a < (0.2 - 0.3)\ \mu\text{m} \tag{1.172}$$

theory 195 cannot be applied without some corrections made necessary by the partially reversible character of the aggregation. The main conclusion is that when

$$a > 0.2\ \mu\text{m and } \varphi > 10^{-2} \tag{1.173}$$

theory 195 does not need corrections respective to the reversibility of flocculation. However, this conclusion will change at the transition to a thicker adsorption layer. As described in Section 1.9.4, the thicker the adsorption layer, the shorter is the doublet fragmentation time.

The electrostatic repulsion decreases the depth of the potential well and correspondingly decreases the doublet lifetime. As a result, flocculation becomes possible for submicrometer droplets as well as for micrometer-sized droplets, if the electrolyte concentration is not too high, the surface potential is rather high, and the droplet volume fraction is not too high. This is seen from Figure 1.31.

The reversibility criterion depends on many parameters in the case of charged droplets. To discriminate and to quantify the conditions of coagulation and flocculation let us consider Rev values lower than 0.3 as low and values higher than 3 as high. In other words, coagulation takes place when Rev > 3, while at Rev < 0.3 there is flocculation; that is, the conditions

$$\text{Rev} = \frac{\tau_d(c_o, \varphi, a)}{\tau_{Sm}(a, \varphi)} > 3 \tag{1.174}$$

$$\text{Rev} < 0.3 \tag{1.175}$$

determine the boundaries for the domains of coagulation and flocculation. These domains are characterized by Figure 1.34 and correspond to fixed values of the droplet volume fraction.

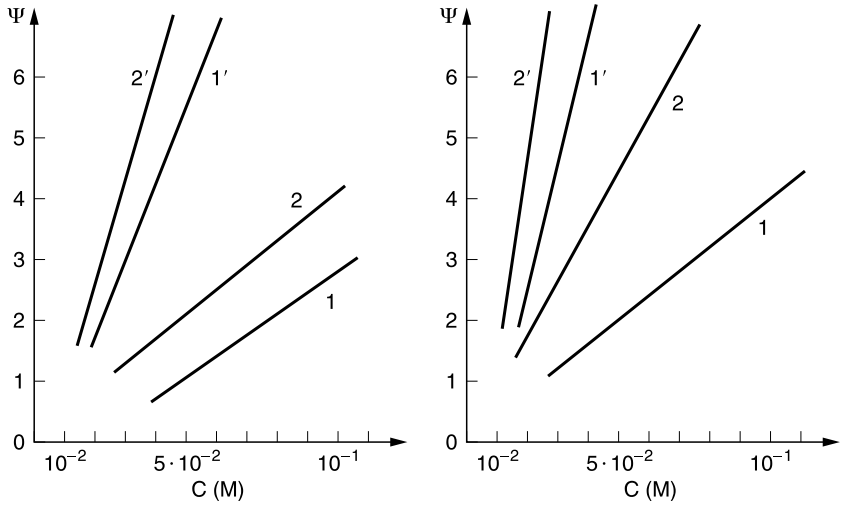

FIGURE 1.34 Domains of coagulation and flocculation. Curves 1 and 2 are calculated with the Rabinovich–Churaev Hamaker function; twice higher value is used for calculation of curves $1'$ and $2'$. The domain of flocculation is located above curve 1, while the domain of coagulation is located beneath curve 2. Volume fraction $\varphi = 0.01$ (*a*); $\varphi = 0.1$ (b). Particle dimension $2a = 4$ μm. (From S.S. Dukhin, J. Sjöblom, D.T. Wasan, and Ø. Sæther, *Colloids Surfaces* 180: 223 (2001).)

In addition, a definite and rather large droplet dimension $2a = 4$ μm is fixed. After fixation of the values of volume fraction and droplet dimension the domains are characterized in coordinates Ψ and C.

The domain of flocculation is located above and to the left of curve 2; the domain of coagulation is located beneath and to the right of curve 1. To characterize the sensitivity of the domain boundaries to the Hamaker function value, curves $1'$ and $2'$ are calculated using values two times higher than those of curves 1 and 2.

In distinction from uncharged droplets flocculation in the range of micrometer-sized droplets is possible. As seen in Figure 1.34, even rather large droplets (4 μm) aggregate reversibly if the electrolyte concentration is lower than $(1 - 5) \times 10^{-2}$ M and the Stern potential is higher than 25 mV. For smaller droplets the domain of flocculation will extend while the domain of coagulation will shrink. For submicrometer droplets flocculation takes place even at high electrolyte concentrations (0.1 M).

1.9.5.3 Hydration Forces Initiate Flocculation

Due to similar dependence on the distance h between hydration forces and electrostatic interaction the doublet lifetime decrease caused by hydration forces of repulsion can be calculated on account of this similarity. It is sufficient to use the substitution h_s for κ^{-1} and K_s for

$$16\varepsilon \left(\frac{kT}{e}\right)^2 \tanh\left(\frac{e\psi}{kT}\right)^2 \tag{1.176}$$

where k is the Boltzmann constant, T is absolute temperature, and e is the elementary charge. The doublet lifetime can be determined with the use of the results presented in Figure 1.31.

For the sake of brevity, the similar figure with K_s given on the ordinate axis and h_s on the abscissa axis is not shown. It turns out that the decrease in τ_d caused by hydration forces leads to flocculation of submicrometer droplets. As to micrometer-sized droplets, coagulation takes place with the exception for the case when both h_s and K_s are rather large.

1.9.6 Applications

The restrictions in Equations 1.121 and 1.135 corresponding to strong retardation of the rate of multiplet formation and slow intradoublet coalescence are not frequently satisfied. Nevertheless, these conditions are important because they correspond to the case of very stable emulsions. As the kinetics of the retarded destabilization of rather stable emulsions is of interest, attention has to be paid to provide these conditions and thus the problem of coupled coalescence and flocculation arises.

There are large qualitative distinctions in the destabilization processes for the coupling of coalescence and coagulation, and coalescence and flocculation. In the first case, rapid aggregation causes rapid creaming and further coalescence within aggregates. In the second case, the creaming is hampered due to the low concentration of multiplets and coalescence takes place both before and after creaming. Before creaming singlets predominate for a rather long period of gradual growth of droplet dimensions due to coalescence within doublets. The discrimination of conditions for coupling of coalescence with either flocculation or coagulation is accomplished in Ref. 184.

The creaming time is much shorter in the coagulation case and correspondingly the equation describing the coupling of coalescence and flocculation preserves its physical sense for a longer time than is the case for coagulation. One concludes that the theory of the coupling of coalescence and flocculation provides a new opportunity for long-term prediction of emulsion stability, although creaming restricts the application of this theory as well. Note that this restriction weakens in the emulsions of low density contrast and in w/o emulsions with a high viscosity continuum.

Long-term prediction is a two-step procedure. The first step is the determination of whether an emulsion exhibits coagulation or flocculation. It means that the characteristic time τ_d must be measured and compared with τ_{Sm}, the value of which is easily evaluated with account for measured concentration using Equation 1.124. A comparison of these times enables the choice between condition 1.121 and the opposite condition ($\tau_{Sm} \ll \tau_d$). The second step is the prediction of the evolution in time for the t.d.c. If condition 1.121 is valid Equation 1.138 has to be used for the prediction. τ in Equation 1.138 has to be specified in accordance with Equation 1.135. In the opposite case DIGB theory must be used.

1.9.6.1 Long-Term Prediction of Emulsion Stability

It is possible, in principle, to give a long-term prediction of emulsion stability based on the first indications of aggregation and coalescence. The next example clarifies the principal difficulty in a reliable long-term prediction, if a dynamic model of the emulsion is not available.

The first signs of aggregation and coalescence can always be characterized by a linear dependence, if the investigation time t is small in comparison with a characteristic time τ for the evolution of the total droplet concentration $n(t)$:

$$n(t) = n_0\left(1 - \frac{t}{\tau}\right) \tag{1.177}$$

This short time asymptotic corresponds to many functions, for example to Equation 1.138 or to Equation 1.156. The first can arise in the case of coalescence coupled with coagulation [195], while the second can arise for coalescence coupled with flocculation [187]. The discrimination between irreversible and reversible aggregations is only one component of emulsion dynamics modeling (EDM) and it is seen that without this discrimination the difference in the prediction of the time necessary for a droplet concentration decrease, for example 1000 times, can be 7τ and 1000τ.

1.9.6.2 Perfection of Methods for Emulsion Stabilization (Destabilization) by Means of the Effect on Both Coalescence and Flocculation

Stability (instability) of an emulsion is caused by the coupling of coalescence and flocculation. Meanwhile, for emulsifiers (or deemulsifiers) the elaboration of their influence on the elementary act of coalescence only is mainly taken into account. The coupling of coalescence and flocculation is reflected in Equation 1.135 and one concludes that it follows the multiplicativity rule and not the additivity rule. This means that the total result of the application of a stabilizer (destabilizer) depends very much on both flocculation and fragmentation. The development of a more efficient technology for emulsion stabilization (destabilization) is possible by taking into account the joint effect on both the coalescence and the aggregation (disaggregation) processes.

1.9.6.2.1 Combining Surfactants and Polymers in Emulsion Stabilization

The coalescence rate depends mainly on the thin (black) film stability and correspondingly on the short-range forces. The flocculation depends on the long-range surface forces. Due to this large difference synergism in the dependence of these processes on the different factors can be absent.

The use of one surfactant only may not provide both the optimal fragmentation and optimal stability of an emulsion film. Probably the use of a binary surfactant mixture with one component which provides the film stability, and a second one which prevents the flocculation, may provide perfect emulsion stabilization. Naturally their coadsorption is necessary. For such an investigation a measurement method for both the doublet fragmentation time and the coalescence time is necessary.

1.9.6.2.2 Strong Influence of Low Concentrations of Ionic Surfactant on Doublet Fragmentation Time and Coalescence Time

Let us consider the situation when an emulsion is stabilized against coalescence by means of an adsorption layer of nonionic surfactant and is strongly coagulated because of the subcritical value of the Stern potential that is usual for inorganic electrolytes [202] at moderate pH. In a large floc any droplet has many neighbors, meaning a rather high number of interdroplet films per droplet. The coalescence rate is proportional to the total number of films and can be rather high. It can be strongly decreased by adding a low concentration of an ionic surfactant. This can be sufficient to provide a supercritical Stern potential value that will be accompanied by a drastic decrease in the doublet lifetime compared to that of weakly charged droplets.

At shorter doublet lifetimes flocculation can become reversible and it can stop at the stage of singlet–doublet equilibrium. It will provide a strong decrease in the coalescence rate because coalescence occurs within doublets only and their concentration can be very low.

Thus, a small addition of an ionic surfactant to higher concentration of a nonionic surfactant sufficient to provide an almost saturated adsorption layer can make the overall emulsion

stabilization more efficient. The nonionic surfactant suppresses coalescence but cannot prevent flocculation, while the ionic surfactant retards the development of flocculation.

We can give an example when both coalescence and flocculation are affected by an ionic surfactant (SDS). In Ref. 233 it is established that coalescence is suppressed at SDS concentrations exceeding 6×10^{-5} M. Meanwhile, the C.C.C. is 2×10^{-2} M NaCl at 10^{-6} M SDS. Thus, SDS concentrations slightly above 10^{-6} M are sufficient to retard flocculation. In this example it is essential that the concentrations needed to retard flocculation are very low compared to those needed to prevent coalescence.

It is noteworthy that low concentrations of an ionic surfactant can increase emulsion stability due to the simultaneous manifestation of three mechanisms. First, the depth of the secondary potential minimum decreases due to the electrostatic repulsion that is accompanied by a τ_d decrease. Second, the transition from the secondary minimum through an electrostatic barrier and into the primary minimum extends the coalescence time. Third, the time of true coalescence, i.e., the time necessary for thin film rupture, increases due to electrostatic repulsion as well [185,217].

1.9.6.3 Standardization of the Measurement of τ_c and τ_d

Direct investigation of the coalescence subprocess in emulsions is difficult. Instead, the entire destabilization process is usually investigated. Meanwhile, the rate of the destabilization process depends on the rates of both flocculation and disaggregation and on the floc structure as well. All these characteristics vary in a broad range. At a given unknown value for the time of the elementary act of coalescence τ_c the different times can be measured for the integrated process and different evaluations of τ_c are possible.

The rate of coalescence in an aggregate essentially depends on the number of droplets within it and the packing type, i.e., on the number of films between the droplets. This complication is absent when considering the case of the s.d.e.

The possible advantage of τ_c measurement at s.d.e. is in avoiding the difficulty caused by polydispersity of droplets appearing during preceding coalescence within large flocs. At the s.d.e. the initial stage of the entire coalescence process can be investigated when the narrow size distribution of an emulsion preserves.

At s.d.e. the determination of the time dependence of the t.d.c. is sufficient for the investigation of coalescence. In Refs. 185 and 186 this was accomplished through direct visual observation. By using video enhanced microscopy and computerized image analysis the determination of the t.d.c. can be automated. Such automated determination of total droplet number in a dilute DCD-in-water emulsion at the s.d.e. can be recommended as a standard method for the characterization of the elementary act of coalescence.

In parallel, the second important characteristic, namely the doublet fragmentation time, is determined by the substitution of τ_c, τ_{Sm}, and measured τ_d into Equation 1.138.

1.9.6.4 Experimental–Theoretical Emulsion Dynamics Modeling

1.9.6.4.1 General

To predict the evolution of the droplet (floc) size distribution is the central problem in emulsion stability. It is possible, in principle, to predict the time dependence of the distribution of droplets (flocs) if information concerning the main subprocesses (flocculation, floc fragmentation, coalescence, creaming), constituting the whole phenomenon, is available. This prediction is based on consideration of the population balance equation (PBE).

The PBE concept was proposed by Smoluchowski. He specified this concept for suspensions and did not take into account the possibility of floc fragmentation. Even with this restriction he succeeded in the analytical solution neglecting gravitational coagulation and creaming, and obtained the analytical time dependence for a number of aggregates n_i comprising i particles ($i = 2, 3 \ldots$).

In the most general case the equation for the evolution of the total droplet number takes into account the role of aggregation, fragmentation, creaming, and coalescence. There is no attempt to propose an algorithm even for a numerical solution to such a problem.

The usual approach in the modeling of an extremely complicated process is the consideration of some extreme cases with further synthesis of the obtained results. The next three main simplifications are inherent to the current state of emulsion dynamics modeling: the neglect of the influence of the gravitational field, i.e., neglect of creaming/sedimentation; in a first approximation it is possible to consider either coagulation or flocculation; finally, the neglect of the rate constant dependence on droplet dimension.

1.9.6.4.2 Combined Approach in Investigations of Dilute and Concentrated Emulsions

The modeling of collective processes in concentrated emulsions is extremely complicated. Recently, the efficiency of computer simulation in the systematic study of aggregates, gels, and creams has been demonstrated [204]. Monte Carlo and Brownian dynamics are particularly suited to the simulation of concentrated emulsions. However, information about droplet–droplet interaction is necessary. The reliability of this information is very important to provide reasonable results concerning concentrated emulsions. In other words, the assumption concerning pair additive potentials for droplet/droplet interaction and the thin emulsion film stability must be experimentally confirmed. The extraction of this information from experiments with concentrated emulsions is very difficult. On the other hand, measurement of the doublet fragmentation time in dilute emulsions is a convenient method to obtain information about pair additive potentials. Information about pair potentials and the elementary act of coalescence obtained in experiments with dilute emulsions preserves its significance for concentrated emulsions as well.

One concludes that modeling of concentrated emulsions becomes possible by combining experimental investigation of the simplest emulsion model system with computer simulation accounting for the characteristics of a concentrated emulsion (high droplet volume fraction, etc.).

1.9.6.4.3 Kernel Determination

Kernel determination is the main task which must be solved to transform the PBE into an efficient method for emulsion dynamics modeling. The levels of knowledge concerning kernels describing different subprocesses differ strongly. There exists a possibility for quantification of kernels related to aggregation and fragmentation [173,194,227]. On the other hand, the current state of knowledge is not sufficient for prediction of the thin film disruption time.

The deficit in knowledge about thin film stability makes purely theoretical modeling of emulsion dynamics impossible. As a result a complex semi-theoretical approach to EDM is necessary. The PBE is the main component of both the experimental and the theoretical stages of this approach. In the experimental stage the PBE simplified regarding s.d.e. provides the background for the determination of the coalescence kernels with the use of the experimental data [185,186].

For the determination of the coalescence kernels the more complicated reverse task must be solved, namely their determination based on the comparison of experimental data about the emulsion evolution in time with the PBE solution. In the absence of an analytical solution the reverse

task is usually very difficult. The most efficient way to overcome this difficulty is the experimental realization with the use of the universally simplest conditions for emulsion time evolution, which can be described analytically.

1.9.6.4.4 Singlet–Doublet Quasi-Equilibrium

Singlet–doublet quasi-equilibrium with slow coalescence within doublets is the simplest emulsion state for which investigation can provide information about coalescence.

The simplest singlet–doublet emulsion can exist at singlet–doublet quasi-equilibrium and slow coalescence within doublets. Its simplicity results in a very simple kinetic law for the entire kinetics of coupled flocculation and coalescence, namely Equation 1.138. Thus, s.d.e. provides the most convenient conditions for investigations of the elementary act of coalescence and the doublet fragmentation time.

The main simplification in all existing models for emulsion dynamics [181,195] is the neglect of the coalescence time dependence on droplet dimensions. This simplification is not justified and decreases very much the value of the prediction, which can now be made with use of the PBE. For elimination of this unjustified simplification it is necessary to determine the coalescence time for emulsion films between droplets of different dimensions i and j, namely τ_{cij}, similar to the existing analytical expressions for the doublet fragmentation time, τ_{dij} [173]. The determination of a large set of τ_{cij} values by means of a comparison of experimental data obtained for an emulsion consisting of different multiplets and the PBE numerical solutions for it is impossible. On the other hand, this paramount experimental–theoretical task can be solved for a dilute emulsion at s.d.e. and slow intradoublet coalescence.

1.9.6.4.5 Substitution of the Coalescence Kernels

Substitution of the coalescence kernels makes the PBE equation definite and ready for the prediction of emulsion time evolution with the restriction of low density contrast and without account for gravitational coagulation and creaming.

With application of the scaling procedure for the representation of the kinetic rate constants for creaming and gravitational coagulation the PBE is solved analytically in Ref. 234. This scaling theory creates a perspective for the incorporation of creaming in the emulsion dynamics model in parallel with coalescence, aggregation, and fragmentation.

1.10 SUMMARY

The mechanisms of kinetic stability in macroemulsions and mini-emulsions are completely different. The strong droplet deformation and flattening in a macroemulsion cause the Reynolds mode of drainage which prolongs the life of the emulsion. This mechanism is not important for mini-emulsion droplet interaction, because either the deformation and flattening are weak (charged droplets) or the Reynolds drainage is rapid due to the small dimension of the interdroplet film (uncharged droplets). The kinetic stability of a mini-emulsion can be caused by floc fragmentation if the electrokinetic potential is not too low and the electrolyte concentration is not too high, corresponding to some electrostatic repulsion.

The potential strength of physicochemical kinetics with respect to emulsions is the population balance equation (PBE), enabling prediction of the time evolution of the droplet size distribution (d.s.d.) when the subprocesses (including droplet aggregation, aggregate fragmentation, droplet coalescence, and droplet (floc) creaming) are quantified. The subprocesses are characterized in

the PBE by the kinetic coefficients. The coupling of the four subprocesses, the droplet polydispersity, and the immense variety of droplet aggregate configurations causes extreme difficulty in EDM. The three processes of aggregation, fragmentation, and creaming can be quantified. In contrast, only the experimental approach is now available for efficient accumulation of information concerning emulsion film stability and coalescence kernel quantification for EDM.

Correspondingly, EDM may be accomplished by combining experiment and theory: (1) the determination of coalescence and fragmentation kernels with the use of emulsion stability experiments at low density contrast (l.d.c.) and singlet–doublet equilibrium (s.d.e.), because this enables the omittance of creaming and gravitational terms in PBE, simplifying it and making solution of the reverse task possible; and (2) the prediction of the droplet size evolution with time by means of solution of the PBE, specified for the determined coalescence and fragmentation kernels. This mathematical model has to be based on the PBE supplemented by terms accounting for the role of creaming and gravitational coagulation in the aggregation kinetics.

Emulsion dynamics modeling with experiments using l.d.c. emulsions and s.d.e. may result in: (1) the quantification of emulsion film stability, namely the establishment of the coalescence time dependence on the physicochemical specificity of the adsorption layer of a surfactant (polymer), its structure, and the droplet dimensions. This quantification can form a basis for the optimization of emulsifier and demulsifier selection and synthesis for emulsion technology applications, instead of the current empirical level applied in this area; (2) the elaboration of a commercial device for coalescence time measurement, which in combination with EDM will represent a useful approach to the optimization of emulsion technology with respect to stabilization and destabilization.

Symbols

LATIN	
a	Radius (m)
A	Hamaker constant
A_{ij}	Hamaker constant for interaction
b	Target distance
c_i	Bulk concentration of surfactant
C	Concentration (mol m^{-3})
D	Diffusion coefficient of a droplet ($m^2\ s^{-1}$)
D	Diffusion coefficient of an ion or a surfactant molecule
e	Elementary charge (C)
f	Friction coefficient (kg s^{-1})
F	Faraday constant (C mol^{-1})
F	Force (N)
g	Standard acceleration of free fall ($m\,s^{-2}$)
h	Shortest distance between colloidal particles, drops (m)
J	Flux ($m^2\,s^{-1}$)
k_f	Flocculation rate constant
K	Boltzmann constant ($J\,K^{-1}$)
n_i	Number concentration of particles (aggregates) of size i
N_A	Avogadro's number
p_{12}	Pair distribution function
Pe	Pecklet number
$\mathbf{r}(r)$	Distance (m)

R	Gas constant ($\mathrm{J\,K^{-1}\,mol^{-1}}$)
R_{ij}	Collision radius
Re	Reynolds number
$R_{ij} = a_i + a_j$	Collision radius
t	Time (s)
t_F	Characteristic flocculation time
T	Temperature (K)
$u_0(\hat{\mu})$	Instantaneous creaming velocity (Eq. 1.42)
u_0	Stokes creaming rate (Eq. 1.117)
U	Energy (J)
U, v	Velocity ($\mathrm{m\,s^{-1}}$)
U_{12}	Potential function between drops 1 and 2
V	Volume ($\mathrm{m^3}$)

GREEK

γ	Interfacial tension ($\mathrm{N\,m^{-1}}$)
Γ	Surface (excess) concentration ($\mathrm{mol\,m^{-2}}$)
δ	Diffusion layer thickness (m)
ε	Relative dielectric permittivity (dielectric constant)
ε_0	Dielectric permittivity of vacuum
χ_r	Retardation coefficient (Eq. 1.45)
ζ	Electrokinetic potential
θ	Angle of rotation
κ	Reciprocal Debye length ($\mathrm{m^{-1}}$)
λ	Size ratio of two drops, $\lambda = a_1/a_2 < 1$
μ	Kinematic viscosity ($\mathrm{J\,mol^{-1}}$)
$\hat{\mu} = \mu_1/\mu_2$	Viscosity ratio
$\Pi(h)$	Disjoining pressure ($\mathrm{N\,m^2}$)
ρ	Density ($\mathrm{kg\,m^{-3}}$)
σ	Surface charge ($\mathrm{C\,m^{-2}}$)
τ	Characteristic time (s)
Ψ	Electric potential (V)

REFERENCES

1. B. V. Derjaguin, Theory of Stability of Colloids and Thin Films, Nauka, Moscow, 1986 [in Russian]; translation: Theory of Stability of Colloids and Thin Films, Plenum, New York, 1989.
2. J. Gregory, Crit. Rev. Environ. Control 19:185 (1989).
3. M. von Smoluchowski, Phys. Z. 17:557, 585 (1916).
4. M. von Smoluchowski, Phys. Chem. 92:129 (1917).
5. Th.F. Tadros and B. Vincent, in Encyclopedia of Emulsion Technology, Vol. 1 (P. Becher, ed.), Marcel Dekker, Inc., New York, 1983, p. 57.
6. E. E. Kumacheva, E. A. Amelina, A. V. Prtsev, and E. D. Shchukin, Kolloidn. Zh. 40:1214 (1989).
7. K. Larsen, in Emulsions – A Fundamental and Practical Approach (J. Sjöblom, ed.), NATO ASI Series Vol. 363, 1991, p. 41.
8. H. J. Junginger, Emulsions – A Fundamental and Practical Approach (J. Sjöblom, ed.), NATO ASI Series Vol. 363, 1991, p. 207.
9. M. van den Tempel, Rec. Trav. Chim. 72:419, 433 (1953).
10. R. P. Borwankar, L. A. Lobo, and D. T. Wasan, Colloids Surfaces 69:135 (1992).

11. Ph.T. Jacger, J. J. M. Janssen, F. G. Groeneweg, and W. G. M. Agterof, Colloids Surfaces 85:255 (1994).
12. B. V. Derjaguin, N. V. Churaev, and V. M. Muller, Surface Forces, Nauka, Moscow, 1985 [in Russian]; translation: Surface Forces, Plenum, New York, 1987.
13. R. J. Hunter, Foundations of Colloid Science, Vol. 1, Oxford Science Publication, Oxford, 1987.
14. H. Sonntag and K. Strenge, Coagulation Kinetics and Structure Formation, VEB Dentscher Verlag der Wissenschaften, Berlin, 1987.
15. D. H. Melik and H. S. Fogler, in Encyclopedia of Emulsion Technology, Vol. 3, Marcel Dekker, Inc., New York, 1988, pp. 3–78.
16. N. A. Fuchs, Mechanika aerosoley, Izd-vo AN SSSR, 1955: The Mechanics of Aerosols, Pergamon, London, 1964.
17. V. M. Voloshchuk and Yu. S. Sedunov, Coagulation Processes in Disperse Systems, Hydrometeoizdat, Leningrad, 1975 [in Russian].
18. S. S. Dukhin, N. N. Rulyov, and D. S. Dimitrov, Coagulation and Dynamics of Thin Films, Naukova Dumka, Kiev, 1986 [in Russian].
19. B. V. Derjaguin, S. S. Dukhin, and N. N. Rulyov, in Surface and Colloid Science, Vol. 13 (E. Matijevich, ed.), Wiley Interscience, New York, 1983, p. 71.
20. H. J. Schulze, Physicalisch-Chemische Elementarvorgange des Flotations Processes, VEB Verlag der Wissenschaft, Berlin, 1981.
21. J. Sjöblom (ed.), J. Disper. Sci. & Technol. 15 (1994).
22. W. Stumm and J. J. Morgan, Aquatic Chemistry, Wiley, New York, 1981.
23. E. Dickenson, in Emulsions – A Fundamental and Practical Approach (J. Sjöblom, ed.), NATO ASI Series Vol. 363, 1991, p. 25.
24. M. P. Aronson, in Emulsions – A Fundamental and Practical Approach (J. Sjöblom, ed.), NATO ASI Series Vol. 363, 1991, p. 75.
25. P. Walstra, in Gums and Stabilizers for the Food Industry, Vol. 4 (G. O. Phillips, P. A. Williams, and D. I. Wedlock, eds.), IRL Press, Oxford, 1988, p. 233.
26. S. R. Reddy, D. H. Melik, and H. S. Fogler, J. Colloid Interface Sci. 82:116 (1981).
27. D. H. Melik and H. S. Fogler, J. Colloid Interface Sci. 101:72 (1984).
28. X. Zhang and R. Davis, J. Fluid. Mech. 230:479 (1991).
29. S. E. Friberg, in Emulsions – A Fundamental and Practical Approach (J. Sjöblom, ed), NATO ASI Series Vol. 363, 1991, p. 1.
30. J. A. Kitcherer and P. R. Musselwhite, The Theory of Stability in Emulsions in Emulsion Science (P. Sherman, ed.), Academic Press, London, 1968.
31. B. Bergenståhl and P. M. Claesson, in Food Emulsions (K. Larsson and S. Friberg, eds.), Marcel Dekker, Inc., 1989, pp. 41–96.
32. Ya. I. Rabinovich and N. V. Churaev, Kolloidn. Zh. 52:309 (1990).
33. H. C. Hamaker, Physica. 4:1058 (1937).
34. B. A. Pailtorpe and W. B. Russel, J. Colloid Interface Sci. 89:56 (1982).
35. N. F. H. Ho and W. I. Hiquichi, J. Pharm. Sci. 57:436 (1968).
36. J. Lyklema, Fundamentals of Interface and Colloid Science, Academic Press, London, 1993.
37. Ya. I. Rabinovich and N. V. Churaev, Kolloidn. Zh. 41:468 (1979).
38. Ya. I. Rabinovich and N. V. Churaev, Kolloidn. Zh. 46:69 (1984).
39. R. J. Hunter, Zeta Potential in Colloid Science, Academic Press, London, 1981.
40. S. S. Dukhin, Adv. Colloid Interface Sci. 44:1 (1993).
41. S. S. Dukhin, B. V. Derjaguin, and N. M. Semenikhin, Dokl. Akad. Nauk SSSR 192:357 (1970).
42. B. V. Derjaguin, Theory of Stability of Colloids and Thin Films, Plenum, New York, 1989, Chap. 5, Sec. 5.
43. S. S. Dukhin and V. N. Shilov, Dielectric Phenomena and the Double Layer in Disperse Systems and Polyelectrolytes, Wiley, Toronto, 1974.
44. J. Kijlstra, H. P. van Leuven, and J. Lyklema, J. Chem. Soc. Faraday Trans. 88:3441 (1992).
45. B. R. Midmore and R. I. Hunter, J. Colloid Interface Sci. 122:521 (1988).
46. J. N. Israelachvili and R. M. Pashley, J. Colloid Interface Sci. 98:500 (1984).

47. P. M. Claesson and H. K. Christenson, J. Phys. Chem. 92:1650 (1988).
48. H. K. Christenson, P. M. Claesson, J. Berg, and P. C. Herder, J. Phys. Chem. 93:1472 (1989).
49. R. M. Pashley and J. N. Israelachvili, J. Colloid Interface Sci. 97:446 (1984).
50. B. V. Derjaguin and Z. M. Zorin, Zh. Fiz. Khim. 29:1010 (1955).
51. G. Frens and J. Th. G. Overbeek, J. Colloid Interface Sci. 38:376 (1972).
52. T. W. Healy, A. Homola, and R. O. James, Faraday Discuss. Chem. Soc. 65:156 (1978).
53. P. Meakin, Phys. Rev. Lett. 51:1119 (1983).
54. M. Kilb, Phys. Rev. Lett. 53:1653 (1984).
55. T. Vicsek and F. Family, Phys. Rev. Lett. 52:1669 (1984).
56. P. Meakin, I. Vicsek, and F. Family, Phys. Rev. B31:564 (1985).
57. A. Einstein, Ann. Phys. 17:549 (1905); 19:371 (1906).
58. A. Einstein, The Theory of the Brownian Movement, Dover, New York, 1956.
59. N. A. Fuchs, Z. Phys. 89:739 (1934).
60. B. V. Derjaguin, Dokl. AN SSSR 109:967 (1956).
61. B. V. Derjaguin and N. A. Krotova, Physical Chemistry of Adhesion. Izd-vo AN SSSR. Moscow, 1949.
62. G. I. Taylor, Proc. Roy. Soc. London A 108:12 (1924).
63. L. Spielman, J. Colloid Interface Sci. 33:562 (1970).
64. E. P. Honig, G. J. Roberson, and P. H. Wiersena, J. Colloid Interface Sci. 36:97 (1971).
65. G. K. Batchelor, J. Fluid Mech. 119:379 (1982).
66. A. Z. Zinchenko, Prikl. Mat. Mech. 42:955 (1978).
67. A. Z. Zinchenko, Prikl. Mat. Mech. 44:30 (1980).
68. A. Z. Zinchenko, Prikl. Mat. Mech. 46:58 (1982).
69. G. Hetsroni and S. Haber, Int. J. Multiphase Flow 4:1 (1978).
70. Y. O. Fuentes, S. Kim, and D. J. Jeffrey, Phys. Fluids 31:2445 (1988).
71. Y. O. Fuentes, S. Kim, and D. J. Jeffrey, Phys. Fluids A1:61 (1989).
72. S. Haber, G. Hetsroni, and A. Solan, Int. J. Multiphase Flow 1:57 (1973).
73. E. Rushton and G. A. Davies, Appl. Sci. Res. 28:37 (1973).
74. R. H. Davis, J. A. Schonberg, and J. M. Rallison, Phys. Fluid A1:77 (1989).
75. X. Zhang and R. H. Davis, J. Fluid Mech. 230:479 (1991).
76. X. Zhang, Ph.D. thesis. University of Colorado, 1992.
77. H. Sonntag, in Coagulation and Flocculation (Dobias, ed.), Marcel Dekker, Inc., New York, 1993.
78. E. B. Vadas, H. L. Goldsmith, and S. G. Mason, J. Colloid Interface Sci. 43:630 (1973).
79. E. B. Vadas, R. G. Cox, H. L. Goldsmith, and S. G. Mason, J. Colloid Interface Sci. 57:308 (1976).
80. H. Siedentopf and R. Zsigmondy, Ann. Phys. (Leipzig) 10:1 (1903).
81. R. Zsigmondy, Z. Phys. Chem. 93:600 (1918).
82. A. Tuorilla, Kolloidchem. Beihefte 22:193 (1926).
83. B. V. Derjaguin and N. M. Kudravtseva, Kolloidn. Zh. 26:61 (1964).
84. A. Watillon, M. Romerowski, and F. van Grunderbeek, Bull. Soc. Chim. Belg. 68:450 (1959).
85. R. H. Ottewill and M. C. Rastogi, J. Chem. Soc. Trans. Faraday Soc. 56:866 (1960).
86. N. H. G. Penners and L. K. Koopal, Colloids Surfaces 28:67 (1987).
87. J. Cahill, P. G. Cummins, E. J. Staples, and L. Thompson, J. Colloid Interface Sci. 117:406 (1987).
88. H. Gedan, H. Lichtenfeld, H. Sonntag, and H.-J. Krug, Colloids Surfaces 11:199 (1984).
89. N. A. Fuchs, Uspechi Mechaniki Aerozoley, lzd-vo AN SSSR. Moscow, 1961 [in Russian].
90. L. A. Spielman and J. A. Fitzpatrick, J. Colloid Interface Sci. 42:607 (1973).
91. L. A. Spielman and J. A. Fitzpatrick, J. Colloid Interface Sci. 43:350 (1973).
92. J. Langmuir and K. Blodgett, Gen. Elec. Comp. Rep., July 1945, pp. 45–58.
93. W. Rybczynski, Bull. Cracovie (A) 40 (1911).
94. J. Hadamard, Comp. Rend. 152:1735 (1911).
95. P. F. Saffman and J. S. Turner, J. Fluid Mech. 1:16 (1956).
96. V. G. Levich, Physicochemical Hydrodynamics, Prentice-Hall, Englewood Cliffs, NJ, 1962.
97. A. N. Frumkin and V. G. Levich, Zh. Fiz. Chim. 21:1183 (1947).

98. S. S. Dukhin, in Modern Theory of Capillarity (A. I. Rusanov and F. Ch. Goodrich, eds.), Springer-Verlag, Berlin, 1981.
99. R. D. Vold and R. C. Groot, J. Colloid Sci. 19:384 (1964).
100. S. J. Rehfild, J. Phys. Chem. 66:1969 (1962).
101. E. R. Garret, J. Am. Pharm. Assoc. 51:35 (1962).
102. H. Brauer, Grandlagen der Ein-und Mehrphasenstronumgen, Verlag Sanerlander, Aarau, 1971.
103. R. G. Boothroyd, Flowing Gas–Solid Suspensions, Chapman & Hall, London, 1971, Sec. 2.2.
104. H. S. Muralidhara, R. B. Beard, and N. Senapti, Filt. Sep. 24:409 (1987).
105. K. L. Sutherland, J. Phys. Chem. 58:394 (1948).
106. B. V. Derjaguin and S. S. Dukhin, Trans. Inst. Mining Metall. 70:221, 231 (1960).
107. L. I. Levin, Research into the Physics of Coarsly Dispersed Aerosols, Izdvo AN SSSR, Moscow, 1961 [in Russian].
108. G. L. Natanson, Dokl. AN SSSR 116:109 (1957).
109. A. Fonda and H. Herne, in Aerosol Science (C. N. Davies, ed.), Academic Press, New York, 1969.
110. W. R. Russel, D. A. Saville, and W. R. Schowalter, Colloidal Dispersions, Cambridge University Press, Cambridge, 1989, Chap. 11.
111. S. S. Dukhin, Kolloidn. Zh. 44:431 (1982); 45:207 (1983).
112. S. S. Dukhin and B. V. Derjaguin, Kolloidn. Zh. 20:326 (1958).
113. M. B. Weber, J. Sep. Technol. 2:29 (1981).
114. A. Nguen Van and S. Kmet, Int. J. Miner. Process. 35:205 (1992).
115. R. C. Clift, J. R. Grace, and M. E. Weber, Bubbles, Drops and Particles, Academic Press, New York, 1978, p. 27.
116. R. H. Yoon and G. H. Luttrel, Miner. Process. Extractive Metal Rev. 5:101 (1989).
117. G. H. Luttrel and R. H. Yoon, J. Colloid Interface Sci. 159:129 (1992).
118. I. O. Protodiaconov and S. V. Uljanov, Hydrodynamics and Mass Transport in Disperse Systems, Liquid–Liquid, Nauka, Leningrad, 1986, pp. 28–48 [in Russian].
119. V. Ya. Rivkind and G. M. Riskin, Izv. AN SSSR MZhG N1:8 (1976).
120. M. B. Weber and D. Paddock, J. Colloid lnterface Sci. 94:328 (1983).
121. J. H. Masliyah, Ph.D. dissertation, University of British Columbia, Vancouver, Canada, 1970.
122. S. W. Woo, Ph.D. dissertation, McMaster University, Hamilton, Canada, 1971.
123. N. N. Rulyov and E. S. Leshchov, Kolloidn. Zh. 42:1123 (1980).
124. A. E. Hamielec and A. I. Jonson, Can. J. Chem. Eng. 40:41 (1962).
125. J. F. Anfruns and J. A. Kitchener, in Flotation (M. C. Fuerstenau, ed.), A. M. Gaudin Memorial Volume, SME-AIME, New York, pp. 626–637.
126. E. S. R. Gopal, in Emulsion Science (P. Sherman, ed.), Academic Press, London, 1969, pp. 69–70.
127. S. S. Dukhin and M. V. Buikov, Zh. Fiz. Chim. 39:913 (1965).
128. L. A. Spielman, Annu. Rev. Fluid Mech. 9:297 (1977).
129. S. L. Goren and M. E. O'Neil, Chem. Eng. Sci. 26:325 (1971).
130. S. L. Goren, J. Fluid Mech. 41:613 (1971).
131. A. I. Goldman, R. G. Cox, and H. Brenner, Chem. Eng. Sci. 22:637 (1967).
132. N. N. Rulyov, Kolloidn. Zh. 40:898 (1978).
133. N. N. Rulyov, Kolloidn. Zh. 40:1202 (1978).
134. V. Shubin and P. Kekicheff, J. Colloid Interface Sci. 155:108 (1993).
135. G. A. Martinov and V. M. Muller, Dokl. AN USSR 207:1161 (1972).
136. D. Reay and G. A. Ratelif, Can. J. Chem. Eng. 51:178 (1973).
137. D. Reay and G. A. Ratelif, Can. J. Chem. Eng. 53:481 (1975).
138. G. L. Collins and G. J. Jameson, Chem. Eng. Sci. 31:985 (1976).
139. G. L. Collins and G. J. Jameson, Chem. Eng. Sci. 31:239 (1977).
140. K. Okada, Y. Akagi, M. Kogure, and N. Yoshioka, Can. J. Chem. Eng. 68:393 (1990).
141. K. Okada, Y. Akagi, M. Kogure, and N. Yoshioka, Can. J. Chem. Eng. 68:614 (1990).
142. Wen Jongsong and G. K. Batchelor, Scintia Sinica 28:172 (1985).
143. G. K. Batchelor and C. S. Wen, J. Fluid Mech. 124:495 (1982).
144. D. J. Jeffrey and Y. Onishi, J. Fluid Mech. 139:261 (1984).
145. R. H. Davis, J. Fluid Mech. 145:179 (1984).

146. L. D. Reed and F. A. Morrison, Int. J. Multiphase Flow 1:573 (1974).
147. Ya. I. Rabinovich and A. A. Baran, Colloids Surfaces 59:47 (1991).
148. V. A. Parsegian, N. Fuller, and R. P. Rand, Proc. Natl. Acad. Sci. USA, 2750 (1979).
149. R. P. Rand, Annu. Rev. Biophys. Bioeng. 10:277 (1981).
150. R. P. Rand, V. A. Parsegian, J. A. Henry, L. J. Lis, and M. McAlister, Can. J. Biochem. 58:959 (1980).
151. H. R. Kruyt, Colloid Science, Vol. 1, Elsevier, Amsterdam, 1952.
152. A. S. Dukhin, Kolloidn. Zh. 50:441 (1988).
153. A. V. Bochko, A. S. Dukhin, E. I. Moshkovski, and A. A. Baran, Kolloidn. Zh. 49:543 (1987).
154. M. Stimson and G. B. Jeffrey, Proc. Roy. Soc. London A110:1117 (1926).
155. N. N. Rulyov, S. S. Dukhin, and V. P. Semenov, Kolloidn. Zh. 41:263 (1979).
156. P. S. Kisliy, Yu. I. Nikitin, V. M. Melnik, and S. M. Uman, Poroshkovaja Metallurgija 6:92 (1982).
157. L. A. Spielman and P. M. Cukor, J. Colloid Interface Sci. 43:51 (1973).
158. M. V. Ostrovsky and R. J. Good, J. Disper. Sci Technol. 7:95 (1986).
159. F. S. Milops and D. T. Wasan, Colloids Surfaces 4:91 (1981).
160. M. Boenrel, A. Graciaa, R. S. Shechtel, and W. H. Waade, J. Colloid Interface Sci. 72:161 (1979).
161. J. Vinatieri, Paper SPE 6675, J. Petrol. Technol. (1977).
162. D. O. Shah and R. S. Shechter, Improved Oil Recovery by Surfactant and Polymer Flooding, Academic Press, New York, 1977.
163. H. K. van Bollen and Associates, Inc., Fundamentals of Enhanced Oil Recovery, Pen Well Publishing Co, Tulsa, OK, 1980.
164. P. Becher (ed.), Encyclopedia of Emulsion Technology, Vol. 1, Marcel Dekker, New York, 1983.
165. P. Becher (ed.), Encyclopedia of Emulsion Technology, Vol. 2, Marcel Dekker, New York, 1985.
166. R. A. Mohammed, A. I. Bailey, P. F. Luckham, and S. E. Taylor, Colloids Surfaces 80:223 (1993); 80:237 (1993); 83:261 (1994).
167. C. I. Chitewelu, V. Hornof, G. H. Neale, and A. E. George, Can. J. Chem. Eng. 72:534 (1994).
168. L. Bertero, A. Di. Lullo, A. Lentini, and L. Terzi, SPE 28543, Society of Petroleum Engineers (1994).
169. J. F. McCafferty and G. G. McClaflin, SPE 24850, Society of Petroleum Engineers (1992).
170. J. N. Israelachvili, Intermolecular and Surface Forces, 2nd ed., Academic Press, London, 1991.
171. J. Sjöblom (ed.), Emulsions and Emulsion Stability, Marcel Dekker, New York, 1996.
172. I. B. Ivanov and P. A. Kralchevsky, Colloids Surfaces 128:155 (1997).
173. S. S. Dukhin and J. Sjöblom, in Emulsions and Emulsion Stability (J. Sjöblom, ed.), Marcel Dekker, New York, 1996, p. 41.
174. P. A. Kralchevsky, K. D. Danov, and N. D. Denkov, in Handbook of Surface and Colloid Chemistry, CRC Press, London, 1996.
175. Chapter 11.4 in Ref. 174.
176. R. K. Prud'homme (ed.), Foams: Theory, Measurement and Applications, Marcel Dekker, New York, 1995.
177. P. A. Kralchevsky, K. D. Danov, and I. B. Ivanov, in Ref. 176.
178. S. A. K. Jeelany and S. Hartland, J. Colloid Interface Sci. 164:296 (1994).
179. P. D. I. Fletcher, in Drops and Bubbles in Interface Research (D. Mobius and R. Miller, eds.), Vol. 6, Elsevier, New York, 1998.
180. P. J. Breen, D. T. Wasan, Y. H. Kim, A. D. Nikolov, and C. S. Shetty, in Emulsions and Emulsion Stability (J. Sjöblom, ed.), Marcel Dekker, New York, 1996.
181. S. S. Dukhin and J. Sjöblom, J. Dispersion Sci. Technol. 19:311 (1998).
182. Ø. Holt, Ø. Sæther, J. Sjöblom, S. S. Dukhin, and N. A. Mishchuk, Colloids Surfaces 123–124:195 (1997).
183. Ø. Sæther, S. S. Dukhin, J. Sjöblom, and Ø. Holt, Colloid. J. 57:836 (1995).
184. S. S. Dukhin, J. Sjöblom, D. T. Wasan, and Ø. Sæther, Colloids Surfaces 180:223 (2001).
185. Ø. Sæther, J. Sjöblom, S. V. Verbich, N. A. Mishchuk, and S. S. Dukhin, Colloids Surfaces 142:189 (1998).
186. Ø. Sæther, J. Sjöblom, S. V. Verbich, and S. S. Dukhin, J. Dispersion Sci. Technol. 20:295 (1999).
187. Ø. Holt, Ø. Sæther, J. Sjöblom, S. S. Dukhin, and N. A. Mishchuk, Colloids Surfaces 141:269 (1998).

188. S. S. Dukhin, Ø. Sæther, and J. Sjöblom, Proc. Symposium on Emulsions, Foams and Thin Films, in honor of D. T. Wasan at Penn State, June 1998.
189. O. Reynolds, Phil. Trans. R. Soc. (London), A177:157 (1886).
190. A. Scheludko, Adv. Colloid. Interface Sci. 1:391 (1967).
191. K. D. Danov, D. N. Petsev, N. D. Denkov, and R. Borwankar, J. Chem. Phys. 99:7179 (1993).
192. D. N. Petsev, N. D. Denkov, and P. A. Kralchevsky, J. Colloid Interface Sci. 176:201 (1995).
193. I. B. Ivanov and D. S. Dimitrov, in Thin Liquid Films (I. B. Ivanov, ed.), Marcel Dekker, New York, 1998.
194. N. A. Mishchuk, J. Sjöblom, and S. S. Dukhin, Colloid J. 57:785 (1995).
195. K. D. Danov, I. B. Ivanov, T. D. Gurkov, and R. P. Borwankar, J. Colloid Interface Sci. 167:8 (1994).
196. L. A. Lobo, D. T. Wasan, and M. Ivanova, in Surfactants in Solution (K. L. Mittal and D. O. Shah, eds.), Plenum Press, New York, 1992, Vol. 11, p. 395.
197. L. Lobo, I. Ivanov, and D. Wasan, Materials Interfaces and Electrochemical Phenomena 39:322 (1993).
198. G. Narsimhan and E. Ruckenstein, in Ref. 176.
199. D. Exerova, D. Kashchiev, and D. Platikanov, Adv. Colloid Interface Sci. 40:201 (1992).
200. B. V. Derjaguin and Yu. V. Gutop, Kolloidn. Zh. 24:431 (1962).
201. A. V. Prokhorov and B. V. Derjaguin, J. Colloid Interface Sci. 125:111 (1988).
202. S. V. Verbich, S. S. Dukhin, A. Tarovsky, Ø. Holt, Ø. Sæther, and J. Sjöblom, Colloids Surfaces 23:209 (1997).
203. D. Kashchiev and D. Exerowa, J. Colloid Interface Sci. 203:146 (1998).
204. E. Dickinson and S. R. Euston, Adv. Colloid Interface Sci. 42:89 (1992).
205. P. Taylor, Adv. Colloid Interface Sci. 75:107 (1998).
206. H. W. Yarranton and Y. H. Masliyah, J. Colloid Interface Sci. 196:157 (1997).
207. G. A. Martynov and V. M. Muller, Kolloidn. Zh. 36:687 (1974).
208. V. M. Muller, Kolloidn. Zh. 40:85 (1978).
209. J. D. Chan, P. S. Hahn, and J. C. Slattery, AIChE J. 34:40 (1988).
210. S. A. K. Jeelani and S. Hartland, J. Colloid Interface Sci. 156:467 (1993).
211. R. W. Aul and W. I. Olbriht, J. Colloid Interface Sci. 115:478 (1991).
212. A. Scheludko and D. Exerova, Colloid J. 168:24 (1960).
213. A. Scheludko, Proc. K. Ned. Akad. Wet. Ser. B. 65:87 (1962).
214. D. Platikanov and E. Manev, in Proceedings 4th International Congress of Surface Active Substances, Plenum, New York, 1964, p. 1189.
215. K. A. Burrill and D. R. Woods, J. Colloid Interface Sci. 42:15 (1973).
216. K. A. Burrill and D. R. Woods, J. Colloid Interface Sci. 42:35 (1973).
217. S. R. Deshiikan and K. D. Papadopoulos, J. Colloid Interface Sci. 174:302 (1995).
218. S. R. Deshiikan and K. D. Papadopoulos, J. Colloid Interface Sci. 174:313 (1995).
219. M. E. Costas, M. Moreau, and L. Vicente, J. Phys. A: Math. Gen. 28:2981 (1995).
220. F. Le Berre, G. Chauveteau, and E. Pefferkorn, J. Colloid Interface Sci. 199:1 (1998).
221. B. J. McCoy and G. Madras, J. Colloid Interface Sci. 201:200 (1998).
222. J. Widmaier and E. Pefferkorn, J. Colloid Interface Sci. 203:402 (1998).
223. I. M. Elminyawi, S. Gangopadhyay, and C. M. Sorensen, J. Colloid Interface Sci. 144:315 (1991).
224. P. Meakin, Adv. Colloid Interface Sci. 28:249 (1988).
225. R. Nakamura, Y. Kitada, and T. Mukai, Planet Space Sci. 42:721 (1994).
226. S. Chandrasekhar, Rev. Mod. Phys. 15:1 (1943).
227. V. M. Muller, Colloid J. 58:598 (1996).
228. D. G. Dalgleish, Colloids Surfaces 46:14 (1990).
229. D. G. Dalgleish and Y. Fang, J. Colloid Interface Sci. 156:329 (1993).
230. D. J. Mitchell and P. Richmond, J. Colloid Interface Sci. 46:128 (1974).
231. V. N. Gorelkin and V.P. Smilga, Kolloidn. Zh. 34:685 (1972).
232. V. N. Gorelkin and V.P. Smilga, in Poverkhnostnye Sily v Tonkikh Plenkakh i Ustoichivost Kolloidov (B. V. Derjaguin, ed.), Nauka, Moskow, 1974, p. 206.
233. S. Usui, Y. Imamura, and E. Barough, J. Disp. Sci. Technol. 8:359 (1987).
234. S. B. Grant, C. Poor, and S. Relle, Colloids Surfaces 107:155 (1996).